

Mitochondrial proteome maintenance in murine spinal motor axons and the role of the RNA-binding protein CLUH

Inaugural-Dissertation

zur

Erlangung des Doktorgrades

Der Mathematisch-Naturwissenschaftlichen Fakultät

Der Universität zu Köln



vorgelegt von

Tim Schlegel

aus Moers

angenommen im Jahr 2025

Berichterstatter (Gutachter):

Prof. Dr. Elena Irene Rugarli

Prof. Dr. Niels Gehring

Tag der mündlichen Prüfung: 05.02.2025

Table of Contents

Abstract	5
Zusammenfassung	7
1 Introduction	9
1.1 Mitochondria in Neurons	9
1.1.1 Mitochondria and neurodegenerative diseases.....	9
1.2 Pathways to maintain mitochondria in axons and dendrites	10
1.2.1 Neuronal polarisation as a challenge for distal maintenance	10
1.2.1 Limited distal maintenance by protein and mitochondrial transport and dynamics	10
1.2.3 Local translation of mRNAs in Neurons.....	12
1.3 RNA binding protein CLUH	17
1.3.1 The role of CLUH in neurons	18
2 Aims	20
3 Materials and Methods	21
3.1 Mouse line	21
3.2 Primary Neuron culture	21
3.3 HeLa cell culture	22
3.4 Preparation and lysis of compartmentalised proteomics	22
3.4.1 LC and MS	22
3.4.2 Data analysis	23
3.5 Fluorescence and brightfield microscopy	24
3.6 Fluorescence immunostaining of primary motoneurons in MFDs	24
3.7 Trafficking of mitochondria	24
3.8 Live imaging of mRNA and endosomes	25
3.8.1 Analysis.....	25
3.9 Fluorescent in-situ hybridisation (FISH)	26
3.9.1 3D colocalisation analysis.....	27
3.10 Cloning of mRNA tether constructs	28
3.11 Statistical analysis, graph, and scheme creation	29
3.12 Data availability	29
3.13 Antibodies, Reagents, Plasmids	30
3.13.1 Primary Antibodies	30
3.13.2 Secondary Antibody.....	30
3.13.3 Reagents	31
3.13.4 Plasmids	32

4 Results	33
4.1 Identifying axon specific changes in the mitochondrial proteome of primary motoneurons	33
4.1.1 Successful set up of an axonal compartment using two chambered microfluidic devices	33
4.1.2 Axonal and whole cell proteome of primary motoneurons at DIV 10 by mass spectrometry	36
4.1.3 The axonal mitochondrial proteome is depleted of OXPHOS proteins and has an overall strong shift in metabolically active proteins	39
4.1.4 Are protein half-life, local translation activity and mRNA levels predictors for enrichment of mitochondrial proteins in axon?.....	43
4.1.5 Differences between axonal and whole cell enriched mitochondrial proteome correlate with more spherical morphology.....	46
4.2 Trafficking of axonal mitochondria is not affected by CLUH	48
4.3 CLUH does not control the abundance of target mRNA in axons by affecting trafficking of target mRNA (Zaninello, Schlegel et al., <i>Science Advances</i>, 2024)	49
4.3.1 Setting up the mRNA tether system for live imaging of mRNA movement	50
4.3.2 Axonal trafficking of CLUH target mRNAs is not substantially affected by absence of CLUH.....	52
4.4 Investigating a CLUH dependent colocalisation and co-transport of CLUH target mRNA with endosomes and mitochondria	53
4.4.1 In HeLa cells CLUH and <i>Atp5a</i> mRNA association occurs away from mitochondria and late endosomes.....	53
4.4.2 Pilot experiment identifying preferential colocalisation of CLUH target <i>Mdh2</i> with late endosomes in WT axons.....	56
4.4.3 Characterising the association and co-transport of <i>Mdh2</i> and <i>ActB</i> mRNA with late endosomes in presence and absence of CLUH	58
5 Discussion	64
5.1 Compartmentalised proteomics of primary motoneurons	64
5.1.1 Robust axon enriched proteome of motoneurons and comparison to other <i>in vitro</i> studies.....	64
5.1.2 Normalisation of proteomics data from compartmentalised cells.....	65
5.1.3 Alterations of mitochondrial metabolic pathways in axons of developing neurons and their possible relevance for neuronal health.....	66
5.1.4 Protein half-life, translation and mRNA levels do not majorly determine axonal enrichment on proteomic scale, but can be influential on pathway level	69
5.1.5 Mitochondrial morphology as a major determinant of protein composition	71
5.2 Relevance of CLUH for mechanisms of axonal mitochondrial maintenance	72

5.2.1 Failure to maintain the axonal mitochondrial proteome under KO of CLUH is not due to mitochondria transport	72
5.2.2 mRNA transport is not affected by loss of CLUH in a way to reduce mRNA levels in axons	73
5.2.3 mRNA localisation to endosomal translation hubs is not affected by CLUH KO in a way that suggests substantially increased mRNA decay	75
5.2.4 CLUH acts on target mRNAs away from mitochondria and late endosomes.....	77
5.2.5 Diminished local translation is likely the cause for the failure to maintain the axonal mitochondrial proteome under KO of CLUH	78
5.3 Limitations of the experimental models.....	80
5.3.1 Primary moto neurons	80
5.3.2 HeLa cells.....	81
Appendix	82
References.....	94
Erklärung zur Dissertation.....	107

Abstract

Mitochondria play a very important role in mediating neuronal activity and survival. Dysfunction of mitochondria is related to a variety of neurodegenerative diseases. Often axons are particularly affected, which is thought to be connected to the high polarisation of neurons. Their long axons and other distal areas make the homeostasis of organelles like mitochondria and the supply of new proteins challenging. Direct transport of proteins or whole organelles over long distances can be limited by protein half-life. Thus, transport of mRNAs and local translation are central alternatives. RNA binding proteins (RBPs) play an important role in this context, by forming complexes that can regulate mRNA stability, transport and translation, and mediate the tethering of mRNAs to organelles to facilitate localised translation. CLUH (Clustered mitochondria protein homolog) is an RBP, which binds to mRNAs of nuclear-encoded mitochondrial proteins. Loss of CLUH not only leads to clustering of mitochondria, but also to an increased decay of its target mRNAs and to a reduced abundance of the corresponding proteins. This defect has also been observed in axons of primary spinal motoneurons of a *Cluh* knock-out mouse model. Thus, suggesting a key role of CLUH in regulating mitochondrial biogenesis at post-transcriptional level.

As mentioned, mitochondria in axons face the challenge of long distances for the maintenance with new proteins and it is unclear what affects this may have on the mitochondrial proteome. Therefore, I wanted to compare the mitochondria annotated proteome of axons to the rest of the cell. I cultured primary spinal motoneurons in a two-chambered microfluidic device, yielding one compartment composed exclusively of axons and another with whole neurons. Analysis of the axonal mitochondrial proteome identified the depletion of proteins involved into oxidative phosphorylation and parts of the citric acid cycle, while proteins involved in fatty acid metabolism and urea cycle were enriched in axons. These proteome changes suggest a metabolic difference between axonal and whole cell mitochondria. By correlating my data to other existing datasets, I explored if mRNA stability, mRNA transport, axonal transcriptome or protein half-life could be factors involved in regulating protein enrichment. While no factor correlated with the mitochondrial proteome in general, protein half-life appeared to play a substantial role in the citric acid cycle. Moreover, the shift from elongated to circular morphology of axonal mitochondria, correlated with an increase of soluble over membrane associated mitochondrial proteins in axons.

In a more specific approach, focusing on the RBP CLUH, I investigated how CLUH may regulate its mRNA targets on a post-transcriptional level in motoneurons. In order to analyse whether the reduced mRNA abundance in axons of primary spinal motoneurons may be caused by altered axonal transport, I used an optimised mRNA-tether system (MS2-MCP) that allows

for live imaging of mRNA at high temporal and spatial resolution. I showed that CLUH has no effect on active and directed transport of target mRNAs (*Mdh2*, *Atp5a*), suggesting that other regulatory mechanisms like increased mRNA decay are involved in the lower mRNA levels. Increased decay could be due to mislocalisation of mRNA away from translational hubs like endosomal and mitochondrial surfaces. However, I found only a small reduction in association length and no change in co-movement of *Mdh2* mRNA with late endosomes in CLUH KO axons. Similarly, in HeLa cells CLUH did not impact co-localisation of mRNA to late endosomes or mitochondria and CLUH preferentially associates with *Mdh2* away from these organelles.

Zusammenfassung

Mitochondrien spielen eine sehr wichtige Rolle für die neuronale Aktivität und die Aufrechterhaltung von Neuronen. Eine Funktionsstörung der Mitochondrien steht in Zusammenhang mit einer Vielzahl neurodegenerativer Erkrankungen. Häufig sind die Axone besonders betroffen, was vermutlich mit der starken Polarisierung der Neuronen zusammenhängt. Die langen Axone und andere distale Bereiche, machen die Aufrechterhaltung von Organellen wie Mitochondrien und die Versorgung mit neuen Proteinen zu einer Herausforderung. Der direkte Transport von Proteinen oder ganzen Organellen über große Entfernungen kann durch die Halbwertszeit von Proteinen begrenzt sein. Daher sind der Transport von mRNAs und die lokale Translation zentrale Alternativen. RNA-bindende Proteine (RBPs) spielen in diesem Zusammenhang eine wichtige Rolle, indem sie Komplexe bilden, die die Stabilität, den Transport und die Translation von mRNAs regulieren können und die Verankerung von mRNAs an Organellen vermitteln, um eine lokalisierte Translation zu erleichtern. CLUH (Clustered mitochondria protein homolog) ist ein RBP, das an mRNAs von Nukleus kodierten mitochondrialen Proteinen bindet. Der Verlust von CLUH führt nicht nur zu einer Haufenbildung der Mitochondrien, sondern auch zu einem verstärkten Abbau der mRNAs die CLUH bindet und zu einer reduzierten Häufigkeit der entsprechenden Proteine. Dieser Defekt wurde auch in Axonen primärer spinaler Motoneuronen eines Cluh-Knockout-Mausmodells beobachtet. Dies deutet auf eine Schlüsselrolle von CLUH bei der Regulierung der mitochondrialen Biogenese auf post-transkriptioneller Ebene hin.

Wie bereits erwähnt, sind die Mitochondrien in den Axonen mit der besonderen Herausforderung konfrontiert, dass sie über längere Strecken mit neuen Proteinen versorgt werden müssen, und es ist unklar, welche Auswirkungen dies auf ihr Proteom hat. Daher wollte ich das mitochondrial annotierte Proteom von Axonen mit dem Rest der Zelle vergleichen. Ich kultivierte primäre spinale Motoneuronen in einem zweikammerigen mikrofluidischen System, in dem eine Seite ausschließlich aus Axonen bestehendes und die andere die ganzen Neuronen enthält. Die Analyse des axonalen mitochondrialen Proteoms ergab, dass Proteine, die an der oxidativen Phosphorylierung und an Teilen des Zitronensäurezyklus beteiligt sind, in den Axonen unterrepräsentiert sind, während Proteine, die am Fettsäurestoffwechsel und am Harnstoffzyklus beteiligt sind, in den Axonen angereichert sind. Diese Veränderungen des Proteoms deuten auf einen Unterschied im Stoffwechsel zwischen axonalen und anderweitigen Mitochondrien hin. Durch Korrelation meiner Daten mit anderen bestehenden Datensätzen untersuchte ich, ob der mRNA-Transport, das axonale Translatom oder die Protein-Halbwertszeit Faktoren sein könnten, die die Proteinverteilung regulieren. Während kein Faktor mit dem mitochondrialen Proteom im Allgemeinen korrelierte, schien die Protein-

Halbwertszeit eine wesentliche Rolle im Zitronensäurezyklus zu spielen. Darüber hinaus korrelierte der Übergang von einer länglichen zu einer kreisförmigen Morphologie der axonalen Mitochondrien mit einer Zunahme der löslichen gegenüber den membranassoziierten mitochondrialen Proteinen in den Axonen.

In einem spezifischeren Ansatz, der sich auf das RBP CLUH konzentrierte, untersuchte ich, wie CLUH seine mRNA-Ziele auf post-transkriptioneller Ebene in Motoneuronen regulieren kann. Um zu analysieren, ob die verringerte mRNA-Häufigkeit in Axonen primärer spinaler Motoneuronen durch einen veränderten axonalen Transport verursacht werden könnte, verwendete ich ein optimiertes mRNA-Adaptersystem (MS2-MCP), das eine Live-Bildgebung von mRNA mit hoher zeitlicher und räumlicher Auflösung ermöglicht. Ich konnte zeigen, dass CLUH keine Auswirkungen auf den aktiven und gerichteten Transport von Ziel-mRNAs (*Mdh2*, *Atp5a*) hat, was darauf hindeutet, dass andere Regulationsmechanismen wie ein erhöhter mRNA-Abbau für das niedrigere mRNA-Level verantwortlich sind. Der verstärkte Abbau könnte auf eine Fehllokalisierung der mRNA weg von Translationszentren wie endosomalen und mitochondrialen Oberflächen zurückzuführen sein. Ich fand jedoch nur eine geringe Verringerung der Assoziationsdauer und keine Veränderung der gemeinsamen Bewegung von *Mdh2* mRNA mit späten Endosomen in CLUH-KO-Axonon. Auch in HeLa-Zellen hatte CLUH keinen Einfluss auf die Kollokalisierung von mRNA mit späten Endosomen oder Mitochondrien, und CLUH assoziiert bevorzugt mit *Mdh2* abseits dieser Organellen.

1 Introduction

1.1 Mitochondria in Neurons

The central nervous system is the most energy demanding organ in the body, having a highly over-proportional rate of metabolism as compared to its weight (Mink, Blumenschine, and Adams 1981; Harbauer 2017). The primary source of the energy carrier adenosine triphosphate (ATP) in neurons has been shown to be oxidative phosphorylation (OXPHOS), which takes place in mitochondria (Hall et al. 2012; Harris, Jolivet, and Attwell 2012). OXPHOS is a process which is fuelled by the electron transport chain (ETC), where the channelling of electrons between four protein complexes (CI-CIV) creates a proton gradient from the mitochondrial inter membrane space to the mitochondrial matrix. This proton gradient is used by the fifth protein respiratory complex (CV) to produce ATP from adenosine diphosphate (ADP) (Zhao et al. 2019). ATP is then used for many functions in the neuron, most importantly to drive the action potential in axons by sodium-potassium pumps which create the resting potential (Bean 2007). In synapses, which are crucial for passing the action potential from one neuron to another, ATP is important for driving the clustering of synaptic vesicles by the assembly of actin cytoskeleton and to recycle and mobilise synaptic vesicles (Verstreken et al. 2005; Pollard 2007). In addition, the mitochondria themselves have been suggested to be important for development by inducing axonal branching (Spillane et al. 2013) and are involved in maintaining the calcium ion (Ca^{2+}) homeostasis in synapses (Billups and Forsythe 2002). Ca^{2+} floods the synapses upon action potential arrival and leads to the release of neurotransmitters from synaptic vesicles to propagate the signal to the post-synaptic neuron and is also involved in synaptic plasticity, where a synaptic connection is strengthened or weakened. Thus, a constant supply of axons and dendrites with functional mitochondria is essential to meet local energy demands and to ensure neuronal function (Schwarz 2013; Sheng and Cai 2012).

1.1.1 Mitochondria and neurodegenerative diseases

Based on the central role mitochondria play in neurons, it is not surprising that mitochondria dysfunction correlates with a variety of neurodegenerative diseases (McFarland, Taylor, and Turnbull 2010), including mutations in proteins of mitochondrial fusion and fission. For example, mutations in *DRP1* can lead to microcephaly and optic atrophy (Waterham et al. 2007), degeneration of the motor and sensory axons in Charcot-Marie-Tooth (CMT) disease are caused by mutations in *MFN2* and *GDAP1* (Züchner et al. 2004; Kijima et al. 2005; Cassereau et al. 2011) and *OPA1* mutations have been connected to optic atrophy and also more widespread neurodegeneration (Alexander et al. 2000; Delettre et al. 2000). Another example is connected to mitochondrial clearance, as *PINK1* and *PRKN* mutations lead to Parkinson's

disease (PD) (Pickrell and Youle 2015). Mutations in the mitochondrial m-AAA metalloprotease SPG7 or in the mitochondrial chaperonin HSP60/ SPG13 cause hereditary spastic paraplegia (HSP), a disease characterised by progressive weakness and spasticity of the legs (Casari et al. 1998; Hansen et al. 2002). And even in cases where a mitochondrial dysfunction is not causative, it can be involved in the disease progression of many neurodegenerative diseases. Examples for this are amyotrophic lateral sclerosis (ALS) mutants of SOD1 and Huntington's disease (HD) mutants of HTT, which can localise to mitochondria where they cause cytochrome c release leading to impaired electron transfer activity and also apoptosis (Lin and Beal 2006). Defects of the bioenergetic functions of mitochondria, like deleterious mutations in OXPHOS complexes, rarely cause neurodegenerative diseases as the effects are too severe and lead to embryonic and infantile lethality, such as Leigh syndrome (Schon and Przedborski 2011).

Many of the aforementioned diseases, like CMT, HSP, ALS and PD are specifically axonopathies, meaning they affect the axons first and majorly, while the soma remains for a much longer time unaffected (Züchner and Vance 2005; Burke and O'Malley 2013). Thus, axons and their mitochondria seem to exhibit a particular vulnerability against deleterious impacts, for which the reasons are not entirely clear yet.

1.2 Pathways to maintain mitochondria in axons and dendrites

1.2.1 Neuronal polarisation as a challenge for distal maintenance

The main role of neurons is to interconnect parts of the brain for signal processing and to relay signals between the central nervous system and all organs, for motility, sensation, and other functions. In order to serve this role and particular in case of motor and sensory neurons, they are not only highly polarised but have axons which in humans can reach a meter of length (Bolam and Pissadaki 2012; Misgeld and Schwarz 2017). These distances also create one of the central challenges, which is to maintain distal neuronal areas with functional organelles and a functional proteome over the whole lifetime of the cell.

1.2.1 Limited distal maintenance by protein and mitochondrial transport and dynamics

The maintenance of neuronal compartments is mainly supported by guaranteeing a complete and functional proteome. For the distal parts of a neuron, like axons, synapses and dendrites, this proteome maintenance is more challenging than for the soma, as almost all proteins are synthesised from mRNA that is encoded in the nucleus. The mitochondrial DNA (mtDNA) in humans only encodes for 13 proteins which are part of OXPHOS, some rRNAs and tRNAs, while the majority of mitochondrial proteins are nuclear encoded (Taanman 1999). Thus, there

needs to be a constant path of proteome homeostasis from the soma to everywhere else in the cell and there are two major ways how this may be achieved.

The first way is the direct or indirect, via organelles and vesicles, transport of proteins synthesised in the soma towards distal areas like the axon. The general existence of this process has been shown by compartmentalised SILAC on human induced pluripotent stem cells (iPSCs) derived dopaminergic neurons, which allows to measure the proportion of soma labelled proteins in the axonal compartment. In this *in vitro* model with limited axon length, protein transport made up the majority of axonal proteins (Cavarischia-Rega et al. 2024). Looking at the processes necessary for protein transport, the main two motor proteins relevant for active anterograde and retrograde transport of cargos like proteins, vesicles or organelles along microtubules are Kinesin and Dynein. In studies investigating the biomechanics of Kinesin, it travels on average at a speed of 0.5 $\mu\text{m/s}$, with the fastest reported velocities at 1.4 $\mu\text{m/s}$ or 12 cm/day (Abraham et al. 2018). In *in vivo* mouse experiments the median half-life of proteins in neurons has been reported at 8-25 days, with a range from a couple of hours to 880 days (Cohen and Ziv 2019; Price et al. 2010; Fornasiero et al. 2018; Heo et al. 2018). In *in vitro* studies on primary cortical or hippocampal neurons these half-lives are shorter than *in vivo* (Median: 2- 5 days) (Cohen et al. 2013; Cohen and Ziv 2019; Hakim et al. 2016; Mathieson et al. 2018; Dörrbaum et al. 2018; Heo et al. 2018). Compared to other cell types like HepG2 or HeLa cells where the average protein half-life has been reported at 9.4 or 37.8 hours, the neuronal protein half-lives are substantially longer (Chen, Smeekens, and Wu 2016; Zecha et al. 2018). The increased half-life of proteins in neurons and neuronal specific proteins is assumed to be an adaptation to the above-mentioned challenges of transport and maintenance in neurons (Cohen and Ziv 2019). It is also important to note that in the range of neuronal protein half-lives, mitochondrial proteins are among the most long-lived ones (Mathieson et al. 2018; Cohen et al. 2013; Dörrbaum et al. 2018; Heo et al. 2018; Fornasiero et al. 2018; Cavarischia-Rega et al. 2024). The longer half-life in neurons and of nuclear encoded mitochondrial (NEM) proteins reduces the need of newly synthesised proteins. Nevertheless, at the reported transport speeds of proteins and even with the extended protein-half-life, many proteins will spend a majority and some even all their lifetime until their degradation en route to a distal part of the neuron.

In case of mitochondrial proteins specifically, mitochondria as a whole organelle may be synthesised in the soma with all the necessary proteins and then transported into axons, synapses and dendrites. For active mitochondrial transport, mitochondria are tethered to the motor proteins Kinesin or Dynein via the adaptors TRAK1 and 2 and the outer mitochondrial proteins Miro1 and 2 (van Spronsen et al. 2013; Guo et al. 2005; Brickley and Stephenson 2011). In this way, mitochondria can be transported into every part of the neuron via the microtubule cytoskeleton at a speed very similar to that of kinesin transport in general (Misgeld

and Schwarz 2017). Mitochondria are highly dynamic organelles, meaning they can undergo fusion and fission, mediated by a well conserved machinery of proteins (Friedman and Nunnari 2014). Through these dynamics older mitochondria can refresh their proteome with proteins from newly transported mitochondria to maintain their functionality (Harbauer 2017). The importance of mitochondrial fusion and fission for axonal health was also described above, by the connection of several neurodegenerative diseases with mutations in fusion and fission factors. In general, while the process of mitochondrial transport in combination with mitochondrial dynamics makes the protein transport more indirect, it does not change its dependency on protein half-life.

1.2.3 Local translation of mRNAs in Neurons

1.2.3.1 Localisation of mRNA

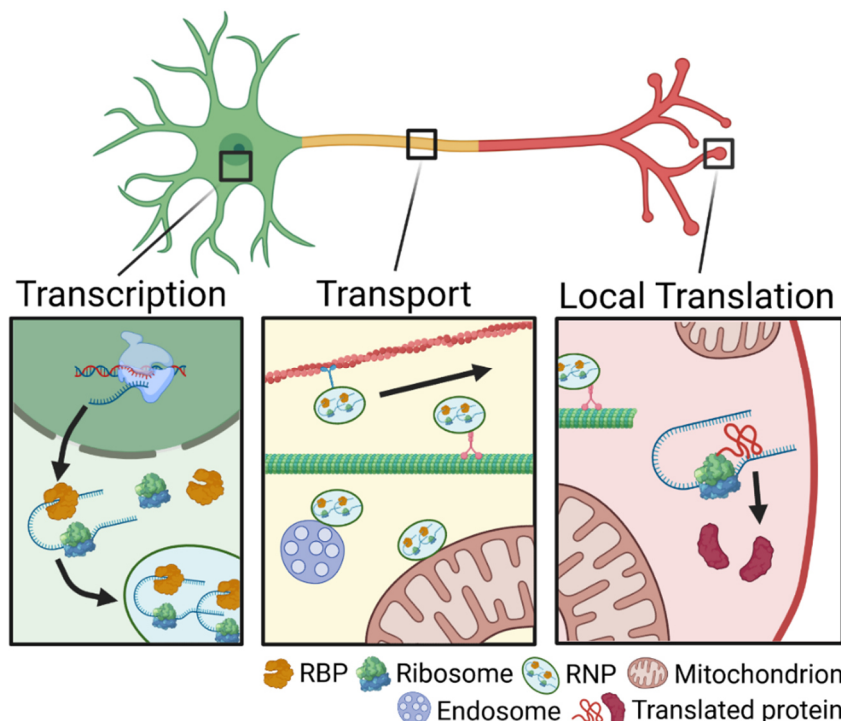


Figure 1: Schematic of processes involved in local translation in axons.

After transcription in the nucleus, mRNA can be bound by RNA binding proteins (RBPs) and Ribosomes, to create ribonucleoproteins (RNPs). With additional adaptors, RNPs can be bound by motor proteins or tethered to organelles like endolysosomes and mitochondria for transport and localisation. Once the targeted location is reached, mRNA may be translated, making newly synthesized protein available locally. Scheme created with BioRender.com.

The second mechanism for distal proteome maintenance is local translation, meaning that the mRNA rather than the protein is transported and then translated distally (Fig 1). In general, localisation of mRNA has been shown to play an important role especially in polarised cells, for coordinating cell physiology, anatomy and responding to local protein requirements. In early embryonic *Drosophila* development for example, 71% of all expressed genes encode for

subcellularly localised mRNAs (Lécuyer et al. 2007). Furthermore, focusing on the neurons, the polarisation of neurons is based on a functional asymmetry, which consequently calls for an asymmetric proteome. These assumptions are confirmed by Cajigas et al. (2012), who identified a list of 2,550 transcripts localised specifically to hippocampal dendrites and axons. Among these mRNAs are also NEM mRNAs which have been found in dendrites and axons (Aschrafi et al. 2016; Jung et al. 2022; Zappulo et al. 2017; Saal et al. 2014). It does however not seem as if NEM mRNAs follow a very clearly defined axonal enrichment state, as there have been publications finding NEM mRNAs to be particularly enriched (Nijssen et al. 2018; Aschrafi et al. 2016; Maciel et al. 2018) but also others where they are underrepresented in axons (Jung et al. 2022; Zappulo et al. 2017) or follow no clear trend (Briese et al. 2016a; Shigeoka et al. 2016).

For mRNA to be located in axons there have to be specific transport mechanisms beyond the frequently reported diffusion. A subset of mRNAs is actively transported at rapid speeds and reaches average speeds of 1.3 – 3 $\mu\text{m/s}$ with the fastest mRNAs being transported at 5 $\mu\text{m/s}$ or 43 cm/day (Muslimov et al. 2002; Park et al. 2014; Lionnet et al. 2011). For mRNAs to be actively transported, association with RNA binding proteins (RBPs) is central for mediating transport and localisation, but also nuclear export, splicing, stability, and translation (Müller-McNicoll and Neugebauer 2013) (Fig 1). The binding to the mRNA can happen via specific consensus sequences, secondary structures or also to the poly(A) tail of the RNA (Änkö and Neugebauer 2012). When they mediate transport and localisation of mRNAs, these sites are called localisation elements, Cis-acting elements or zip codes, usually found in the 3'UTR of a transcript. mRNAs and RBPs, together with other components like ribosomal proteins and translation regulators, then form dynamic ribonucleoprotein complexes (RNPs) (Buxbaum, Haimovich, and Singer 2014; Eliscovich and Singer 2017). RNPs can recruit motor proteins to the complex for active transport along the cytoskeleton or the RNPs can be tethered to organelles like mitochondria, endosomes and lysosomes to hitchhike on these (Cohen et al. 2022; Cioni et al. 2019; Liao et al. 2019) (Fig 1). It is generally assumed that mRNAs are translationally repressed during transport and activated again when they reach a certain location (Besse and Ephrussi 2008; Graber et al. 2013).

An example for an RBP important for mRNA transport and translational silencing is ZBP1 (zip code-binding protein 1). It binds β -actin mRNA, via a 54-nucleotide motif and regulates the myosin-dependent transport of β -actin mRNA to the leading edge of fibroblast (Oleynikov and Singer 2003; Latham et al. 2001) or dendrites of hippocampal neurons (Eom et al. 2003), dependent on synaptic activity (Yoon et al. 2016). When ZBP1 binds the β -actin mRNA it prevents the translation during transport until arrival at the endpoint, where ZBP1 is removed after phosphorylation by the kinase Src (Hüttelmaier et al. 2005). Another example is the protein

SFPQ (splicing factor, poly-glutamine rich) which has been found to bind to granules of mRNAs associated with neuronal survival like *Lmnb2*, *Bclw*, *Impa1* and *Creb1* via conserved binding motives in the 3'UTR (Cosker et al. 2016). SFPQ mediates the axonal transport of these RNA granules by interaction with the adaptor KLC1 (tetrameric kinesin containing the adaptor) and the motor KIF5A (Kinesin family member 5A), to maintain axonal health (Fukuda et al. 2021).

Two examples of RBPs which specifically bind NEM mRNAs are Puf3 and CLUH. CLUH will be introduced in more depth further down. PUF (Pumilio-Fem-3 binding factor) proteins are conserved from yeast to humans and are defined by the existence of Puf repeats which are crucial for their ability to bind 3' UTRs of mRNAs (Wickens et al. 2002). The yeast protein Puf3 has been shown to localise to the OMM, preferentially bind NEM mRNAs and regulating the mRNA localisation to mitochondria (García-Rodríguez, Gay, and Pon 2007; Saint-Georges et al. 2008). Binding of Puf3 furthermore promotes decay of the target mRNA by increasing deadenylation and decapping (Olivas and Parker 2000; Miller et al. 2014). However, if the yeast is grown under conditions requiring more mitochondrial activity, like on galactose, the decay promoting activity is inhibited, even though mRNA binding is still present (Miller et al. 2014). This shift is mediated by a glucose depletion dependent phosphorylation of Puf3, which prevents association with translating polysomes (Lee and Tu 2015).

1.2.3.2 Translation of localised mRNA

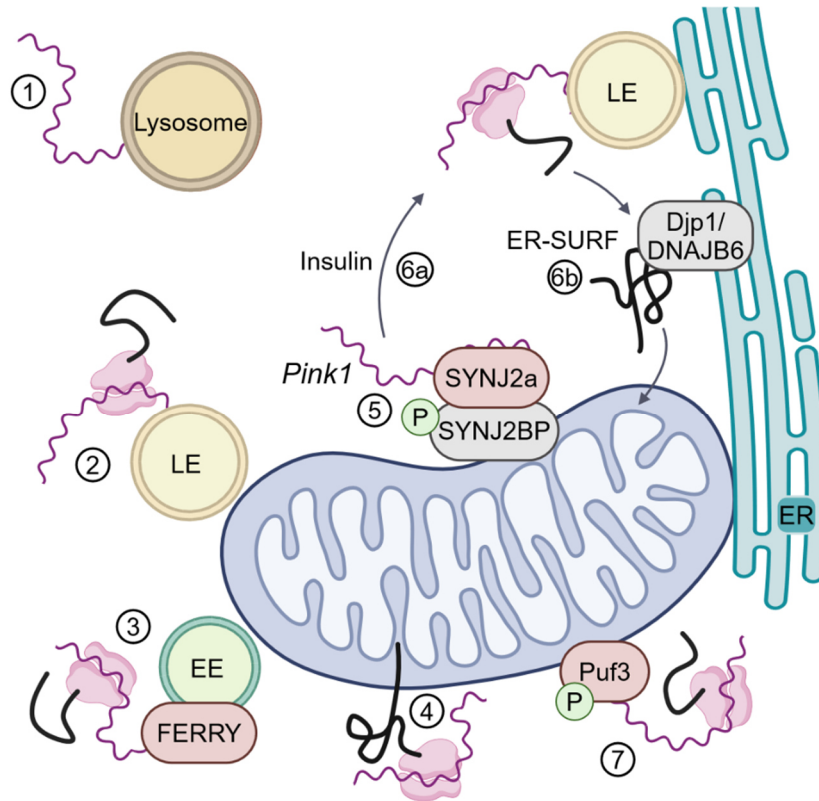


Figure 2: Regulation of local translation of NEM mRNAs.

NEM mRNAs in neurons can be tethered to lysosomes (1), to late endosomes (LE) (2) and to early endosomes (EE) via the FERRY complex (3). This tethering facilitates mRNA trafficking and thereby enables localized translation in axons and on LEs and EEs in immediate proximity to mitochondria. The newly synthesized peptides of NEM mRNAs being translated directly on mitochondria can also be simultaneously imported into the mitochondria (4). Multiple RBPs that couple NEM mRNAs with the mitochondria have been reported, including SYNJ2a, which binds to Pink1 and other NEM mRNAs and is attached to the OMM via the phosphorylated adaptor SYN2BP (5). Upon insulin stimulation, the AMPK mediated phosphorylation of SYNJ2BP is inhibited, leading to the release of Pink1 mRNA and association with LEs. The release of mRNA increases translational activity particularly at the contact sites of ER, LE and mitochondria (6a). A mechanism called ER-SURF promotes the delivery of proteins to mitochondria via the chaperone DNAJB6 (yeast: Djip1) (6b). Another example of an RBPs with a role in tethering translation of NEM RNAs to the OMM is the yeast protein Puf3. Scheme created with BioRender.com.

After mRNA has been successfully localised to the target location it can be translated to provide fresh proteins directly where needed (Bourke, Schwarz, and Schuman 2023; Das et al. 2021) (Fig 1). The mRNA molecules can also be used as a template for multiple rounds of translation, making the transport of one mRNA molecule more energy efficient than transport of proteins. Some of the first evidence for mRNA translation in axons, has been found by Lee and Hollenbeck (2003). Newer studies have expanded on this and added neurite and axon specific

translatomes (Jung et al. 2022; Zappulo et al. 2017). The relevance and prevalence of local translation for neurons is exemplified by a study on retinal ganglion cell (RGC) axons from eye explants, where approximately one third of the axonal proteome was found to be locally translated (Cagnetta et al. 2018). A direct correlation between neurite transcriptome and translome has been found in cultures of mouse induced neurons (Zappulo et al. 2017), while in axons of RGCs *in vivo* no such relation was identified and simply four subgroups with different axonal transcript enrichment and translation activity were found. NEM mRNAs were herein present in the group with axonal transcript depletion with a low or a high level of axonal translation (Jung et al. 2022). Thus, at least some of the NEM proteins are dependent on regulation by local translation. This regulation can be induced by stimuli like glutamate or NMDA in dendritic spines or synaptosomes, which promotes the localization and local translation of transcripts such as those of NEM proteins at the position of stimulation. These findings suggest a direct relation between synapse activity, the needed mitochondrial activity and local translation (Yoon et al. 2016; Kuzniewska et al. 2020). Reciprocally, mitochondria have been shown to be an essential energy supplier for stimuli induced local translation in dendrites near synapses. Under basal conditions local translation is however independent of mitochondria, suggesting that only concentrated stimuli induced translation events are dependent on the additional energy supply (Rangaraju, Lauterbach, and Schuman 2019).

As mentioned above, using neurons as a model and smFISH or a fluorescent tagging system that allows to express and detect specific mRNAs, not only mitochondria but also late endosomes (LE), early endosomes (EE) and lysosomes have been found to be associated with mRNAs, including NEM mRNAs, in axons and dendrites (Cioni et al. 2019; Schuhmacher et al. 2023; De Pace et al. 2024; Cohen et al. 2022; Harbauer et al. 2022). In the case of mitochondria, these associations can be mediated by the coding sequence of the mRNA, like it has been shown for *Cox7c* mRNA (Cohen et al. 2022) or RBPs like the above mentioned Puf3 (Lee and Tu 2015) (Fig 2). For at least a fraction of mitochondria localised NEM mRNAs it has been suggested that translation happens by cytosolic ribosomes directly on the mitochondria in combination with co-translational import of the nascent peptide by the TOM complex (Gold et al. 2017; Eliyahu et al. 2010). In case of other organelles, the tethering of mRNAs is mediated by specific adaptors like the five-subunit FERRY complex for EE and the RBP SYNJ2a with the adaptor SYN2BP for mitochondria (Cioni et al. 2019; Schuhmacher et al. 2023; De Pace et al. 2024; Harbauer et al. 2022) (Fig 2). Interestingly, the endolysosomal system is not only relevant for localisation of NEM mRNAs but also plays a central role as hub of translation of the mRNAs. Translation activity has been identified on LEs, frequently in proximity to mitochondria (Cioni et al. 2019) and the FERRY complex on EEs associates with ribosomes and can localize together with mRNA of NEM proteins to mitochondria (Schuhmacher et al.

2023): Furthermore, knock-out of the lysosomal BORC complex which mediates anterograde lysosomal trafficking, depleted axons not only of some NEM mRNAs but also those for ribosomal proteins (De Pace et al. 2024) (Fig 2).

How contact sites and interactions of multiple organelles can play a role for translation of NEM mRNAs was first identified in yeast as a process named ER-SURF. It describes the delivery of mitochondrial proteins via the ER and ER-localized chaperones to mitochondria (Hansen et al. 2018). The process is dependent on close ER-mitochondria contact sites and particularly important for hydrophobic mitochondrial precursor proteins (Koch et al. 2024). This pathway was recently suggested to also occur in neurons and in combination with translation hubs on the endolysosomal system. The RNA binding protein SYNJ2a which can bind 90 NEM mRNAs, one of which is *Pink1* mRNA, is tethered to the mitochondrial surface by SYNJ2BP (Harbauer et al. 2022). *Pink1* mRNA tethered to mitochondria via this mechanism can be released upon insulin signalling which inhibits the kinase AMPK, leading to a dephosphorylation of SYNJ2BP and a release of SYNJ2a with the mRNA (Hees, Wanderoy, et al. 2024). Released *Pink1* mRNA associates to ribosomes on the endolysosomal system and the ER, where the nascent chain is bound by the ER membrane-bound chaperon DNAJB6, which transports PINK1 back to the mitochondria for import (Hees, Segura, et al. 2024) (Fig 2). For which specific NEM mRNAs this pathway is relevant and whether the organelle the mRNA is tethered to or released from is really important for the pathway remains to be clarified.

1.3 RNA binding protein CLUH

CLUH (CluA homologue, clustered mitochondria homologue) is a conserved protein found in a variety of organisms from *Dictyostelium discoideum* (CluA), over *Saccharomyces cerevisiae* (Clu1), *Arabidopsis thaliana* (FRIENDLY or FMT) and *Drosophila melanogaster* (Clueless, Clu) to the mammalian CLUH. In all these organisms, the loss of CLUH and its homologues has been associated with the hallmark phenotype, clustering of mitochondria (Zhu et al. 1997; Fields, Conrad, and Clarke 1998; El Zawily et al. 2014; Cox and Spradling 2009; Gao et al. 2014; Schatton et al. 2017). Furthermore, *clu* mutants have a reduced lifespan and ATP production in adult but not larval *Drosophila* and mice with full body KO of CLUH have respiratory deficiencies in mouse embryos and exhibit lethality shortly after birth (Sen, Damm, and Cox 2013; Schatton et al. 2017). This defects are caused as CLUH is needed to increase the respiration activity and starvation responses, like amino acid catabolism and β -oxidation, during the switch from glycolysis to OXPHOS after birth or as a general answer to starvation (Schatton et al. 2017). Overall, these data support the role of CLUH in mitochondrial biogenesis and homeostasis.

Of the mRNAs bound by CLUH in human embryonic kidney (HEK) cells, more than 90% are transcripts of NEM proteins, related to central mitochondrial pathways of OXPHOS, citric acid cycle, fatty acid oxidation and other (Gao et al. 2014). The loss of CLUH leads to major dysregulation of the mitochondrial proteome, as shown in liver specific KO of CLUH, where protein level almost exclusively of NEM proteins are downregulated. Transcript levels correlate with the protein level changes and mRNA half-life is reduced in CLUH KO, suggesting the proteomic changes are, that at least in part, due to decreased mRNA levels and stability (Schatton et al. 2017). On a global level translation is indeed not reduced in MEF or NSC34 cell lines depleted of CLUH. However, translational activity specifically of CLUH targets has been reported to be down. Some CLUH targets show barely affected mRNA levels, but their encoded proteins are characteristically downregulated in CLUH KO (*Opal*, *Ogdh*, *Got2*, *Spg7*, *Pdha*, and *Sdha*), thus suggesting reduced translational activity as the cause of protein loss (Gao et al. 2014). Even for CLUH targets where depletion of mRNA in CLUH KO is substantial (*Atp5a1*, *Hadha*, *Pcca*), impaired translation additionally reduces protein levels. This is indicated by the reduced presence of CLUH target mRNAs in the polysome fraction of CLUH KO MEF cells compared to the WT (Schatton et al. 2017). The evidence that CLUH and all other homologues play an important role in the translation of NEM mRNAs is additionally supported by its association with ribosomes specifically at the OMM in *Drosophila* ovaries (Sen and Cox 2016). CLUH and FMT also co-immunoprecipitate with ribosomal subunits and translation factors (Antonicka et al. 2020; Hémono, Haller, et al. 2022; Hémono, Salinas-Giegé, et al. 2022) and CLUH is present in the polysome fraction in HCT116 and HeLa cells (Hémono, Haller, et al. 2022; Schatton et al. 2022). In addition, CLUH has been shown to exhibit not only stable interaction with itself, SPAG5 and KNSTRN, but also more transient interactions with many NEM proteins which must occur in between cytosolic synthesis and mitochondrial import (Hémono, Haller, et al. 2022; Schatton et al. 2022).

1.3.1 The role of CLUH in neurons

In the nervous system CLUH has only recently been characterised (Zaninello et al. 2024). It was found that deletion of *Cluh* in mouse neural progenitor cells (CLUH KO) led to peripheral neuropathy and impaired locomotor activity, defined by an increased crossing time and more slips when crossing a walking beam and impaired rotarod performance from 5 months onwards. Furthermore, the compound muscle action potential (CMAP), which is the sum of hind paw action potentials after stimulating the sciatic nerve, is halved in CLUH KO mice at 8 months. These findings were substantiated by increased axonal degeneration in the peroneal branch of the sciatic nerve from 5 months onwards and an increased number of poorly innervated and smaller neuro muscular junctions (NMJs) at the tibialis anterior muscle in 14 months old CLUH KO mice. The number of motoneurons present in the spinal cord was however not changed,

suggesting an axonopathy. Mitochondria in nerves of aged CLUH KO mice were more frequently swollen and showed dilated cristae than the WT. In comparison, in primary motoneurons *in vitro*, it was determined that at this embryonic stage of development mitochondria were normal in terms of morphology, distribution, membrane potential and axonal density. However, in growth cones (GCs) ATP production by mitochondria in CLUH KO was found to be reduced, while unchanged in the soma. This defect correlated with a reduced GC size and fewer synaptic vesicles. Since CLUH binds many NEM mRNAs, including those of OXPHOS proteins, it is not surprising to find reduced ATP levels in absence of CLUH. In fact, mRNA levels of the CLUH targets *Atp5a* and *Pink1*, but not the control *ActB*, were reduced in CLUH KO and especially in axons. This also correlated with a downregulation of NEM proteins in neurons with a particularly high decrease in axons specifically. These results were obtained by using a compartmentalised culture of primary motoneurons, separating neurites from soma via a porous membrane (Boyden chamber). In summary, CLUH has been shown to prevent a peripheral neuropathy and maintain the levels of NEM mRNA and proteins especially in axons of motoneurons. How the lack of CLUH may induce this neuropathy and axonal defects by post-transcriptional regulation of its targets will be investigated and discussed in this thesis.

2 Aims

- Identify the differences between the mitochondrial proteome in axons and the rest of the neuron, to elucidate possible variations in their composition and related metabolic changes. This could help to resolve the cause for the vulnerability of axons and mitochondria in axons as compared to soma.
- Investigate how the RNA binding protein CLUH regulates mRNA targets on a post-transcriptional level and thereby mitochondrial homeostasis in primary motoneurons

3 Materials and Methods

3.1 Mouse line

The animal procedures were carried out according to the European (EU directive 86/609/EEC), national (Tierschutzgesetz), and institutional guidelines and were approved by local authorities (Landesamt für Natur, Umwelt und Verbraucherschutz Nordrhein-Westfalen, Germany). Animals were kept in the Cologne Excellence Cluster on Cellular Stress Responses in Aging-Associated Diseases (CECAD), University of Cologne, Germany, in individually ventilated cages at 22°C (\pm 2°C), at a relative humidity of 55% (\pm 5%), under a 12-hour light cycle, on sterilized bedding (Aspen wood, Abedd, Germany) and with access to a sterilized commercial pelleted diet (ssniff Spezialdiäten GmbH) with acidified water ad libitum. Previously described *Cluh*^{fl/fl} Cre^{wt/tg} (CLUH KO) mice, with *Cluh* knocked out in neural progenitors, were used for primary cultures. To generate embryos with that genotype, *Cluh*^{fl/fl} Cre^{wt/wt} (WT) females, were mated with CLUH KO males, resulting in 50/ 50 occurrence of CLUH KO and WT embryos of which the WT ones were used as a control. For experiments which were only done on wild type mice, pure wild type breeder mice were mated. Mice were kept on a pure C57/BL6NRj background.

3.2 Primary Neuron culture

Motoneurons were plated on coverslips coated with poly-d-lysine (20 μ g/ml) for 2 hours and laminin (0.1 μ g/ml) over-night at a density of 120,000 cells/cm² in DMEM, supplemented with 5% FBS, 0.6% Glucose, 1% penicillin/ streptomycin and amphotericin B (250 μ g/ml). After 1 day in culture the medium was fully exchanged by growth medium consisting of Neurobasal medium supplemented with 2% B-27, 1% glutamine, 1% penicillin/streptomycin, amphotericin B (250 μ g/ml), 1 μ M cytosine arabioside (not for MFD cultures), brain-derived neurotrophic factor (BDNF; 10 ng/ml), ciliary neurotrophic factor (CNTF; 10 ng/ml), and glia cell line-derived neurotrophic factor (GDNF; 10 ng/ml). Cells were cultured in a humidified incubator with 5% CO₂ at 37°C. For neuronal cultures in MFDs (Xona, RD150) 35 mm glass bottom μ -Dishes (Ibidi, 81158) were coated as described above, dried, and then the sterilised MFDs were mounted on top. 300k cells in 7 μ l growth medium were slowly injected into the seeding well towards the growth compartment. After an initial attachment time in the incubator, both sides of the MFD were topped up with 180 μ l growth medium. From day in vitro (DIV) 2 onwards, medium was changed every two days. The medium was supplemented with growth factors for the whole-cell side (1x) and five times growth factor concentration for the axonal compartment (5x). Medium changes were done by removing almost all medium in the wells of the MFD and then adding 117 μ l of 1x medium to the whole cell side and 153 μ l of 5x medium to the axonal

side. Medium was added in a way that more of the medium was added to the top well than the bottom well, to create a flow of exchange. Cells were kept in humidified incubators at 37°C and 5% CO₂.

3.3 HeLa cell culture

Cells were cultured in DMEM supplemented with 10% FBS, 2 mM L-Glutamine and 1% of Penicillin and Streptomycin. The cells were kept at confluences below 70% and split by incubation in Trypsin-EDTA for 3-5 min after washing with PBS. Cells were spun down at 100 x g, re-suspended and a small fraction was re-seeded in the culturing flask. Cells were kept in humidified incubators at 37°C and 5% CO₂.

3.4 Preparation and lysis of compartmentalised proteomics

As lysis buffer an in-solution-digest (ISD) buffer was used, which is based on 2% SDC (Sodium deoxycholate) and 100 mM HEPES (pH 8.5) and added TCEP (Tris(2-carboxyethyl)phosphine) (10 mM), CAA (2-chloroacetamide) (20 mM), LysC (0.5 µg/ µl) and Trypsin (0.5 µg/ µl). At DIV10, medium was removed from both sides of the MFD and 100 µl PBS were added on both sides instead. To lyse the axonal side, the PBS from the axonal side was removed and 7 µl of ISD buffer was added. After 30 seconds the axons were fully dissolved, and the buffer was transferred from the axonal compartment into an Eppendorf tube. To lyse the whole cell (WC) compartment, the MFD was carefully removed and cell clusters in the well areas were scraped away. Afterwards 20 µl of ISD-buffer was added on the WC material and incubated for 1 minute, while constantly pipetting the buffer up and down. The WC lysate was also transferred into an Eppendorf tube, and both were incubated for 4 hours at 37°C. In this time the buffer polymerised, but this did not affect digestion. After the digestion, formic acid was added to a final volume of 1%, mixed and centrifuged at full speed for 5 min. The addition of formic acid let the SDC precipitate and thereby create a white SDC pellet and a liquid supernatant which was taken and stored at -20°C till analysis.

3.4.1 LC and MS

LC-MS/MS instrumentation consisted of an Easy-LC 1200 (Thermo Fisher Scientific) coupled via a nano-electrospray ionization source to an Exploris 480 mass spectrometer (Thermo Fisher Scientific, Bremen, Germany). An in-house packed column (length, 20 cm; inner diameter, 75 µm) was used for peptide separation. A binary buffer system (A, 0.1% formic acid; and B, 0.1% formic acid in 80% acetonitrile) was applied as follows: linear increase of buffer B from 4 to 25% within 25 min, followed by a linear increase to 40% within 2 min. The buffer B content was further ramped to 70% within 2 min and then to 70% within 2 min. Buffer B (70%) was kept for a further 1 min to wash the column. Before each sample, the column was washed using

5 μ l of buffer A, and the sample was loaded using 8 μ l of buffer A. The flow rate was 250 nl/min. The radio frequency lens amplitude was set to 45%, the capillary temperature was 275°C, and the polarity was set to positive. MS1 profile spectra were acquired using a resolution of 60,000 [at 200 mass/charge ratio (m/z)] at a mass range of 320 to 1150 m/z and an automatic gain control target of 1×10^6 .

For MS/MS-independent spectra acquisition, 30 equally spaced windows were acquired at an isolation m/z range of 13 Thomson, and the isolation windows overlapped by 1 Th. The fixed first mass was 200 m/z . The isolation centre range covered a mass range of 456 to 804 m/z . Fragmentation spectra were acquired at a resolution of 30,000 at 200 m/z with stepped normalised collision energies of 25, 30, and 42 and using a maximal injection time of 55 ms. The default charge state was set to 3. The AGC target was set to 3e6 (900%, Exploris 480). MS2 spectra were acquired in centroid mode. Field Asymmetric Ion Mobility Spectrometry was enabled and used at a compensation voltage of -50 for all samples using an inner electrode temperature of 89°C and an outer electrode temperature of 99.5°C.

3.4.2 Data analysis

Acquired raw files were analysed using Spectronaut (version 18.1) build directDIA pipeline using the Uniprot reference proteome (Mus Musculus, 21,448 sequences). The settings were set as default; the q-value cutoff for precursors, peptides and proteins was set to 0.01. The MS2 signals were utilized for quantification. The peptide quantification was calculated by the mean of the precursors and the protein intensity was calculated by the mean peptide intensity. No imputation was performed. The cross-run normalization was enabled. The protein group table was exported and the MaxLFQ intensities as well as iBAQ intensities were exported. The MitoCarta 3.0 (Rath et al. 2021) was annotated using the Uniprot identifiers.

Before further processing, all entries with more than one associated gene, the common serum contaminant albumin and the growth factors used for culturing were removed from the dataset. With Perseus (1.6.15), CLUH target and UniProt-based gene ontology annotations were added. Two versions, one with the total proteome and one with MitoCarta 3.0 annotated proteins, were exported again and relative iBAQ values were calculated in MS Excel. For each embryo two to three lysates from different MFDs were analysed. The median of those riBAQs was calculated for each embryo, followed by filtering for proteins for which at least three values in axonal and WC compartment were measured. On these shared proteins a two-sample student's T-test were done, with an S_0 of 0.01 and a permutation-based FDR of 0.01 for the total proteome and a permutation-based FDR of 0.05 for the MitoCarta annotated proteins. Volcano plots were generated using Instant Clue (Nolte et al. 2018) and heatmaps were created using GraphPad Prism. Gene ontology analysis of significantly enriched or depleted proteins was performed

using the GProfiler webtool (Kolberg et al. 2023). Correlations between datasets were calculated in Perseus or GraphPad Prism and are reported as Pearson correlation.

3.5 Fluorescence and brightfield microscopy

All live imaging and most fixed experiments were performed using the LSM980 Airyscan 2 confocal microscope (Carl Zeiss Microscopy) equipped with a Plan-Apochromat 63×/1.4 oil differential interference contrast objective. For live imaging the Multiplex CO-8Y mode was used, to get confocal resolution imaging at the best possible temporal resolution and the incubator of the microscope was used to maintain a temperature of 37°C and 5% CO₂. For fixed imaging of HeLa cells, the Multiplex SR-8Y mode was used to reach super resolution of 120 nm (x/y) and 350 nm (z). Furthermore, after selecting several fields per coverslip to image, those positions were all automatically imaged in one go. For fixed images of neurons MFD cultures stained with GFAP, TAU and CNP, GFAP I used a 10x/0.45 air objective in a tile-scan of eight images, merged by ZEN blue software. For the fixed image of a primary neuron MFD culture stained for TAU and MAP2 the TCS SP8 (Leica Microsystems) with a PL Apo 40x/0.85 CORR CS objective was used. A tile-scan of 91 images was taken and merged using the LAS X software (3.5.7.23225).

3.6 Fluorescence immunostaining of primary motoneurons in MFDs

At DIV10, MFDs were gently removed from the glass bottom of the dish, by pulling slowly from the top-right well. Afterwards the medium left was removed, the cells were washed once with PBS and then fixed in room temperature PFA (4%) for 15 min. Afterwards cells were washed two times in PBS, followed by permeabilization in 0.1% Triton-X (in PBS) for 10 min. For all of these and the following washing steps it was crucial to pipet very gently and never directly on top of the cells. Triton-X was removed after 10 min and the cells were washed three times in PBS, before blocking with 10% goat serum for 30 min. Primary antibodies were incubated for 1 hour at room temperature, dissolved in 300 µl of 1% goat serum. Afterwards cells were washed three times in PBS and then incubated with the secondary antibody and DAPI at 4°C overnight. After another two washes, PBS was removed, and cells were mounted using ibidi Mounting Medium (ibidi, 50001).

3.7 Trafficking of mitochondria

Neurons were loaded with 60 nM MitoTracker Green (Thermo Fisher) for 20 min. Images were acquired every second for 6 min. The first and last 20 seconds were excluded from analysis to avoid influences from microscope movement. Axons were straightened using the Straighten plugin of ImageJ and kymographs were generated. Trafficking was analysed on the kymographs by measuring the distance between the most proximal and the most distal position in the axon,

with a threshold of 2 μm to be regarded as moving. Directionality of motion was analysed by calculating the distance between the mitochondrial position in the first and last frame. If this distance was below 2 μm , as the mitochondrion moved back to its original position, directionality was undefined.

3.8 Live imaging of mRNA and endosomes

For mRNA trafficking experiments, cells were transfected with 2 μg of DNA and 0.9 μl Lipofectamine per Well of an Ibidi 4-Well chamber and a 24:1 ration of plasmid DNA from the reporter to RNA construct. For experiments on association of mRNA with endosomes or mitochondria, 2.2 μg of DNA (1.8 μg for mRNA, 0.4 μg for eGFP-RAB7) in 1.6 μl of Lipofectamine were transfected. Medium on the cells was not exchanged before transfections and the cells were incubated for 1 hour in the incubator with the transfected. Afterwards, medium was replaced by new medium, and cells were incubated for another 24 hours before imaging. Live imaging and analysis of mRNA trafficking in neurons was done as described in (Zaninello et al. 2024). For co-imaging of mRNA and late endosomes, cells were incubated with a final concentration of 20 nM Halo-Ligand JF 549 (Promega, GA1110) for 20 min, followed by one full replacement and one 70% replacement of the medium. Axons were selected based on thin and long morphology and movies were taken with two seconds per frame over 90 frames (180 seconds). To get the whole axon in focus, a Z-Stack of 9 – 11 slices (1.36 - 1.7 μm) was taken of every frame. For all samples the pixel size of 85 x 85 x 170 nm was kept.

3.8.1 Analysis

Movies were analysed using two approaches. On the one hand, Kymographs were generated from maximum projected time lapses using ImageJ. The Kymographs were used to manually trace mRNA tracks, and analyse them using the “step-3 measure” of the Kymolyzer macro (Basu et al. 2020). On the other hand, the movies themselves were analysed using the automatic tracking module of the NIS-Elements AR software (Nikon), considering only tracks with more than 20 frames. A custom add-on MATLAB script was employed to examine the type of movement and directionality of mRNA trajectories in neurites. In particular, the type of movement was determined by calculating the MSD of each particle as follows:

$$\text{MSD}(\tau) \leq [x(t + \tau) - x(t)]^2 + [y(t + \tau) - y(t)]^2 > \quad (\text{Eq. 1})$$

where x and y are the coordinates describing the mRNA position along the neurite, τ and t are the lag and absolute times, respectively, and the brackets are representing the time average. This calculation was performed for $\tau = 25\%$ of the total time of the trajectory (Ruthardt, Lamb, and Bräuchle 2011).

The MSD data were fitted with an anomalous diffusion model:

$$\text{MSD} = A\tau^\alpha + B \quad (\text{Eq. 2})$$

where A depends on the motion properties of the particle, B is the residual MSD, and the coefficient α indicates the type of particle motion (Otero et al. 2014). Trajectories were classified as actively driven ($\alpha > 1.5$), diffusive ($0.9 < \alpha < 1.1$), or confined ($\alpha < 0.5$). Lastly, to define the motion type based on the lateral displacement of mRNAs, the net displacement (ND) and lateral maximal displacement (LMD) were measured. ND was defined as the difference in x coordinates of the first point and the last point of the mRNA trace. LMD was defined as the difference between the most proximal and the most distal point of the trace. mRNAs with a ND $> 5 \mu\text{m}$ were defined as directed; mRNAs with ND $< 5 \mu\text{m}$ and LMD $< 1 \mu\text{m}$ were defined as stationary, while particles with ND $< 5 \mu\text{m}$ and LMD $> 1 \mu\text{m}$ were defined oscillatory (Zhao et al. 2020).

Association of mRNA-MS2 with GFP-RAB7 was analysed fully manually, using Fiji. Videos were adjusted in the brightness and contrast to make the signal clearly visible. Especially for the GFP signal these adjustments had to be done for every video separately, as signal intensity could differ. The axon initial segment and the growth cone were not analysed, as the density of signal was usually too high for a meaningful analysis. For the rest of the axon, every time an mRNA spot associated with the GFP-RAB7 signal (also partial signal overlap), the frame of association, the frame of dissociation the state of motion when associated and when dissociated (Stationary, Diffuse oscillation, Directed motion) and special behaviours (Ping-Pong, Yo-yo, Pit stop) were noted in an MS Excel table. Every motion ending up more than around $1.5 \mu\text{m}$ more distal or proximal from the start point was regarded as directed. Locations and times of each association event were also saved as ROIs for possible confirmation of the observations. For most criteria assessed data was analysed by averages per axon, like for all measures just comparing WT and CLUH KO of both mRNAs. Averages per embryo were only used for the reporting of different state of motion, as the number of spots would have been too low for some axons when divided over three motion states.

3.9 Fluorescent in-situ hybridisation (FISH)

HeLa cells were seeded on coverslips placed in 24-well plates, at 50k or 60k cells per well for WT and CLUH KO respectively and grown for 24 hours. For FISH and immune co-staining, the ViewRNA™ Cell Plus Assay-Kit (Invitrogen, 88-19000-99) was used, with different fixation and permeabilization steps. Instead of using the provided Fixation/ Permeabilization Solution, after washing the cells once with PBS, they were first fixed in 4% PFA for 15 min at room temperature, followed by two washes with PBS + RNase inhibitor (1/100),

permeabilization with 0.1% Triton-X for 8 min and another three washes with PBS + RNase inhibitor. Afterwards, with the blocking step the protocol was continued as described by the protocol of the kit. The alteration was necessary in order to prevent mitochondrial signal from dissolving, which happened when fixation and permeabilization were combined.

3.9.1 3D colocalisation analysis

Preprocessing of FISH images was done initially in ZEN 3.8 (ZEISS). The files with multiple positions imaged were split into their separate scenes using the function “Split Scenes”. These single scenes were then aligned based on a recording of multi-coloured beads, using the same imaging settings on the same day. In detail, the image file of the beads was used to create a file containing all processes necessary to perfectly align the bead signals from the different colours. This was done by using the “Channel Alignment (Extended)” function, marking the “Save Transformation” field, setting quality to medium, as registration method “Translation + Iso scaling”, linear interpolation and using the Z-dimension for 3D data. The transformation file created from the beads was then applied to all of the actual images taken, using single scenes one by one and saving the bead aligned images. These images were then further processed using a self-made half-automated Fiji macro (Cell segmentation for FISH_Thesis.ijm), which opens the images, enhances the contrast of each channel for better visibility, giving the user the chance to manually outline as many cells from the image as they want, saving those single cells without any surrounding signal in separate files and then continuing with the next image. Only cells fully on the image, with one nucleus and not visibly in mitosis were used for analysis.

For the actual analysis of colocalisation between mRNA FISH signal and antibody staining Imaris 10.0.1 (Oxford Instruments) was used. Before importing, images had to be converted into an Imaris compatible file format using the ImarisFileConverter 10.0.1. In Imaris all images from one biological replicate were then processed together using the batch function. In detail, a surface for DAPI signal was created (Smoothing: 50 nm and thresholding on absolute intensities, threshold > 525- 800, number of voxels above 25), a surface for TOM20 (Smoothing: 0.025 and thresholding on background subtracted signal (0.75 μm ball size), threshold > 320- 600, number of voxels above 40) or a surface for RAB7 (No smoothing and thresholding on background subtracted signal (0.35 μm ball size), threshold > 315-340, number of voxels above 15), a surface for CLUH (No smoothing and thresholding on absolute intensities, Threshold > 940-1150, Number of Voxels above 10) and spots based on the mRNA FISH signal (Estimated diameter: 180 nm and with background subtraction, quality threshold > 200). Thresholds were adapted for each biological replicate in order to maintain similar surface sizes and for CLUH signal adapted in a way that no surfaces were created in the images of CLUH KO cells.

After batched processing, the results tables were exported for further processing in MS Excel. The results tables on the mRNA spots contain a sub table for the distance to each of the three created surfaces, which were all sorted according to the spot IDs to be in the same order. This data was then combined into one table with the information on the spot ID, sample of origin, cell of origin and distances to all three surfaces. Using the HSTACK function in MS Excel, for each cell the number of cytosolic spots (distance to DAPI ≥ 0) and the percentage of how many spots colocalised (distance ≤ 0) with one or both protein surfaces was calculated. The average of all cells within a biological replicate was then reported in the figure and used for statistics.

3.10 Cloning of mRNA tether constructs

Two goals needed to be achieved by re cloning the mRNA tether constructs, based on the HaloTag-bActinCDS-bActinUTR-MS2V5 (Addgene #102718) by (Yoon et al. 2016). On the one hand, all protein tags were to be removed. On the other hand, besides of the ActB-MS2V5 construct used as a control, I wanted to create two mRNA-MS2V5 constructs of CLUH targets including their 5' and 3' UTR. *Atp5a* mRNA was selected as one of these, as it was also used as a target in previous experiments on mRNA in neurons. For the selection of a second target, I needed one which would not be too long, in order to still allow for efficient transfection of the final plasmid. From a list of CLUH target mRNAs downregulated in CLUH KO axons, I selected *Mdh2* as the shortest candidate with a full mRNA of 1,456 base pairs. Additionally, I created a version of the plasmid without any coding or UTR sequence, but just a small linker and the MS2V5 sequence (only-MS2).

The cloning strategy was based on a Gibson assembly (NEB, E2621S) and all cloning was planned by using the online NEBuilder Assembly Tool, with the projects saved on the Rugarli server for later revisiting. From the origin plasmid (Addgene #102718), everything between UBC promoter and MS2V5 sequence was removed with a digestion using AgeI and NotI. The sequences of *Atp5a* (ENSMUST0000002649) and *Mdh2* (ENSMUST00000019323) were amplified by PCR using mouse cDNA as a template (MEF, Oligo (dT), 0.75 μ l). *Atp5a* was divided in two pieces for better PCR efficiency. ActB sequence was taken from the original plasmid. All PCRs were done using Q5 polymerase and 50 μ l reaction volume. Products of PCRs and digests were run on a 1% agarose gel and eluted using the QIAquick PCR & Gel Cleanup Kit (Qiagen, 28506). For the final assembly, 15 μ l of Gibson Assembly Mix were combined with 17 fmol Vector and 60 fmol insert for ActB, 20 fmol vector and 40 fmol of each half of the *Atp5a* insert, or 20 fmol vector and 40 fmol insert for *Mdh2*. The final reaction volume was topped up to 20 μ l with water. Samples were incubated for 60 min at 50°C, before moving on ice.

For the only-MS2 plasmid, a small linker based on two annealed primers with the overhangs for NotI and AgeI restriction was created by mixing the primer pair, boiling for 1 min and then reducing the temperature to 25°C over 1 min. Linker (320 pg) and vector (35 ng) were ligated using a T4 DNA Ligase.

The resulting plasmids were transformed into home amplified NEB Stable competent *E. coli* (NEB, C3040H), by adding 4 µl of the reaction volume to 50 µl thawed bacteria, incubating on ice for 30 min, heatshock at 42°C for 90 seconds, incubate on ice for 2 min, followed by incubation at 37°C, with 250 rpm shaking for 30 mins. The bacteria solution was plated onto LB-Agar plates containing Ampicillin for the selection of single clones after growth for 14-16 hours over night at 37°C.

Plasmids were sequenced to confirm correct cloning assembly, by using a UBC Fwd and a MS2 Rev primer. For the pUbC-ActBCDS(hu)-ActB3'UTR(ms)-MS2V5 plasmid clone 1 was picked, for pUbC-Atp5a(CDS+UTRs)-MS2V5 clone D and for pUbC-Mdh2(CDS+UTRs)-MS2V5 clone B. Full plasmid sequences and aligned sequencing results can be found on benchling.com in the project “Cloning of CLUH target mRNA live imaging construct”.

Table 1: Primers used for cloning

Atp5a1 FWD Part 1	cgctgtgatcgtcacttgccgctcctctggttctgc
Atp5a1 REV Part 1	caatcgcgacgtagatgcagtagcagcttcttc
Atp5a1 FWD Part 2	ctgcatctacgtcgcgattggtcagaag
Atp5a1 REV Part 2	ctccaccggtttgtaggttatccggagcagagttctcttttaac
Mdh2 FWD	cgctgtgatcgtcacttgccggcccgagcccagagatga
Mdh2 REV	ctccaccggtttgtaggttacgggtcagagcctgctttactgtcattatc
MS2-only linker FWD	ggccaagcgtcttcggatc
MS2-only linker REV	ccgggatccgaagacgctt

3.11 Statistical analysis, graph, and scheme creation

All statistical analysis, except of the proteomics, were done using GraphPad Prism 8, which was also used to make all graphs. Schemes were created using BioRender, except of the two schemes on MFD principle and lysis which were done using Microsoft PowerPoint. The Venn diagram was made using a freely available tool called Venn Diagram Plotter (Kyle Littlefield, Matthew Monroe). Figures were created using CorelDRAW X8.

3.12 Data availability

Proteomics data in raw and processed form, and imaging data in raw and processed form is available on the servers of the Rugarli lab. All processing and analysis steps are described in

the Materials and Methods part. Macros used are also available on the servers of the Rugarli lab. Experiment protocols are available from the elabjournal.

Adress any requests to Dr. Tim Schlegel via E-Mail to tim.schlegel2@gmail.com.

3.13 Antibodies, Reagents, Plasmids

3.13.1 Primary Antibodies

Table 2: List of primary antibodies

Target	Host	Company (ID)	Dilution
CLUH (eIF3X)	Rabbit	Novus Biologicals (NBP1-91866)	1/750-1/1,000
TOM20	Mouse	Santa Cruz (sc17764)	1/500
ATP5A	Mouse	Abcam (ab14748)	
ATP5A1	Rabbit	Proteintech (14676-1-AP)	1/500
NFH (SMI-31)	Mouse	BioLegend (801601)	1/1,000
RAB7	Rat	BioLegend (W16034A)	1/400
CNP	Mouse	Sigma (C5922)	1/1,000
GFAP	Rabbit	Dako (Z0334)	1/1,000
TAU1/ MAPT	Mouse	Santa Cruz (sc-390476)	1/1,000
MAP2	Rabbit	Cell Signaling (4542)	1/200

3.13.2 Secondary Antibody

Table 3: List of secondary antibodies

Host and target	Fluorophore	Company (ID)
Goat anti-Rabbit IgG (H+L) HCA	Alexa Fluor 488	ThermoFisher (A-11034)
Goat anti-Rabbit IgG (H+L) HCA	Alexa Fluor 546	ThermoFisher (A-11035)
Goat anti-Rabbit IgG (H+L) HCA	Alexa Fluor 647	ThermoFisher (A-21245)
Goat anti-Mouse IgG (H+L) HCA	Alexa Fluor 488	ThermoFisher (A-11029)
Goat anti-Mouse IgG (H+L) HCA	Alexa Fluor 647	ThermoFisher (A-21236)
Goat anti-Rat IgG (H+L) CA	Alexa Fluor 488	ThermoFisher (A-11006)

HCA: Highly Cross-Adsorbed, CA: Cross-Adsorbed

3.13.3 Reagents

Table 4: List of fluorescent and cell culture related reagents

Reagent	Company (ID)	Concentration (If applicable)
<u>Fluorescent reagents</u>		
DAPI	Sigma Aldrich (D9542)	
Hoechst 33342	Invitrogen (H1399)	0.4 µg/ml
MitoTracker Green FM	Invitrogen (M7514)	60 nM
Janelia Fluor® 549 HaloTag® Ligand	Promega (GA1110)	16-20 nM
Janelia Fluor® 647 HaloTag® Ligand	Promega (GA1120)	
<u>Cell culture</u>		
Lipofectamin 2000	ThermoFisher (52887)	
DMEM (+ 4.5g/l D-Glucose)	Invitrogen (11960044)	
Fetal Bovine Serum	Gibco (A5256701)	
L-Glutamine	Gibco (25030-024)	
Penicillin and Streptomycin	Sigma Aldrich (P4333)	
Trypsin-EDTA (0.05 %)	ThermoFisher (25300-054)	
DMEM (+ 4.5g/l D-Glucose, + L-Glutamin, + Pyruvate)	Invitrogen (41966)	
Amphotericin B	Promocell	
Neurobasal Medium	Invitrogen (21103)	
B-27 Supplement (50x)	Invitrogen (17504)	
BDNF	Peprotech	
GDNF	Peprotech	
CNTF	Peprotech	
AraC	Sigma Aldrich	
PDL	Sigma Aldrich (P7886)	
Laminin	Sigma Aldrich	
Trypsin	AppliChem (A3964)	
DNase I	AppliChem (A3778)	

3.13.4 Plasmids

Table 5: List of Plasmids used and their origin

Plasmid	Origin
pUbC-ActBCDS(hu)-ActB3'UTR(ms)-MS2V5	Cloned by me (Zaninello et al. 2024)
pUbC-Atp5a(CDS+UTRs)-MS2V5	Cloned by me (Zaninello et al. 2024)
pUbC-Mdh2(CDS+UTRs)-MS2V5	Cloned by me (Zaninello et al. 2024)
pUbC-MS2V5	Cloned by me
pUbC-NLS-stdMCP-stdHalo	(Voigt et al. 2017) Addgene #104999
eGFP-RAB5A (Homo Sapiens)	Provided by AG Kononenko
eGFP-RAB7A (Canis Lupus)	Provided by AG Kononenko
eGFP-RAB11A (Canis Lupus)	Provided by AG Kononenko
MTS-GFP	

4 Results

4.1 Identifying axon specific changes in the mitochondrial proteome of primary motoneurons

Neurons are highly polarised and specialised cells, mediating a fast signal transduction between different cells. Motoneurons are examples of particularly long axons which can reach a meter in length in humans. Polarisation of neurons also means that there are different parts with different functions, such as axons for action potential relaying, dendrites for action potential receiving and the soma which contains the nucleus, where most proteins are encoded and synthesised. Based on this functional and distance related variability within neurons, substantial differences between the neurite or axon enriched proteome and the proteome enriched in the rest of the cell have been found (Zappulo et al. 2017; Chuang et al. 2018). However, none of these studies take a closer look at how mitochondria, an organelle of central importance for neuronal function, are altered by their localisation in axons compared to the soma. Therefore, I aimed to develop a robust compendium of axon specific proteins which allows me to take a more detailed look at mitochondrial proteins and how the proteome composition of mitochondria in axons may be altered or adapted. This knowledge could give a better understanding on why axons are so much more susceptible to damage than the rest of the neuron, as can be observed in many mitochondria-related neurodegenerative diseases. Motoneurons suit particularly well as a model for this task, as they are some of the longest neurons in the body and thus are most prone to polarisation dependent problems.

4.1.1 Successful set up of an axonal compartment using two chambered microfluidic devices

In order to obtain an axonal proteome, primary spinal motoneurons from WT mouse embryos at embryonic day 12.5 were grown in a two-chambered microfluidic device (MFD). The two chambers of these MFDs are only connected by 150 μm long microchannels which allow neurites but not cell bodies to pass. To further support the recruitment of neurites to the second compartment, a gradient of neurotrophic factors was being applied, which was held up by the fluidic isolation in the MFD (Taylor et al. 2005). Especially for motoneurons, dendrites grow much slower and shorter than axons (Dotti, Sullivan, and Banker 1988; Snider and Palavali 1990), so within ten days of culture (day in vitro (DIV) 10), axons but not dendrites manage to grow into the other side of the MFD, leading to a purely axonal compartment (Fig 3 A). By an immunostaining of the compartmentalised culture at DIV 10, I could nicely proof this concept for my culture (Fig 3 B). Nuclei in the left side mark the seeding compartment, throughout which both dendrites (MAP2) and axons (TAU) were spread. However, while dendrites of the

motoneurons do not manage to cross the microchannels within the ten days in culture, axons have extended deep into the right compartment, resulting in a clean axonal compartment on the right and a mixed whole-cell (WC) compartment on the left.

To successfully achieve primary motoneuron cultures in the MFDs several alterations from normal cultures were needed. Firstly, it was necessary to dramatically increase the seeding density in a very low seeding volume to have enough cells flow from the seeding well into the actual growth chamber. Furthermore, not treating the culture with mitosis inhibitors like AraC, which are frequently used to achieve glia depleted cultures, helped to achieve better developing neurons in these MFDs. Even without mitosis inhibitor, glia cells like astrocytes (GFAP) or oligodendrocytes (CNP) only showed limited presence or were almost fully absent from the growth chamber area at DIV 10 (Fig 3 C, D). It can only be assumed that the very confined space in the growth chamber was unfavourable for these glia cells. Lastly, it was beneficial to use medium which was pre equilibrated in the CO₂ incubator and to not fully replace the medium to avoid introduction of bubbles.

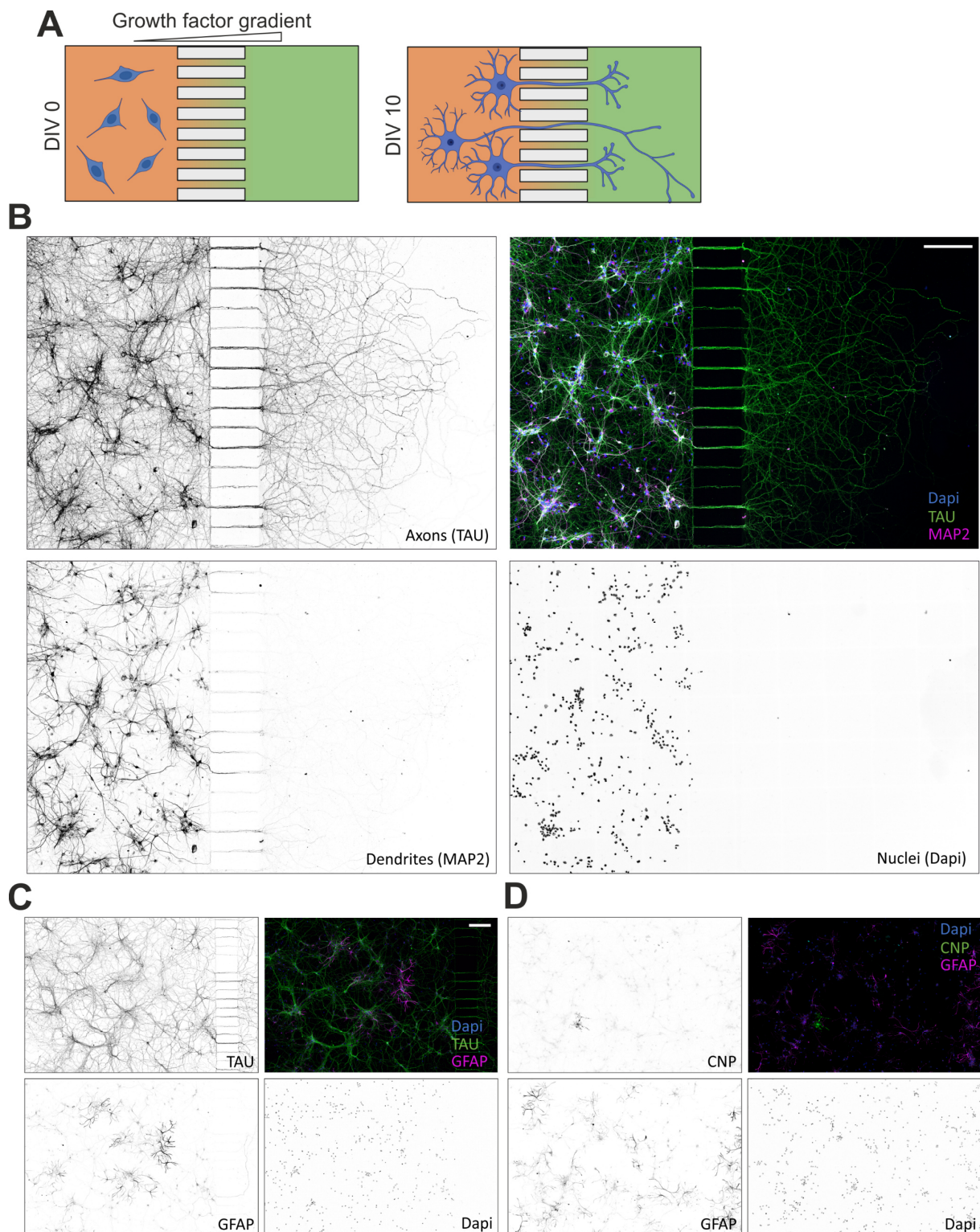


Fig 3: Compartmentalised culture of primary motoneurons in MFDs

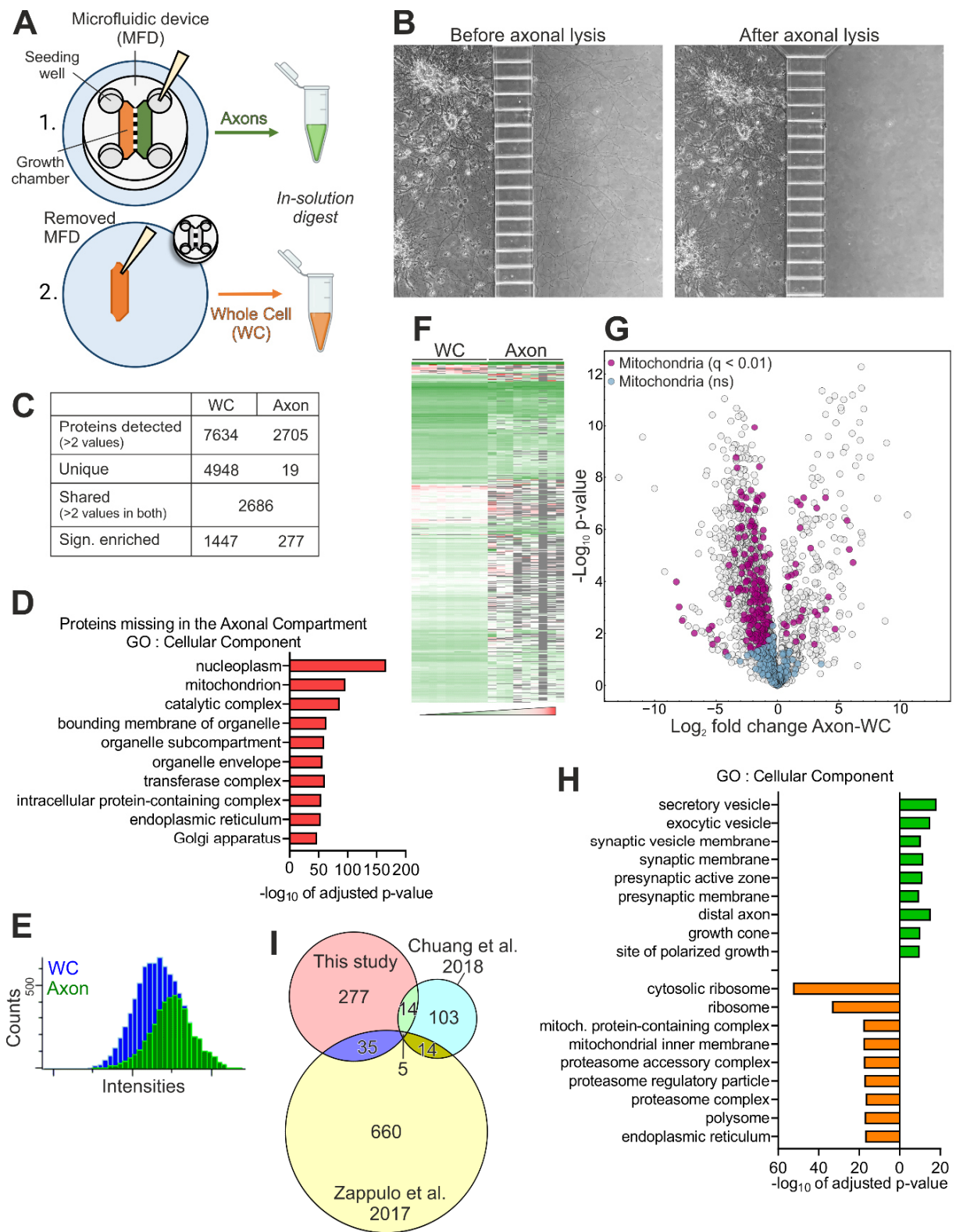
A) Scheme of basic principle of the MFDs, where primary motoneurons are seeded in the left compartment and a growth factor gradient of GDNF, BDNF and CNTF is applied. By DIV 10, the neurons have grown and axons but not dendrites have crossed through the microchannels into the right compartment. **B)** Representative immunostaining of a motoneuron MFD culture at DIV 10, with a staining for axons (TAU), dendrites (MAP2) and nuclei (Dapi). **C)** and **D)** show similar images but with staining for two types of glia cells, astrocytes (GFAP) and oligodendrocytes (CNP). Scalebar 150 μ m.

4.1.2 Axonal and whole cell proteome of primary motoneurons at DIV 10 by mass spectrometry

After having demonstrated the successfully compartmentalised culture of primary motoneurons with an axonal and a WC compartment, I used this model to produce a proteome of axons and define how it is changed compared to the whole cell. To this end I lysed the compartments separately, by first adding a large volume of PBS to the WC compartment and then removing all liquid from the axonal compartment to add lysis buffer (Fig 4 A). In this way, the fluidic isolation prevents any lysis buffer from entering the WC compartment, thus avoiding a contamination of the axonal lysate (Fig 4 B). Afterwards, I gently removed the MFD, scraped of any cells in the seeding well areas where big clusters of neurons and glia from the seeding were concentrated and lysed the cells in the growth chamber area of the WC compartment (Fig 4 A). Both compartments were lysed by in-solution digest, followed by label-free LC-MS/MS combined with FAIMS in a collaboration with Hendrik Nolte from the group of Prof. Dr. Thomas Langer. Of the total 7,653 unique detected proteins, 2,705 were detected in the axon compartment and 7,634 in the WC compartment, with 2,686 proteins being found in at least three of the nine samples of both compartments (Fig 4 C). Thus, 4,948 proteins were only detected in the WC compartment. Many of these were expected to be missing from axons, as they belong to the nucleus (1,212 proteins) or other soma and dendrite specific areas (Fig 4 D). It is furthermore evident that most of the proteins not detected in the axons also exhibit low measured intensities in the WC compartment, suggesting they are generally low abundant proteins (Fig 4 E). One reason for this observation was likely the difference in amount of lysed material between both compartments, leading to much lower protein concentrations in the axonal compartment. In combination with the detection minimum of the MS it was therefore only consequential that more peptides were detected in the WC lysate than the axonal. This means, some of the proteins absent from the axonal but not the WC proteome may have not actually been fully absent from axons. The concentration differences in the starting material were normalised for during the processing of the data to reach comparable intensities of protein detected in samples of both compartments. Data normalisation was done in two steps. Initially the data was processed by intensity Based Absolute Quantitation (iBAQ), where the sum of all peptide intensities is divided by the number of measured tryptic peptides. This method has empirically been found to correlate best with absolute protein concentrations. To get better comparability between axonal and WC reads, the iBAQ values of each protein were then divided by the sum of all iBAQ values within each sample, resulting in a relative iBAQ (riBAQ) (Shin et al. 2013). While this normalisation was a way to allow for comparability, it could not rescue the lower intensity tail of the axon data, thus making interpretations of the axonal absent proteins complicated.

In an unsupervised clustering of all samples based on the proteins shared between both compartments, a full separation of both compartments was the result, showing the clear differences between both compartments. But it was also visible that the variability in measurements was much higher for the axonal compartment than the WC (Fig 4 F). Nevertheless, even with a stringent statistical test ($q \leq 0.01$, $S0 = 0.1$), I found 277 significantly enriched proteins in the axonal compartment and 1,447 proteins enriched in the WC compartment (Fig 4 C, G). With a simple gene ontology enrichment search focusing on cellular components of the axon and WC enriched proteins, I confirmed the successful separation of axons from the rest of the cell. Of the proteins more frequently found in axons some general neuronal components were enriched but also some axon specific ones, like the presynaptic active zone, presynaptic membrane, distal axon and the growth cone. Proteins depleted in axons or enriched in the WC related to ribosomes, organelles like mitochondria and the endoplasmic reticulum and the proteasome complex (Fig 4 H). Organelles were also overrepresented in the proteins not detected in axons (Fig 4 D), however as mentioned above this data cannot be clearly interpreted.

Comparing my data to the other two comparable studies with compartmentalised proteomes of neuronal cultures, it becomes clear that there is only a very small overlap of five proteins which are found to be enriched in axons or neurites in all three studies (Zappulo et al. 2017; Chuang et al. 2018). Also, between each couple of these studies the overlap was minimal (Fig 4 I). These differences are likely connected to the use of three different neuronal models (mouse motoneurons, mouse iNeurons, rat cortical neurons) and three different methods of compartmentalisation (MFDs, Boyden Chamber, Micropattern chips), creating low comparability between the results.



For figure legend, see next page.

Fig 4: Compartmentalised proteomics of axon and WC motoneuron compartments

A) Scheme depicting the layout of a MFD and how the separated lysis procedure is done. B) Brightfield image of MFD culture showing the WC and axon compartment. The second image shows the same area but after axonal lysis. C) Table with numbers of detected, unique and shared proteins which are used for the statistical testing. D) Gene ontology cellular component enrichment of the proteins uniquely detected in the WC compartment. E) Graph of protein counts over measured intensities. All proteins detected in the WC compartment are marked in blue, while proteins detected in both compartments and uniquely in axons are green. F) Heatmap of shared proteome after unbiased clustering, depicting all analysed samples and the measured protein intensities. G) Vulcano blot of shared and statistically analysed proteome. Specifically shown are MitoCarta 3.0 annotated proteins and whether they are significantly enriched (+) or not (-) with a q-value of ≤ 0.01 . H) Gene ontology cellular component enrichment of the proteins significantly enriched in axons (green) or the WC (orange).

4.1.3 The axonal mitochondrial proteome is depleted of OXPHOS proteins and has an overall strong shift in metabolically active proteins

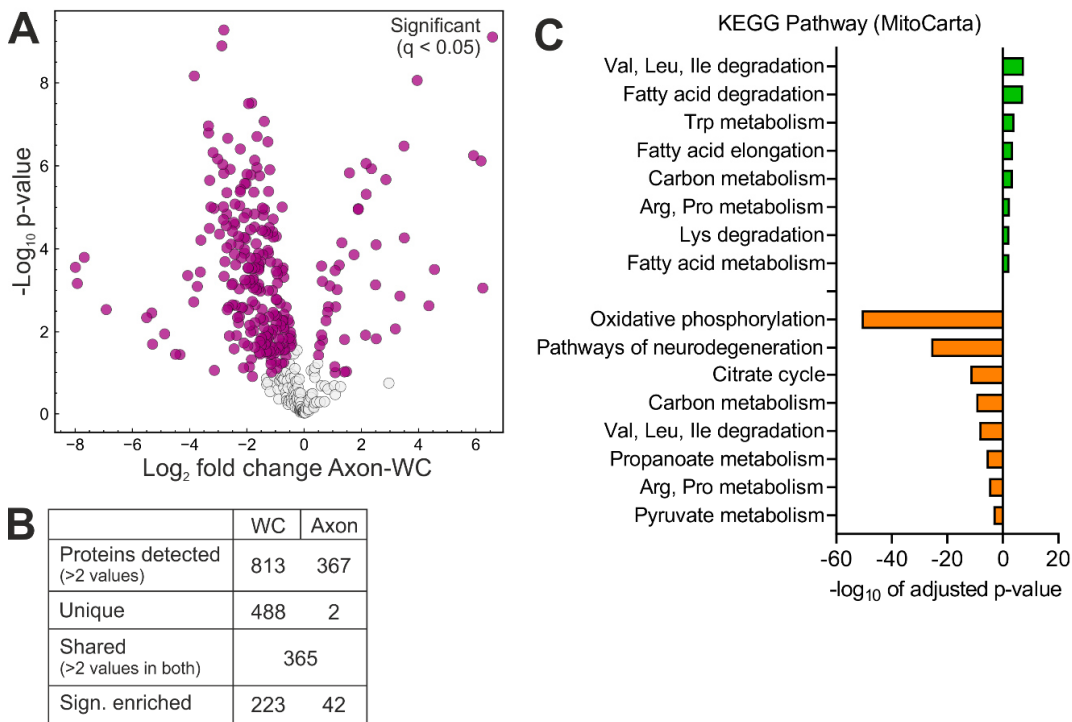


Fig 5: Changes in mitochondrial proteome between axon and WC

A) Vulcano plot of MitoCarta annotated proteins with marked statistically significant changed proteins. B) Table with numbers of detected, unique and shared proteins which are used for the statistical testing. C) KEGG pathway enrichment, of all proteins enriched in axons (green) or enriched in the WC (orange).

To identify adaptations in the mitochondrial axonal proteome, I focused on proteins annotated by the MitoCarta 3.0 database (Rath et al. 2021). Of 815 mitochondrial proteins, 488 were uniquely detected in the WC compartment and two (Bco2, Dmgdh) were unique for the axons. Axon unique proteins were likely artifacts, as axons were also present in the WC compartment.

The 365 shared proteins were normalised like explained above, to get comparable readouts of axonal and WC mitochondria, no matter any differences in mitochondria mass. Statistical testing resulted in 233 WC and 42 axon enriched proteins (Fig 5 A, B, Table S1). To get an idea of the overall pathways which are most affected by these proteomic differences, I checked the respective protein lists for enrichment of terms from the KEGG pathway database. The clearest trend was a depletion of axons from proteins related to oxidative phosphorylation (OXPHOS) which are also the key proteins in the KEGG pathway of neurodegeneration (Fig 5 C). Subunits of OXPHOS complex I- V were detected in the proteome and more than three quarters of these subunits were depleted in axons (54/ 78 depleted), with *Sdha*, *Atp5mf* and *Atp5if1* being the only axonal enriched OXPHOS proteins (Table S2). Additionally, the citric acid cycle, carbon metabolism, some amino acid metabolism related pathways, propanoate and pyruvate metabolism come up from the KEGG pathway screen of axon depleted or WC enriched mitochondrial proteins (Fig 5 C). Of the eight core enzymes or complexes of the citric acid cycle, three (*Idh*: isocitrate dehydrogenase, *OGDC*: oxoglutarate dehydrogenase complex, *Sucl*: succinate-CoA ligase) had the majority of subunits or isozymes depleted from axonal mitochondria, while for the other five steps in the citric acid cycle no change was detected. Interestingly, the three depleted steps cover two out of four electron carrier production (NADH or FADH₂) and the only energy (ATP/GTP) producing step of the citric acid cycle. Additionally, pyruvate metabolism which can provide acetyl-CoA for the citric acid cycle and produces NADH was also strongly depleted from axons (4/5 proteins depleted) (Fig 6 A, Table S3). This data suggests a lower output of electron carriers from the citric acid cycle and pyruvate metabolism.

Looking at proteins which are enriched in axons, there were some proteins involved in amino acid metabolism related pathways, fatty acid metabolism and carbon metabolism (Fig 5 C). The fatty acid metabolism related proteins were particularly interesting in this case, as this pathway did not come up from the WC enriched proteome. Looking at the actual proteins involved into fatty acid β -oxidation, in every of the steps one or more isozymes were axonal enriched, even if there were also some depleted isozymes (Fig 6 B, Table S4). β -oxidation of Acyl-CoA creates not only Acetyl-CoA which could feed into the citric acid cycle, but also two electron carriers (FADH₂ and NADH) for every round of oxidation. Thus, an axonal upregulation of β -oxidation could supplement and potentially partially replace the reduced protein abundance related to the citric acid cycle.

Another mitochondrion related pathway is the urea cycle (Krebs 1973). Some part of the urea cycle takes place in the cytosol, which could be a reason why it did not come up in the pathway enrichment of mitochondrial proteins. However, as the two mitochondrial proteins which are directly related to the urea cycle (*Otc* and *Cps1*) were some of the most highly axonal enriched

proteins and Cps1 was one of the five proteins also found in the other two axon enriched proteomes, I investigated how the residual proteins of this cycle, mitochondrial or not, were regulated (Fig 6 C, Table S5). All extramitochondrial parts of the urea cycle (Ass1, Asl, Arg1) were highly upregulated or uniquely found in axons. Arginase was a special case, as while the cytosolic version Arg1 was only found in axons, the mitochondrial version Arg2 was only found in the WC. Nevertheless, proteins of the urea cycle were clearly enriched in axons, mitochondrial or not, suggesting a possibly increased activity of the urea cycle and more urea production. This finding raised the question whether any of the inputs or outputs of the urea cycle may be regulated in a similar way. Of the proteins related to the urea cycle only Nos1 was enriched in axons as well. Nos1 produces nitric oxide by processing arginine to citrulline under consumption of one NADH (Picón-Pagès, Garcia-Buendia, and Muñoz 2019). Proteins of supporting pathways like the production of the Cps1 cofactor NAG or reactions that feed ammonia into the urea cycle through glutamine and glutamate metabolism had reduced protein abundance in axons or were not detected. Fumarate is an intermediate product of the urea cycle and is also a substrate of the citric acid cycle, linking both cycles. Furthermore, oxaloacetate can be transformed to aspartate via Got, creating a parallel cycle of communication between both, which is called aspartate-argininosuccinate shunt (AAC) (Fig 6 C). Interestingly, the proteins in the citric acid cycle which are also part of the AAC were exactly those discussed above which were stable in their axonal level. Thus, it seems like there may potentially be a connection between the axonal maintenance of this part of the citric acid cycle and the ability of the axonal enriched urea cycle to feed the necessary metabolites processed by the enzymes.

Overall, when relating the proteomic differences between WC and axonal mitochondria to cellular pathways, it turns out that some of the central functions of mitochondria, like OXPHOS and parts of the citric acid cycle had reduced protein levels in axons, while fatty acid beta-oxidation and the urea cycle behave majorly in the opposite way. Pathways related to amino acid metabolism were also heavily impacted by the localisation of the mitochondria, but no clear trend could be identified. Considering pathways like the urea cycle and citric acid cycle are strongly involved in amino acid metabolism and also differentially regulated it makes sense to see this variability reflected on the more general amino acid metabolism level. In summary, at least on a protein level, the observed mitochondrial proteome changes seem to suggest a stark difference in metabolism, caused by mitochondrial localisation in axons.

4.1.4 Are protein half-life, local translation activity and mRNA levels predictors for enrichment of mitochondrial proteins in axon?

I found many significant differences in the (mitochondrial) proteome between axons and the WC, and those changes could quite drastically impact mitochondrial metabolism. However, I could not yet answer based on what level of regulation these proteomic differences occur. The levels of regulation which can most directly be controlled by the cell, are mRNA enrichment by transport of a specific mRNAs into the axon and local translation activity of the mRNA. As I did not measure these factors for my experiment, I investigated their possible impact by correlating my data with published data from other groups that investigated these factors. Axonal transcriptome datasets were acquired from multiple studies using different types of mouse neurons (Jung et al. 2022; Briese et al. 2016b; Loedige et al. 2023; Zappulo et al. 2017). Overall, no substantial correlation of axonal transcript enrichment with the mitochondrial or total axonal proteome enrichment was found (Fig 7 A). An axonal translome was measured by Jung et al. (2022), who used TRAP (translating ribosome affinity purification) to measure the translation activity in the axons of retinal ganglion cells (RGC). Axonal enrichment of mitochondrial proteins was minimally negatively correlated with their axonal translation activity, while on the total proteome level no correlation was found (Fig 7 A). These results suggest that neither mRNA enrichment nor local translation activity are responsible for enriching the axonal proteome of specific proteins. Other factors, which are less regulated by the cell itself but can still define the final protein level in axons and the WC, are mRNA stability and protein half-life. Stability or decay rate of mRNA as the first point, can be investigated by giving a pulse of RNA labelling 5-ethynyl uridine, followed by a chase and capture of the remaining RNAs. Comparing the initially labelled to the remaining mRNA allows to define mRNA stability, as done by Jung et al. (2022) in axon terminals of RGC neurons. Interestingly, the mRNA stability did not correlate with the changes on the total proteome but had a minimal positive correlation with mitochondrial protein enrichment in axons. This finding makes sense as the situation was exactly the opposite for the axonal transcriptome and it has been shown that RNA stability and translational activity stand in a negative correlation to each other (Jung et al. 2022). As the second factor of interest, the half-life of proteins in neurons could have an influence on how well they are retained and how quickly they need to be re-synthesised in axons. There are multiple studies which have investigated protein half-lives in neurons by a SILAC labelling approach followed by mass spectroscopy (Cohen and Ziv 2019). Six different publications have investigated protein half-lives in neurons *in vitro* using primary cultures of mouse embryonic cortical neurons (Mathieson et al. 2018), rat cortical neurons (Cohen et al. 2013; Hakim et al. 2016; Heo et al. 2018), rat hippocampal neurons (Dörrbaum et al. 2018) or human iPSC-derived cortical neurons (Hasan et al. 2023). I also created a list with average half-

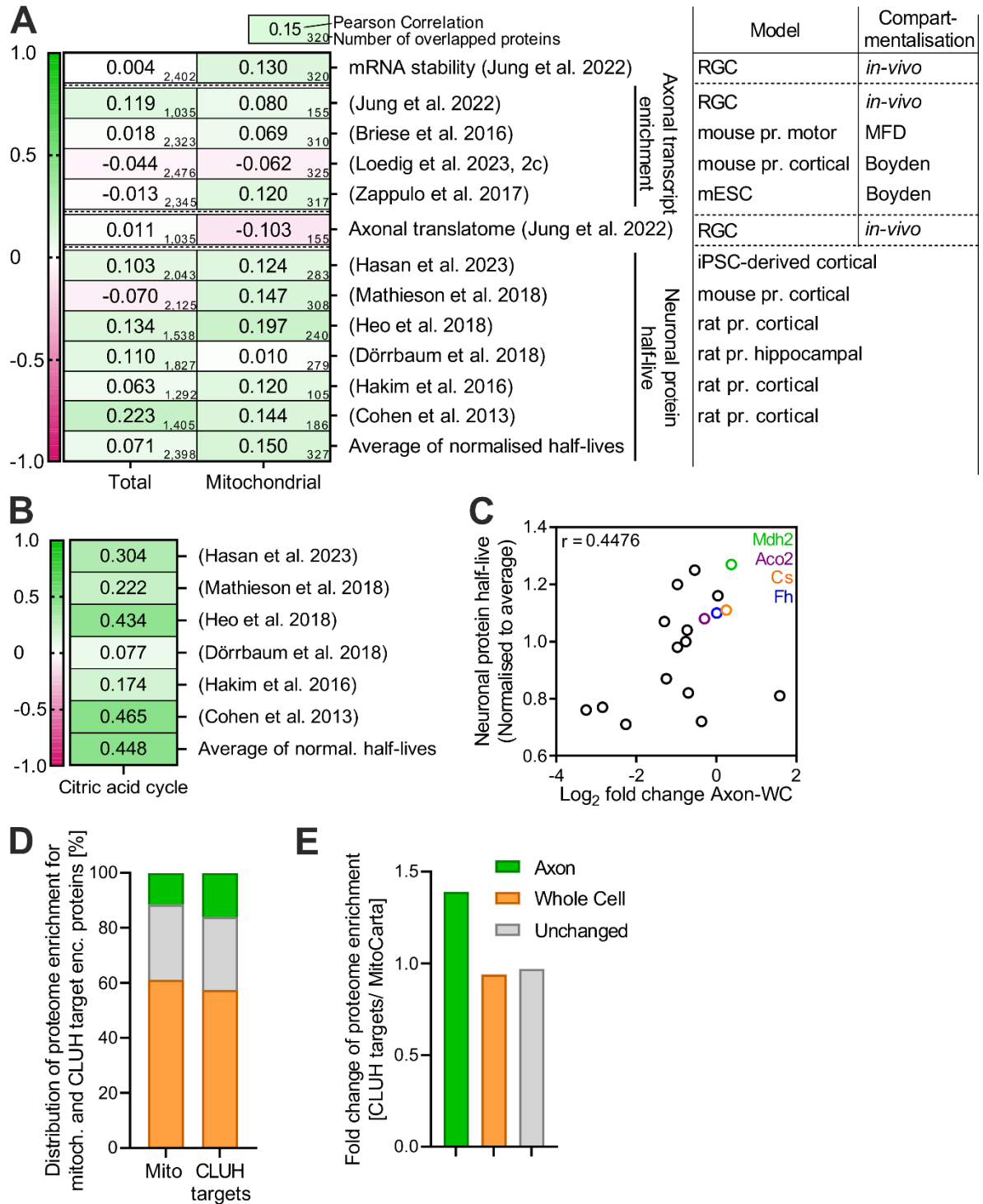
lives from all studies except Hasan et al. (2023), by first normalising the half-lives within each study to make them comparable with each other. In general, for all except one dataset the mitochondrial protein enrichment in axons correlated very lightly with an increased *in vitro* protein half-life in neurons (Fig 7 A). Which also means that proteins depleted from axons were more likely to have lower half-lives. On the total proteome level this correlation was less expressed.

In summary, I have found that axonal enrichment of mitochondrial proteins is very mildly correlated with protein half-life and mRNA stability, minimally negatively correlated with axonal translation activity and uncorrelated with axonal transcript enrichment. These correlations suggest that mitochondrial proteins which are enriched in axons are on average more stable proteins which are translated at a lower frequency from transcripts with no particular axonal enrichment but higher mRNA stability. Differences between the general and the mitochondrial proteome are only in the minimal positive and negative correlation with mRNA stability and local translation activity seen for mitochondrial proteins, which was not found in the general proteome.

On the very broad scale of the total shared proteome or even the mitochondrial proteome, I only detected minimal correlations to regulating factors. One possible reason for this is that in the heterogenous group of hundreds or thousands of proteins, it is unlikely to find one factor that by itself majorly determines most proteins. Thus, I also looked more specifically at one pathway. The citric acid cycle consists in its core of 18 detected proteins. I made the intriguing observation that one part was depleted from axons while the other was maintained, which then led me to test whether difference in protein levels within this pathway could be explained by a specific regulator like protein half-life. Therefore, I correlated axonal protein enrichment data of these proteins with the protein half-lives from the afore mentioned studies. And indeed, I found a substantial correlation of the citric acid cycle axonal protein enrichment with neuronal protein half-lives which was on a much higher level than for the mitochondrial proteins in general ($r=0.448$ vs $r=0.15$) (Fig 7 B). Additionally, when plotting half-life and enrichment, the proteins of the four unchanged steps were some of the proteins with the highest half-lives (Fig 7 C). Therefore, this suggests that protein half-life was a major regulator of the axonal citric acid cycle protein levels.

RBPs, are one way for the cell to influence protein levels in certain areas by regulating some of the above-discussed processes like localised translation and stability of mRNA. CLUH is of particular interest here as it specifically binds mRNAs of NEM proteins and has been shown to affect their mRNA stability and protein levels in axons (Zaninello et al. 2024). Thus, I wanted to see whether the proteins encoded by CLUH's mRNA targets are regulated differently

compared to the mitochondrial proteins in general. For both groups of proteins, the vast majority was enriched in the WC and only few were enriched in the axon (Fig 7 B). However, on this low level I still saw an almost 50% higher share of axon enriched proteins for the CLUH targets than the total mitochondrial proteome (Fig 7 C). This indicates that CLUH is not a major regulator of the axonal mitochondrial proteome but may play a role for some proteins.



For figure legend, see next page.

Fig 7: Correlations of axonal protein enrichment with protein expression regulating steps

A) Heatmap of correlations of the protein abundance (Log2 fold change Axon-WC) from this work to datasets of mRNA stability, axonal transcript enrichment, axonal translome and protein half-life from other studies. Pearson correlation coefficients are written inside each cell in addition to the colour coding by the heatmap. **B)** Pearson correlation of protein half-lives from the core citric acid cycle proteins with the axonal enrichment. **C)** Correlation graph of axonal protein enrichment and the average half-life of citric acid cycle proteins. **D)** Bar graph showing the distribution of protein enrichment groups (Axon, WC, unchanged) in the total mitochondrial proteome and only of the CLUH targets. The differences in this distribution are calculated in **E)**, where for each enrichment group the ratio of its share in the CLUH target proteome over the mitochondrial proteome is reported.

4.1.5 Differences between axonal and whole cell enriched mitochondrial proteome correlate with more spherical morphology

It is well known that mitochondria morphology is very different depending on the localisation in neurons. While in axons mitochondria are round and small, in dendrites and soma the mitochondria are on average several times longer and have a higher complexity with branches. Furthermore, density of mitochondria in dendrites increases with distance from the soma but decreases with distance from the soma in axons (Faitg et al. 2021; Donovan et al. 2024; Turner et al. 2022). These studies focused on neurons *in vivo* in the brain, but I saw very similar morphology and density differences in my MFD culture of mouse embryonic primary motoneurons. Mitochondria in the axonal compartment were almost like spots, while in the WC compartment and especially around the nuclei, mitochondria were elongated and bigger (Fig 8 A). I wanted to see whether these morphological changes may also be reflected in proteome differences. The idea was that the sphere-shaped mitochondria of the axons had a higher volume to surface ratio than the complex and elongated mitochondria of soma and dendrites. As mitochondria are double membrane organelles their surface would roughly equate to their outer and inner membrane (OM and IM) and their volume to the matrix and inter membrane space (IMS). Assuming protein concentration per area of membrane or per volume is stable, the changes in morphology should roughly correlate with protein enrichment and volume-to-membrane ratios in the compartments. And indeed, when dividing the mitochondrial proteins into membrane proteins and soluble “volume” proteins by their MitoCarta annotation, the ratio of soluble proteins over membrane bound proteins was almost four times higher for the axon enriched than for the WC enriched mitochondrial proteins (Fig 8 B). A similar approach could be used to gather an idea about changes in cristae density, by taking the ration of IM to OM proteins. This ratio was similar for both WC and axon compartment. In summary, I have shown that the mitochondrial proteome composition in axons and the rest of the cell directly correlates with their morphological differences, meaning relatively more proteins of the matrix and IMS and less membrane proteins in mitochondria of axons. The ratio of the

membranes to each other was similar though, potentially meaning a similar cristae density in both compartments.

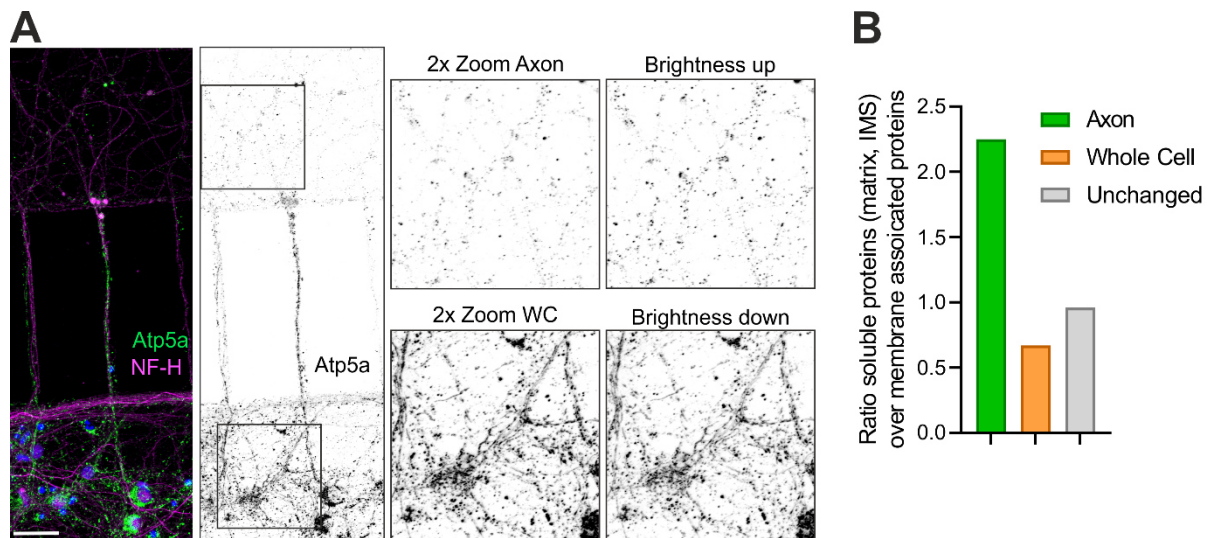


Fig 8: Mitochondrial morphology correlates with proteome changes of membrane associated and soluble proteins

A) Representative immunostaining of MFD culture with WC and axonal side in the same frame. Zoomed in crops to the right only showing the ATP5A staining allow to compare the mitochondrial morphology. For better visualisation, a second version of the crop with adjusted brightnesses of both compartments was added. **B)** Graphical depiction of the ratios of soluble mitochondrial proteins in the matrix and IMS over membrane associated proteins, within the three protein enrichment groups (Axon, WC, unchanged).

4.2 Trafficking of axonal mitochondria is not affected by CLUH

Maintenance of mitochondria and a functional mitochondrial proteome is challenging in neurons due to long distances in the neurites and limited protein half-lives (Kim et al. 2012; Price et al. 2010). As I have shown in the previous chapter, these challenges can indeed be key determinants for the composition of the axonal mitochondrial proteome. Mechanisms to overcome these challenges and maintain distant mitochondria are active transport of mitochondria and transport of mRNA with local translation of nuclear encoded mitochondrial proteins (Harbauer 2017). CLUH is a protein specifically binding to mRNAs of nuclear encoded mitochondrial proteins and is important for mitochondrial biogenesis and homeostasis. Furthermore, lack of CLUH leads to a clustering phenotype of the mitochondria, where they group around the nucleus and away from the cell periphery (Gao et al. 2014; Schatton et al. 2017). Therefore, it seems reasonable to assume that CLUH could also play a role in the processes of distal mitochondrial maintenance in neurons. Thus, I wanted to check whether the axonal transport of mitochondria as one mechanism of mitochondrial renewal may be affected by loss of CLUH. I imaged mitochondria of WT and CLUH KO axons of primary motoneurons using MitoTracker in live movies of 320 seconds. In Kymographs I tracked the motion of each mitochondrion (Fig 9 A) but found no significant change in the percentage of mitochondria in motion (Fig 9 B, C). or their directionality (Fig 9 D, E). The two version of the graphs show on the one hand the statistic if all axons of an embryo are averaged into one value or when every axon is depicted individually. The results that axonal mitochondria trafficking is not altered by CLUH KO, goes along with a recent study of CLUH in the nervous system, not finding any substantial effect of the lack of CLUH on mitochondria density, morphology or membrane potential in primary motoneurons (Zaninello et al. 2024).

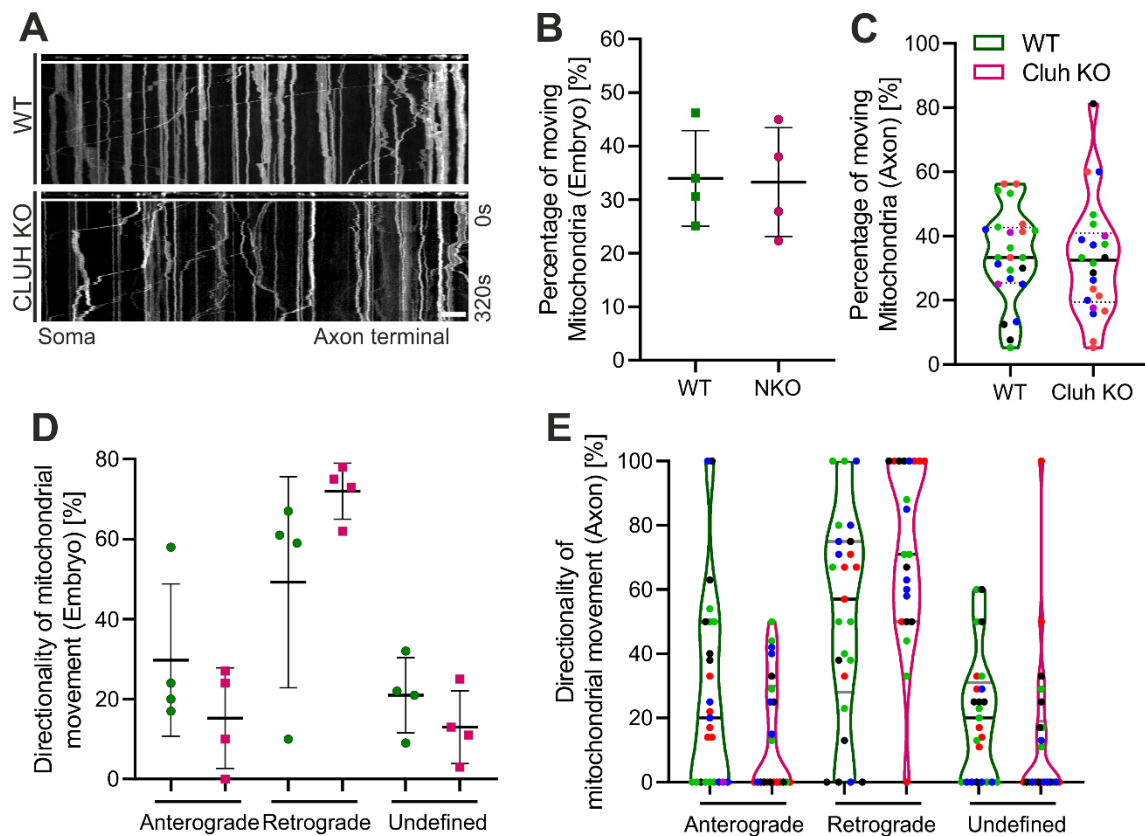


Fig 9: Mitochondria trafficking in axons is not affected by loss of CLUH

A) Representative kymograph of a straightened axon (first frame shown above the kymograph), depicting the trafficking of mitochondria in axons over time (Scalebar 10 μm). Percentages of moving mitochondria are quantified by the average per embryo **(B)** and per axon **(C)**. Furthermore, directionality of motion has been quantified (anterograde, retrograde and undefined) and is depicted by per embryo **(D)** and per axon **(E)**. Data represent the mean ±SD of 4 cultures (5-9 axons per culture) for the embryo averaged statistics. In the axon averaged quantifications, the data is visualised as a violin plot and different cultures are visualised by different colours.

4.3 CLUH does not control the abundance of target mRNA in axons by affecting trafficking of target mRNA (Zaninello, Schlegel et al., *Science Advances*, 2024)

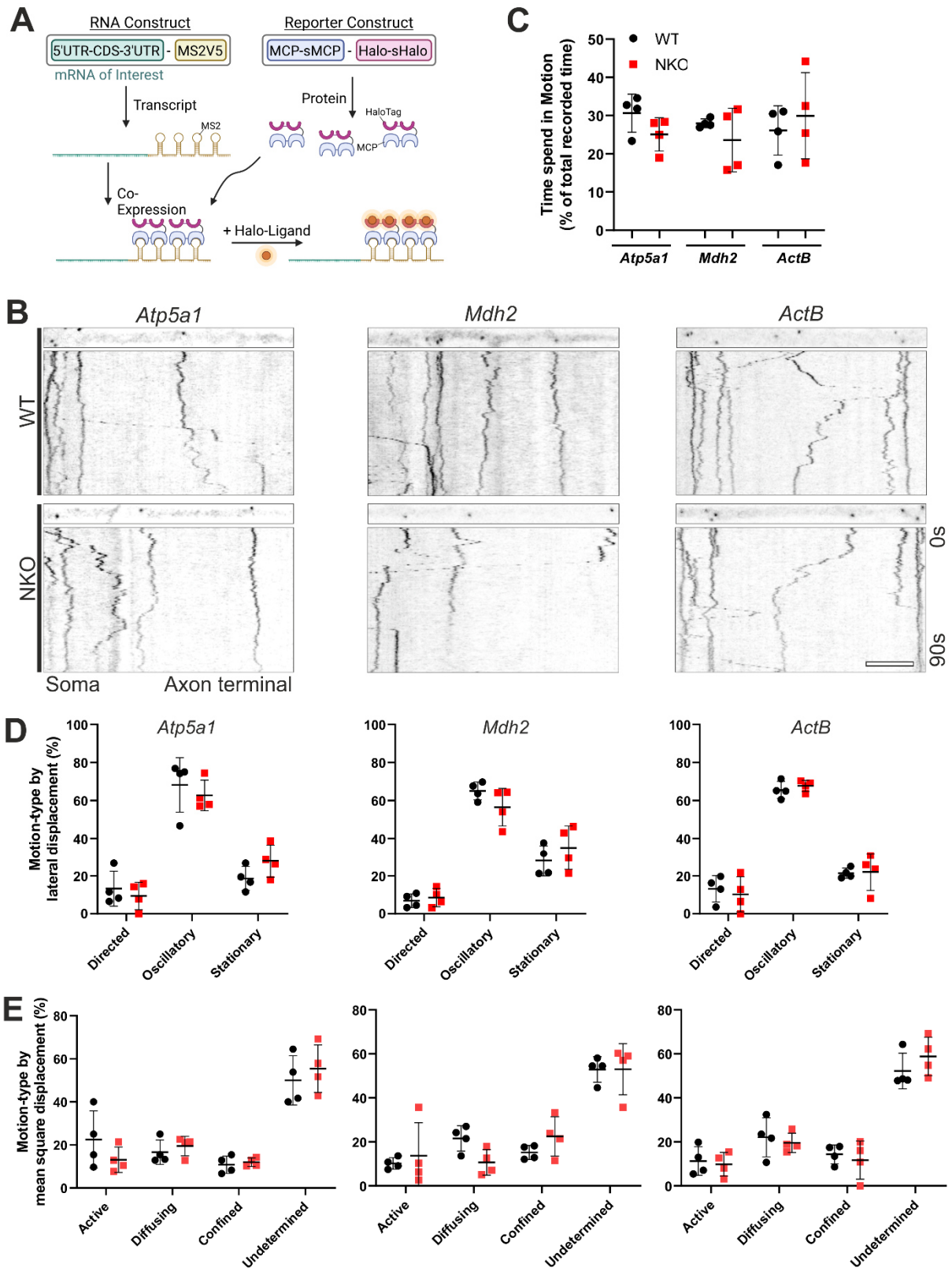
No immediate effect of CLUH depletion on general mitochondrial properties was found in primary motoneurons, except of the reduced ATP abundance in GCs. On a molecular level however, the characteristic depletion of the mitochondrial proteome in CLUH KO primary motoneurons has been identified. Particularly in axons, the proteins encoded by CLUH targets were overrepresented in the pool of depleted proteins and this decrease on a protein level correlated with mRNA levels. The abundance of CLUH target mRNAs *Atp5a* and *Pink1* were found to have reduced levels specifically in axons of CLUH KO primary motoneurons, while

in soma this reduction was less pronounced for *Atp5a* and fully absent for *Pink1*. The control mRNA *ActB* which is not bound by CLUH did not exhibit any changes in mRNA levels for either compartment (Zaninello et al. 2024). A possible explanation for reduced axonal mRNA abundance is a reduced transport of specific mRNAs into axons in CLUH KO conditions. This pathway would also relate back to maintenance of distal mitochondria by local translation of the transported mitochondrial mRNA.

4.3.1 Setting up the mRNA tether system for live imaging of mRNA movement

As reduced transport of specific mRNAs into axons under CLUH KO was identified as a possible cause for diminished CLUH target mRNA abundance in axons, I needed a way of imaging the movement of mRNA molecules in live axons to investigate this hypothesis. One method prevalently used for this task is the bacteriophage-derived MS2 tether system. It uses two constructs which are co expressed in the cell, one RNA construct with the RNA of interest tagged with 24 repeats of MS2 stem-loops after the 3' untranslated region. The stem-loops on the RNA molecule are bound by the MS2 coat protein (MCP) fused with a HaloTag for fluorescent detection, which is encoded by the reporter construct (Fig 10 A). The system first published by Bertrand et al. (1998) in yeast, was optimised over time. New versions already contain various improvements for more accurate expression of proteins and nucleotides by avoiding repetitive nucleotides in the MS2 repeats (MS2V5) and synonymously transforming the tandem dimers in the coat protein (stdMCP) (Wu et al. 2015). In this version of the system GFP is used as a reporter, which for me suffered from low signal intensity and signal to noise ratio, to the point where barely any signal was detectable at all. Same was true for split protein-based systems, utilising a second stem-loop structure (PP7) and coat protein (PCP), with both coat proteins being fused to one part of a split YFP (Wu, Chen, and Singer 2014). This system is supposed to reduce unspecific background in the cell from reporter protein not bound to mRNA, but I could not detect signal at a sufficient level. Instead, I explored using other reporter proteins which promise higher signal intensity and stability. The HaloTag is a modified haloalkane dehalogenase which covalently binds to synthetic ligands (HaloTag ligands). So, while the HaloTag in itself possesses no fluorescence, by adding cell permeable Halo-Ligands with attached synthetic dyes (Janelia Fluor 549) rather than organic fluorescent proteins, this system can excel with improved brightness and photostability (Grimm et al. 2015). A version of the reporter construct with HaloTag instead of GFP has already been successfully used for RNA imaging in neurons (Yoon et al. 2016) and also in my case led to results with great signal intensity and a high signal-to-noise ratio (Fig 10 B). In summary, the MS2 tether system using HaloTag as a reporter allows for imaging of single mRNA molecules, inside live cells, thus being the perfect tool for assessing the mRNA transport. Other systems for live imaging of

mRNA such as RNA aptamers were considered (Cawte, Unrau, and Rueda 2020), however, not followed up upon due to the successful set up of the MS2 tether system.



For figure legend, see next page.

Fig 10: CLUH does not alter the transport of CLUH target mRNAs (adapted from (Zaninello et al. 2024))

(A) The MS2-MCP system consists of an “RNA construct” with the target mRNA and MS2V5 sequence attached after the 3’UTR (RNA-MS2), which is co-expressed with a “reporter construct”, coding for the MCP coating protein tagged with a HaloTag as the reporter (MCP-Halo). After the RNA construct is transcribed, MS2 stem loops form, which MCP-Halo binds. Addition of a Halo-ligand with a fluorophore (JF546) enables the visualization of the mRNA. **(B)** Kymographs of *Atp5a1*, *Mdh2* and *ActB* mRNAs in axons of primary motoneurons using the MS2-MCP system depicted in (A). The first frame of the recording is shown as a straightened segment in the image above the kymograph. Bar, 5 μm . **(C)** Quantification of time spent in motion relative to the total tracked time and using a speed cut-off of more than 0.1 $\mu\text{m}/\text{s}$ in experiments as in (B). **(D)** Division in three different motion-types (directed, oscillatory, stationary) as defined by total and maximal lateral displacement over the whole track or **(E)** by the mean square displacement in the first 25% of the track (active, diffusing, confined) in experiments as in (B). Data represents the mean \pm SD of 4 cultures (10-93 mRNA dots per culture).

4.3.2 Axonal trafficking of CLUH target mRNAs is not substantially affected by absence of CLUH

The CLUH mRNA targets *Atp5a* and *Mdh2* and the control mRNA *ActB* were tagged with MS2 loops as described above and transfected into primary motoneurons at DIV4, together with the reporter construct stdMCP-stdHalo (Fig 10 A). After 24 hours the HaloTag was visualised fluorescently by adding HaloTag ligand-JF546, and neurons with RNA spots in their axons were imaged in 90 second movies. As a more general readout of trafficking, the time spent in motion of each mRNA molecule was quantified using kymographs (Fig 10 B), where motion was defined as movement with a speed of more than 0.1 $\mu\text{m}/\text{s}$. The time spent in motion was similar for WT and CLUH KO for all mRNAs, with only minimal and non-significant changes between genotypes (Fig 10 C). When looking at the movies or kymographs it becomes apparent that not all mRNAs behave the same way and they in fact exhibit a wide variety of speeds and directionality. In an attempt to take this high variability into account, I wanted to divide the population into several more biologically relevant subgroups. In a collaboration with the group of Dr. Jean-Michel Cioni, we therefore traced the motion of each particle again, but this time via single particle tracking for more detailed results. We divided the mRNA population into motion types either by their lateral displacement over the whole movie (directed, oscillatory, or stationary) (Fig 10 D) or by their mean square displacement in the first 25% of the movie (active, diffusive, or confined) (Fig 10 E). However, also in these specified subgroups I could not identify significant changes between WT and CLUH KO for any mRNA. The minimal trends towards less motile motion-states for *Atp5a* and *Mdh2* in CLUH KO are statistically insignificant and too small for biological relevance. Thus, I can conclude that the reduced axonal localisation of CLUH target mRNA does not appear to be caused by a defect in trafficking along the axons, but rather has another cause.

4.4 Investigating a CLUH dependent colocalisation and co-transport of CLUH target mRNA with endosomes and mitochondria

I have shown that the reduced abundance of CLUH target mRNA in axons is likely not caused by transport. If the transport is the same, then the other option for this outcome is a destabilisation of the mRNA in CLUH KO. A possible explanation for destabilised mRNA could be mislocalisation of the mRNA, potentially leading to altered translational activity and enhanced mRNA decay. While direct evidence of RNA mislocalisation leading to decay is missing, distinct localisations of mRNAs have been shown to influence protein synthesis. For example, beta-actin and ribosomal protein-coding mRNA which have been reported to exhibit increased translation activity when localised to lamellipodia and cell protrusions (Hüttelmaier et al. 2005; Dermit et al. 2020). Increased translation activity can then lead to faster mRNA decay, as has been shown for RNA in axons of retinal ganglion cells (Jung et al. 2022). Additional neuronal examples of mRNA localisation or tethering which directly affect translation are *Pink1* mRNA on mitochondria and the identification of late endosomes as general hubs of local translation (Harbauer et al. 2022; Cioni et al. 2019). These examples also show how, especially for mitochondrial mRNAs, like the CLUH targets, early endosomes, late endosomes, lysosomes and mitochondria themselves may be important localisation anchors, likely serving a role in regulating their local translation and thus also the mRNA stability (Cioni et al. 2019; Harbauer et al. 2022; Schuhmacher et al. 2023; De Pace et al. 2024).

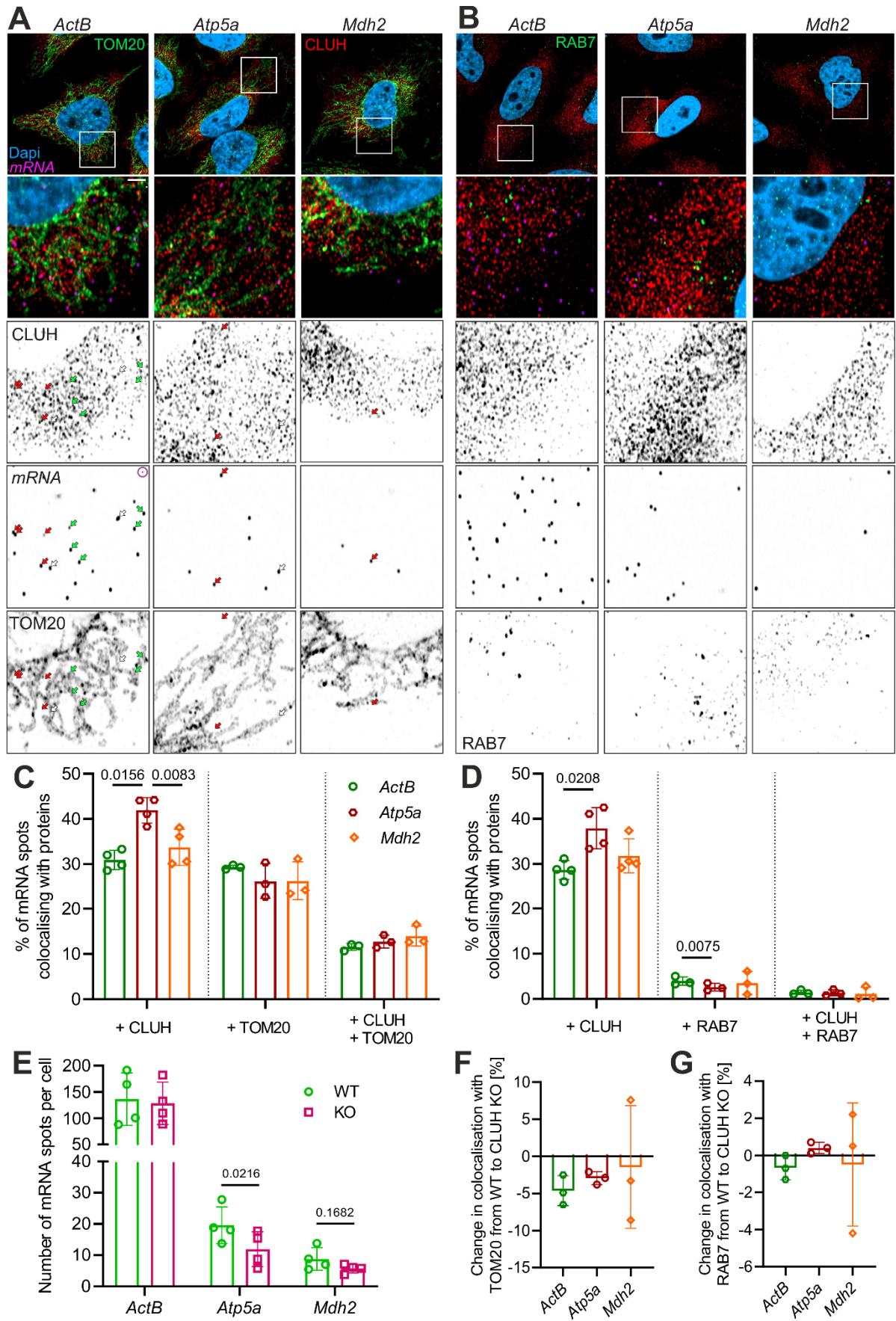
4.4.1 In HeLa cells CLUH and *Atp5a* mRNA association occurs away from mitochondria and late endosomes

Before proceeding to test the essentiality of CLUH for mRNA localisation in neurons, I attempted to investigate whether CLUH preferentially interacts with mRNAs on an organelle identified as a potential anchor for mitochondrial mRNAs and translation. This approach was based on the assumption that an enriched interaction of CLUH with a target mRNA on a specific organelle, results in a high probability that CLUH is involved in a localised activity, such as anchoring or translation, at this organelle. If any localised CLUH to mRNA preference could be observed this would further allow me to reduce the number of candidate organelles in further localisation and co-trafficking studies using neurons.

I used HeLa cells for this exploratory experiment to facilitate higher statistical robustness by imaging more cells, gain better separation of organellar signal in the big cytosol and for the possibility of using the human specific CLUH antibody. In murine neurons I would have had to overexpress tagged CLUH instead. I investigated the colocalisation of endogenous *ActB*, *Atp5a* or *Mdh2* mRNA detected via FISH (Fluorescence in situ hybridisation) with endogenous CLUH

and TOM20 (mitochondria) or RAB7 (late endosomes) (Fig 11 A, B). Images were acquired in super resolution and analysed using the 3D analysis software Imaris, where colocalisation was counted when the centre of the mRNA spot was inside the volume of the proteins. In a first step, I quantified the number of mRNA spots per cell in WT and CLUH KO condition, which confirmed the reduced abundance of CLUH target mRNA in a CLUH KO background as *Atp5a* mRNA was significantly reduced from 19.6 (\pm 5.8) to 11.9 (\pm 5.6) spots and *Mdh2* from 8.8 (\pm 3.6) to 5.7 (\pm 1.4) spots per cell, while *ActB* was relatively unaffected (136.2 ± 49.9 to 128.3 ± 40.2) (Fig 11 E). This quantification also revealed that for *Mdh2* the number of assessed spots is very low, increasing its susceptibility to noise and artifacts. Moving towards colocalisation of the mRNA spots with proteins, I found that the colocalisation of *Atp5a* mRNA spots with CLUH was significantly and on average 10% higher than for *ActB* ($41.9\% \pm 2.8$ vs $30.9\% \pm 2.1$). The colocalisation of CLUH with *Mdh2* was, however, only marginally higher than with *ActB* (2.8%) (Fig 11 C). As *ActB* has not been identified as a CLUH target, the 30.9% colocalisation with CLUH should be interpreted as a measure of random colocalisation and the 9% higher colocalisation with *Atp5a* as specific interaction between mRNA and CLUH. Looking at the association of mRNA with mitochondria and late endosomes, colocalisation with TOM20 was at a very similar level for all three mRNAs (*ActB*: $29.3\% \pm 0.5$, *Atp5a*: $26.2\% \pm 3.9$ & *Mdh2*: $26.3\% \pm 4.3$) (Fig 11 C). For RAB7 the colocalisation was generally much lower, but on that low level a small significant difference could be identified between *ActB* ($4\% \pm 0.9$) and *Atp5a* ($2.6\% \pm 0.8$) (Fig 11 D). The main focus of the experiment, triple colocalisation of mRNA, CLUH and organelle, surprisingly showed no difference in levels of mRNAs colocalising with CLUH and TOM20 or RAB7 for all three tested mRNAs (Fig 11 C, D). This suggests that the clear preferential colocalisation between CLUH and its target mRNA *Atp5a* that was seen, occurs neither on TOM20 nor on RAB7 as on these proteins colocalisation of CLUH to target mRNAs (*Atp5a*, *Mdh2*) was as high as colocalisation to non-targets (*ActB*). Confirming this, no substantial difference between WT and CLUH KO was detected for the colocalisation of the mRNAs to TOM20 or RAB7, further indicating that CLUH has no role in the location of mRNA towards mitochondria or late endosomes (Fig 11 F, G).

Overall, I have shown by imaging that CLUH does preferentially colocalise with the CLUH target mRNA *Atp5a* over a non-target mRNA. This preferential association takes place neither on late endosomes nor mitochondria, but in the cytosol or on another organelle. CLUH seems to also play no role in the localisation of the tested mRNAs towards the organelles.



For figure legend, see next page.

Fig 11: CLUH preferentially associates with *Atp5a* mRNA in the cytosol away from mitochondria and late endosomes in HeLa

A) and B) depict representative images of *ActB*, *Atp5a* and *Mdh2* mRNA (magenta) FISH staining, with TOM20 or RAB7 (green) and CLUH (red) immune staining. A magnified image according to the white frame with each channel separately is shown below. All images are a maximum projection of three z-slices with a total z-depth of 300 nm. Scale bar 2 μ m. In A), arrows are used to indicate mRNA spots colocalising with CLUH (red), TOM20 (green) or both (white), based on the analysis as in C). The purple spot in the purple circle of the *ActB* mRNA image has a size of 180 nm to visualise the spot size used for mRNA colocalisation analysis. C) Percentage of *ActB*, *Atp5a* and *Mdh2* mRNA FISH spots colocalising with CLUH, TOM20 or both. D) shows the same measures but with RAB7 for late endosomes. E) Quantification of the number of mRNA spots per cell in WT and CLUH KO HeLa, from experiments such as A) and B). F) and G) Quantification of the changes in colocalisation of mRNA FISH spots of *ActB*, *Atp5a* and *Mdh2* with RAB7 or TOM20. Data depicted as bar-graph \pm SD, with each point representing one biological replicate. N=4 for CLUH colocalisation and mRNA number quantification and N=3 for the rest. 25-49 cells per N and mRNA. Statistics are calculated with a repeated measures one-way ANOVA followed by Tukey multiple comparisons post-hoc test.

4.4.2 Pilot experiment identifying preferential colocalisation of CLUH target *Mdh2* with late endosomes in WT axons

Results from the HeLa model cannot exclude a neuron specific function of CLUH in mRNA localisation. While the HeLa allowed for a quick, robust experiment they do not exhibit the level of polarisation and long distances, leading to the uniquely challenging conditions in neurons. Therefore, I followed up with another exploratory experiment, to identify which one of the organelles previously identified as tether locations for mRNA (mitochondria, late and early endosomes) has the highest level of association with CLUH target mRNA in WT axons of motoneurons. I focused on *Mdh2-MS2* as mRNA in combination with reporters of early endosomes (GFP-RAB5), late endosomes (GFP-RAB7), recycling-endosomes (GFP-RAB11) and mitochondria (MTS-GFP). I imaged axons at DIV 5 which co-expressed the constructs of the mRNA tether and the GFP marker. As a measure of random or unspecific colocalisation I included an *only-MS2* control, which still creates spots of signal in the axon, but not connected to any specific mRNA. A direct comparison between random and specific colocalisation to organelles is shown in Fig 12 A, B. As this test was only done on one embryo, in addition to the statistics per embryo it was also depicted per axons. On the embryo level the sum of colocalised spots is divided by the sum of all spots, disregarding the specific axon the spots are from (Fig 12 A). In this case of the axon-based graph, only axons with three or more spots were considered and each of those axons is represented as a spot in the graph (Fig 12 B). For more simple interpretation, the data is additionally represented as normalised by the random colocalisation (*Mdh2-MS2* - *only-MS2*) (Fig 12 C, D). On the embryo level, RAB7 clearly had

the highest normalised association to *Mdh2* with 21.8%, followed by RAB11 (8.4%), RAB5 (7.4%) and mitochondria (1.4%). When reported as averages per axon, RAB7 exhibits the second highest association (16.8% \pm 12.8) after RAB11 (24.1% \pm 20.5). This difference in results between the forms of data reporting is the result of the different number of spots per axon and excluding axons with less than three spots for the per axon measure. Interestingly, when including presumed dendrites into the analysis the association to mitochondria rose to almost 13.3% and for RAB5 to 15.9% per embryo. As the focus of this pilot was to identify effects of CLUH on organelle tethering in axons, late endosomes (RAB7) were picked for further analysis since they exhibited the by far highest association on a total number of spots basis and second highest when averaged per axon.

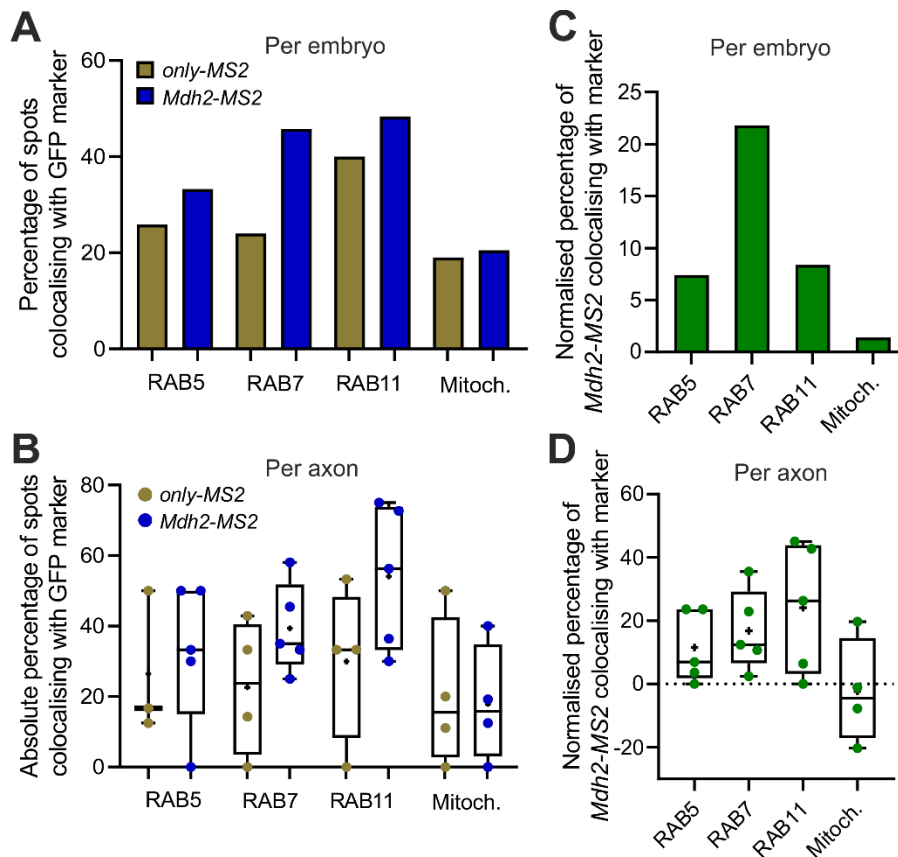


Fig 12: Stationary co-localisation of *Mdh2* with organelles in axons of primary motoneurons

A) Shows the quantification of colocalisation in still frames, between *Mdh2-MS2* as a CLUH target mRNA or the MS2 loops (*only-MS2*) as a negative control with overexpressed markers of endosomes (GFP-RAB5, GFP-RAB7, GFP-RAB11) or mitochondria (MTS-GFP). In **A)** this quantification is colocalisation percentage of all imaged spots. In **B)** the same measure is quantified but displaying the colocalisation percentage per imaged axon with three or more spots. In **C)** and **D)** random colocalisation as defined by *only-MS2* has been subtracted. Data is from one embryo per condition, with 4-6 axons or 3-5 axons (≥ 3 spots) and 21-72 spots per embryo.

4.3.3 Characterising the association and co-transport of *Mdh2* and *ActB* mRNA with late endosomes in presence and absence of CLUH

Based on the results from the pilot experiment I investigated the association of *Mdh2-MS2* as a CLUH target and *ActB-MS2* as a control with GFP-RAB7 in WT and CLUH KO axons. *Atp5a-MS2* was not used for this experiment, because it exhibits fewer spots of signal and it would therefore be extremely challenging to image enough axons for robust numbers in a colocalisation study. Co-expressing axons were imaged at DIV5 with a time lapse of 90 seconds and a two second frame interval. For the analysis, I focused on areas after the axon initial segment and association events were visually defined by an overlap of mRNA and RAB7 signal (Fig 13 A). I observed a small reduction in the average time of association events in WT compared to CLUH KO for both *Mdh2* (21 ± 10 to 16 ± 8 seconds) and *ActB* (19 ± 7 to 13 ± 4 seconds). Yet, only for *ActB* this reduction was significant (Fig 13 B). The majority (median of 66-75%) of spots associated with late endosomes at least once in all conditions (Fig 13 C). One spot could also have multiple association events in case of an interruption of some kind. However, there was no detectable difference in the number of association events per spot (Fig 13 D). These results in part confirm what I observed with endogenous protein and mRNA in HeLa, where no change in the colocalisation of *ActB*, *Atp5a* and *Mdh2* with RAB7 could be found between WT and CLUH KO (Fig 11 G). However, in difference to the results in HeLa, the reduction of association time in axons suggests that while the frequency of association may be the same, the overall association of *Mdh2* and *ActB* mRNA with RAB7 in CLUH KO was less than in WT motoneuronal axons.

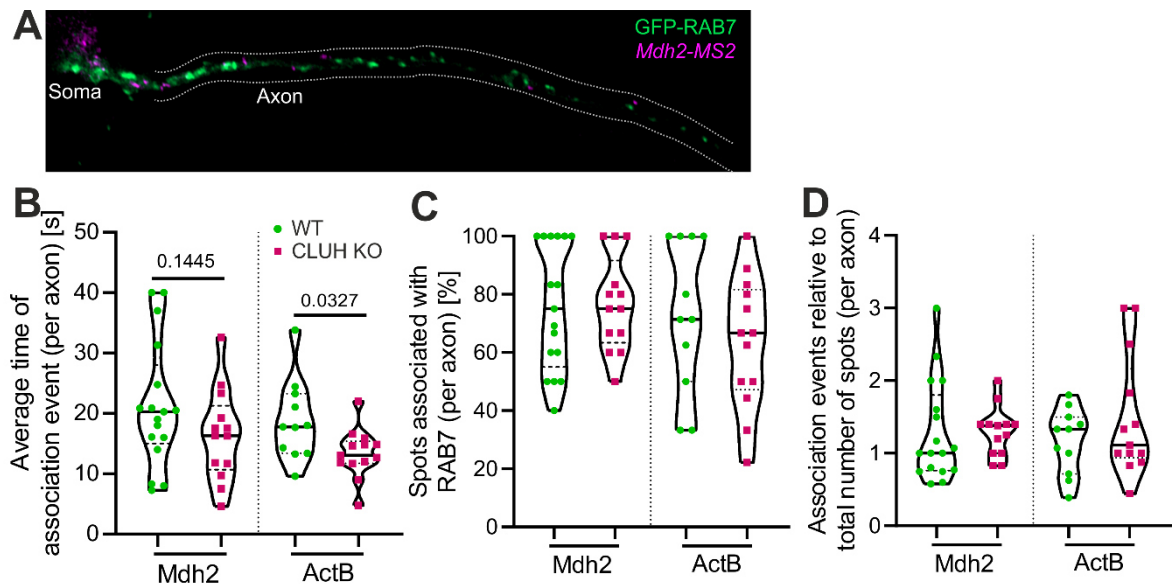


Fig 13: Temporal differences in association of *Mdh2* and *ActB* mRNA with RAB7 in WT and CLUH KO

A) shows a WT example of a neuron imaged to investigate the association over time between mRNA constructs (*Mdh2-MS2*, *ActB-MS2*) and GFP-RAB7 in live axons (3 min with 2 seconds per frame). WT and CLUH KO axons were analysed for the average time of association per event (B), the percentage of spots which at some point associated to an endosome (C) and the number of association events relative to the number of visible spots (D). Data is shown in a violin plot with each dot representing an axon (≥ 3 spots), with 13-17 (*Mdh2*) or 11-13 (*ActB*) axons per genotype from 5 or 3 different embryos respectively. For statistics, in B) and D) a Welch's test per mRNA was used and for C) a Mann-Whitney test (No Gaussian distribution). Only P values of ≤ 0.2 are shown.

Another readout I was interested in, was how the association of mRNA to late endosomes alters the mRNA motility. The idea being, that CLUH somehow mediates the localisation of mRNAs to a certain pool of late endosomes with particular motility or lack thereof. Hence, three states of motion with increasing motility were defined (stationary, diffusive oscillation and directed motion) and manually assigned based on the movement in the movies of mRNA and RAB7 while together. Examples are shown in the Kymographs of Fig 14 A-E, which are created from selected the linearised axons which are shown in their first frame above each kymograph. The best examples for stationary and directed motion can be seen in Fig 14 E, while a great example for diffusive oscillation is in Fig 14 D. These kymographs only suite the purpose of visualising examples of the motion types, while the actual analysis was done on the time lapse movies. Therefore, care has to be taken in the interpretation of the kymographs, as colocalisation in a kymograph can be misleading. When comparing the percentages of the assigned motion-states in WT and CLUH KO no change was found for *Mdh2* and *ActB* (Fig 14 F, G). Most spots exhibited a stationary behaviour when associated with RAB7, and a much smaller percentage

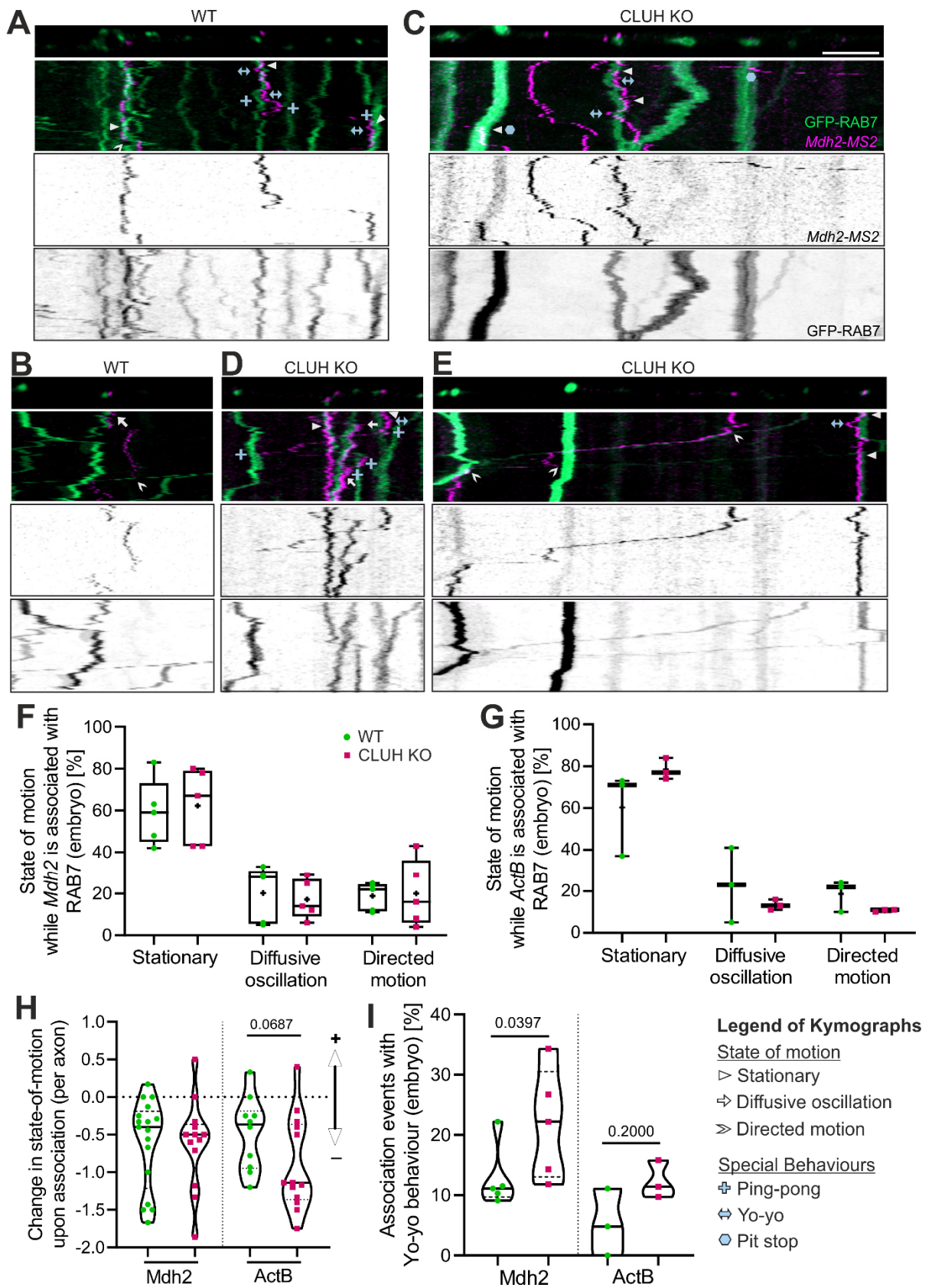
exhibit diffusive oscillation or directed motion (mean: 10-20% each). Thus, presence of CLUH appeared to not impact the motility of associated mRNA and RAB7.

I wanted to confirm this finding by characterising the difference in motility of single and associated mRNA, which should not be substantially different between WT and CLUH KO as the genotype had no impact on trafficking of these mRNAs in general (Fig 10 C, D, E) and also not on the state of motion when associated to RAB7. As mentioned above, the motion-states are defined with an increasing motion in mind, from stationary over diffusive to directed. As such, I had assigned numbers to the states mirroring their motility (stationary: 1, diffusive: 2, directed: 3). By subtracting the state of motion before or after association from the state during association, the result describes how the association of mRNA with RAB7 affected the motility. If the index is below zero it corresponds to an average reduction of the motion state in associated compared to disassociated mRNA. Interestingly, for all tested mRNAs and conditions the average index was less than - 0.5, meaning mRNA was less mobile when associated then alone. This reduction was most clear for *ActB* in CLUH KO where the average index was -0.9 (\pm 0.6) (Fig 14 H). Therefore, as expected, loss of CLUH had no impact on the motility change of dissociated or RAB7 associated *Mdh2* mRNA and only a small, non-significant effect for *ActB*. However, I also showed that mRNA in general seems to exhibit reduced motility when associated to RAB7 positive vesicles.

In addition to the motion states, I identified other distinct behaviours that seemed to characterise and define the interaction of mRNA and RAB7. Frequently, mRNAs and late endosomes that were associated with each other would briefly and sometimes abruptly be separated by small distances, just to associate a few seconds later again. This back-and-forth similar to the motion of a “Yo-yo” appeared frequently as interruptions of stationary associations and can best be seen in the kymographs of Fig 14 E and A (\leftrightarrow). For transparency it has to be noted, that due to the brevity of these events and as I could not judge their relevance, the Yo-yo was ignored for the previous analysis of association times and events, and the interrupted events were still counted as one continuous rather than two separated associations. When quantifying the percentage of association events which were interrupted or composited with a Yo-yo behaviour, the mean percentage was roughly doubled from WT to CLUH KO to 21.9% (\pm 9.2) and 12.3% (\pm 3.1) for *Mdh2* and *ActB* (Fig 14 I). Two additional behaviours which I observed but too infrequent to quantify, were oscillations of mRNA between two or more different endosomes like in a game of “Ping-pong” (Fig 14 A, D), and the tendency of long moving mRNA spots to take brief breaks or “Pit stops” on endosomes they meet on their way (Fig 14 C). All three of the behaviours were mostly characterised by mRNAs moving without endosomes and interacting with them on a stationary level. In general, it seemed to be more frequently the case

that a moving endosome “picks up” a stationary mRNA for a combined movement, then the other way around.

In summary, the small decrease in the association length between *Atp5a* or *ActB* mRNA and late endosomes in CLUH KO and the increase in brief detachments (Yo-yo), suggest that the lack of CLUH impacts the interaction between some mRNAs and late endosomes in axons, seemingly decreasing the stability of their association. In addition, CLUH unrelated, I have shown that during interaction of mRNA and late endosomes, the vast majority of events were stationary interactions and only around 20% exhibited directed motion. In combination with the finding that association of mRNA with late endosomes resulted in reduced motility of said mRNA, these results suggest that late endosomes do not majorly play a transport but a localisation role for mRNAs.



For figure legend, see next page.

Fig 14: Comparing different states of motion and other distinct behaviours of *Mdh2* and *ActB* mRNA when associated to RAB7 in WT and CLUH KO axons

A-E) Kymographs of *Mdh2-MS2* and GFP-RAB7 mRNAs in axons of primary motoneurons. The first frame of the recording is shown as a straightened segment in the image above the kymograph. Kymographs are shown as coloured merge and single channel grayscale. Depicted is not the whole analysed axon, but only selected parts to show representative examples of states of motion (stationary, diffusive oscillation, directed motion) and other behaviours (Ping-pong, Yo-yo, Pit stop). The behaviours are indicated by specific pointers given in the legend below. **A)** and **B)** are from WT axons, while **C)-E)** are from CLUH KO axons. Bar, 5 μ m. The distribution of states of motion as described in **A)-E)** is depicted in **F)** for *Mdh2-MS2* and **G)** for *ActB-MS2*. Data is shown in Boxplots with each dot representing an embryo of 5 (*Mdh2*) or 3 different embryos (*ActB*) with 3-7 or 4-7 axons respectively. Statistical test, two-way ANOVA followed by Sidak multiple comparisons. **H)** Average change in state-of-motion from disassociated to RAB7-associated. Data shown in a violin plot per axon (≥ 3 spots), with 13-17 (*Mdh2*) or 11-13 (*ActB*) axons per genotype from 5 or 3 different embryos respectively. **I)** Percentage of association events exhibiting the Yo-yo behaviour. Data shown in a violin plot per embryo. Statistical test for **H)** and **I)** is a Mann-Whitney per mRNA. Only P values of ≤ 0.2 are shown.

5 Discussion

5.1 Compartmentalised proteomics of primary motoneurons

5.1.1 Robust axon enriched proteome of motoneurons and comparison to other *in vitro* studies

I have successfully obtained a detailed and statistically robust dataset of axonal enriched proteins in primary motoneurons. Of a total of 7,653 proteins, 2,686 were identified in the axonal and the WC proteome. Gene ontology enrichment analysis showed that of the 277 axon enriched proteins, axonal proteins were clearly overrepresented, while axonal depleted or missing proteins were related to ribosomes, organelles (mitochondria, endoplasmic reticulum, proteasome) and the nucleus. Thereby, I demonstrated the effectiveness of the neuronal compartmentalisation.

Only two other studies with compartmentalised proteomics of primary neuron cultures have been published (Zappulo et al. 2017; Chuang et al. 2018). However, the similarity between the neurite or axonal enriched proteome from all three datasets is very low, with only five proteins that are shared among all three (Bhmt, Cps1, Pygl, Ugdh, C3). This was also reflected in the gene ontology cellular component enrichment analysis. Chuang et al. (2018) found an axonal enrichment of nuclear proteins, followed by components of the endoplasmic reticulum, the large ribosomal subunit, and the extracellular matrix. Particularly the prevalence of nuclear proteins and histones seems unexpected. Zappulo et al. (2017) have obtained results much more similar to mine. In their study, nucleus related components are depleted from neurites, as well as some mitochondria associated components and the ribonucleoprotein complex. On the enriched side, components of the cytoskeleton, vesicular trafficking, adhesion molecules, and other synaptic markers were found. However, due to their neurite rather than axon compartmentalisation they did not find exclusively axon related components to be enriched. When looking at the cell models and compartmentalisation methods used, it becomes apparent what is likely the cause for these differences. Chuang et al. (2018) used embryonic rat cortical neurons which were compartmentalised using glass chips which had a poly-l-lysine coated micropattern on the surface, only allowing the long axons to cross into another compartment. Two replicates of these cultures were analysed by MS after dimethyl labelling and quantified using a normalised iBAQ, like I have done. They identified 1,314 proteins in axons and 1,690 in the WC compartment. Zappulo et al. (2017) used mESC which were differentiated into iNeurons by expression of pioneer proneural transcription factor ASCL1. Three biological replicates of cells were grown in Boyden chambers analysed by MS and quantified using label-free quantification (LFQ) without further normalisation. A total of 7,323 proteins were measured, however, to

allow for statistical testing in case values were missing from one compartment, they imputed these values. Thus, it is unclear how many of the reported proteins were actually measured in neurites or just imputed. In an experimental setting where one specific compartment of the cell is compared to everything else, imputation of non-measured proteins could lead to artefactual results, as for example a nucleus specific protein should not be artificially added back in the neurite data. Imputation can also in part explain the more than two times higher number of axon enriched proteins, as I only looked at the actually shared proteins, which were 2,686 in my case.

In summary, all three studies used very different neuronal models and started from a different number of proteins detected or imputed for statistics. Furthermore, Zappulo et al. (2017) used a method for compartmentalisation which cannot differ between dendrites and axons, while Chuang et al. (2018) and I generated the data with methods allowing for theoretically purely axonal samples. Lastly, while the other two studies base their whole dataset on only two or three biological replicates, my dataset is based on nine biological replicates. This allowed me to do very robust and stringent statistics ($q \leq 0.01$), in comparison to Chuang et al. (2018) who have no statistics or Zappulo et al. (2017), who only use a t-test ($p \leq 0.05$) combined with a minimum fold change, but no multiple comparison test as should be done for such big datasets. All these differences evidently lead to barely comparable compartmentalised proteomic datasets, with the data presented by me, arguably being the only statistically robust axon-specific proteome *in vitro*.

Newer publications have focused on using *in vivo* models to get axon-specific proteomes, from cortical neurons or midbrain dopaminergic neurons and their striatal projections in the mouse brain. The cell specificity is reached by using APEX2-based proximity labelling which is only expressed in specific cells (Dumrongprechachan et al. 2022; Hobson et al. 2022). These results from fully mature neurons relate however to a very different developmental state than my data, thus limiting comparability. The cytoplasmic APEX2 labelling does not enrich proteins within membrane-enclosed structures, therefore missing mitochondrial proteins (Hobson et al. 2022). Nevertheless, on a cellular component enrichment level these studies report similar enriched and depleted components as reported by me.

5.1.2 Normalisation of proteomics data from compartmentalised cells

Normalisation between proteomics from different compartments of a cell is challenging and can have a big impact on the data reported. One specific compartment of the cell (Axons) was compared to the rest of the cell. That means overall protein concentrations and also the protein composition were expected to differ greatly. When comparing similar samples, one could usually control for different protein concentrations by a control protein that would be assumed to be expressed equally in all samples. However, since we are looking at a sub-compartment of

the cell compared to a whole cell such an assumption cannot genuinely be made. Therefore, care must be taken when selecting the way of quantifying the MS data and normalising between the samples, to achieve a result that is as close to the real values as possible. I have used iBAQ to quantify the MS data, where the sum of all peptide intensities is divided by the number of measured tryptic peptides, to receive a value regarded as the absolute abundance of each protein. This process was followed by dividing the iBAQ of each protein by the sum of all iBAQ values within a sample, resulting in a relative iBAQ (riBAQ). The riBAQ was calculated in an attempt to make the different starting concentrations of axonal and WC reads comparable and was also used in similar studies (Shin et al. 2013; Chuang et al. 2018). Zappulo et al. (2017) used a different approach, with LFQs for quantification of protein intensities and no additional normalisation. The LFQ algorithm assumes that it works with two similar samples in which the majority of proteins are represented in the same amount (Zappulo et al. 2017). Using such a method in an experimental setting where one should expect that the majority of proteins are differentially expressed, could skew the data by adapting intensities in ways which are not real. This shift towards a more equalised expression pattern can also be seen when comparing the ratio of axon enriched to depleted proteins for my data ($277/1447 \approx 0.19$) and Zappulo et al. (2017) ($660/1162 \approx 0.57$). The experimental setup in these compartmentalised studies makes it inherently difficult to evaluate what is the best processing path to reach data most close the real data. However, I find the riBAQ to appear as the best approach of getting to a realistic normalisation, considering the criteria discussed above.

5.1.3 Alterations of mitochondrial metabolic pathways in axons of developing neurons and their possible relevance for neuronal health

By focusing on the 365 mitochondrial proteins detected in both compartments, and renormalising the data for MitoCarta annotated proteins, I could assess differences in the mitochondrial proteome composition no matter the differences in mitochondria density or mass. In this way I identified OXPHOS related proteins to be the most enriched group of the axon depleted proteins, followed by the citrate cycle. The only unique enriched pathway in the axon enriched proteome was fatty acid metabolism. In the neurite depleted and enriched proteins of Zappulo et al. (2017) and the axon enriched proteins from Chung et al. (2019), these pathways did not come up in a KEGG pathway enrichment. As discussed above this suggests these changes to be specific for axons of mouse motoneurons and not shared by dendrites.

5.1.3.1 Urea cycle in neurodegeneration

The urea cycle, with its mitochondrial and cytosolic part, turned out as another pathway with drastically enriched protein levels in axons for all core proteins, except the mitochondrial isoform of arginase (Fig 6 C). The mitochondrial protein Cps1 was also one of the five proteins

confirmed by the other two proteomics studies (Chung et al. 2019; Zappulo et al. 2017). The urea cycle might usually be more considered when talking about the liver, but the nervous system seems to be one of the major affected parts of the body by urea cycle disorders (UCDs). These UCDs are characterised by a reduction in activity of at least one of the core urea cycle enzymes, leading to hyperammonaemia. The prevalence of the whole group is reported to be between 1/8,000 and 1/44,000 births. The clinical symptoms are especially for complete deficiencies very severe, with 50% mortality. The surviving cases suffer from developmental delay and brain damage, encephalopathy, seizures, altered levels of consciousness, multiorgan failure, vomiting and ataxia (Häberle et al. 2012; Duff and Baruteau 2022). As ammonia are free to diffuse through the blood-brain-barrier, severe toxic effects are observed in the brains in these diseases (Gropman, Summar, and Leonard 2007). There are two forms of UCDs which are also directly related to the neurodegenerative disease hereditary spastic paraplegia (HSP). Arginase (Arg1) deficiency (Argininemia, OMIM 207800) and ornithine translocase (Slc25a15) deficiency (HHH syndrome, OMIM 238970) have multiple reported patients with spastic paraplegia (Panza et al. 2019). Furthermore, increased levels of brain urea have been measured in models and human postmortem-tissue of Huntington (HD) and Alzheimer's disease (AD) (Handley et al. 2017; Xu et al. 2016). For AD, it was also found that the full cyclic activity of the urea cycle in astrocytes can have an A β -detoxification effect (Ju et al. 2022). A similar correlation with neurodegenerative diseases can also be found for nitric oxide synthesis, which is directly related to the urea cycle. Nitric oxide can work in neurotransmission and immune response, but nitrotyrosination of proteins can also be involved in AD (OMIM 104300) and Parkinson's disease onset (Picón-Pagès, Garcia-Buendia, and Muñoz 2019). In summary, the urea cycle and its related pathways activity can affect neuronal health and even lead to multiple neurodegenerative diseases when mis-regulated. Thus, the fact that these proteins are particularly enriched in axons could be because the urea cycle plays a neuroprotective role with specific relevance for axons.

5.1.3.2 Citric acid cycle and the aspartate-argininosuccinate shunt

The urea cycle and the citric acid cycle are linked via oxaloacetate and fumarate and the aspartate-argininosuccinate shunt (AAS) (Fig 6 C). This is particularly interesting as the citric acid cycle enzymes which are part of the AAS (Fh and Mdh2) were not altered in their level between WC and axon, while three out of the five other detected core enzymes or complexes of the citric acid cycle were significantly depleted from axons (Fig 6 A). This finding opened the question why particularly the enzymes in the citric acid cycle which are also connected to the urea cycle maintained their concentration in axonal mitochondria. I identified that those steps of the citric acid cycle which were maintained in their level in axons had a higher protein half-life than those depleted from axons (Fig 7 C). Thus, meaning that protein half-life is a

major determinant of the axonal enrichment or depletion of citric acid cycle proteins. This also suggests that the neuron is not actively counteracting this imbalance by upregulation of mRNA transport or local translation. If protein levels translate to enzymatic activity, a consequence of this imbalance could be that only a part of the citric acid cycle can work at unchanged capacity. One could hypothesise that a partial or linear citric acid cycle activity, may actually be an advantage or at least no disadvantage for axons of developing neurons. Axons in developing neurons may not need as much energy and electron carriers as other compartments of the cell. The low protein half-life of the axonal depleted citric acid cycle proteins could therefore potentially be an evolutionary adaptation to solely focus on Mdh2 for electron carrier production without the need for an active regulatory mechanism. The ASS could be a way of making this partial citric acid cycle possible, as processing of oxaloacetate to fumarate is taken over by the urea cycle, thereby skipping all axonal depleted steps of the citric acid cycle. For this to work it may be necessary to upregulate the urea cycle in the axons, compared to the rest of the cell, as the urea cycle is more needed in axons. And while I have no way of proving any causative connection between the partial citric acid cycle and upregulated urea cycle, the ASS will certainly be beneficial for overall energy efficiency of both pathways by feeding into NADH production by Mdh2 and channelling the efficient usage of metabolites. From protein levels alone, this can however not be deduced, and metabolites and their flow would have to be measured.

5.1.3.3 Enriched fatty acid metabolism and the bottleneck OXPHOS

Fatty acid metabolism was one of the pathways enriched in the axonal mitochondrial proteome, including most isozymes involved in β -oxidation. Fatty acids are important for brain development, particularly during growth, for the synthesis of diverse lipids (Rae et al. 2024). However, from the KEGG pathway enrichment it was less fatty acid synthesis and more fatty acid degradation which was enriched in axons. Fatty acid oxidation as a mechanism for energy production, has so far been reported to be mostly present in adult brains and particularly astrocytes (Carey 1975; Edmond et al. 1987). This idea is already very old, but also more new studies find important proteins for mitochondrial fatty acid import to be absent from neurons (Jernberg et al. 2017). However, none of these studies have used compartmentalised cultures, meaning an axon specific activity of fatty acid oxidation may have not be detected so far as it would have been overshadowed by somatic inactivity. I found that at least the proteins needed for β -oxidation were detected in axons and enriched compared to the WC. It could therefore be very interesting to investigate whether fatty acid oxidation may have a bigger role in developing neurons and particularly their axons, than expected.

As mentioned, fatty acid oxidation produces electron carriers and acetyl-CoA, which can be used in the citric acid cycle (Fig 6 B). Thus, neurons could potentially support the partly

depleted citric acid cycle in axons by an upregulated fatty acid β -oxidation activity. OXPHOS components were however severely depleted from axons. Thus, no matter how the axon may maintain the electron carrier output, the bottle neck will still be OXPHOS as the final step of ATP production. The relation of these pathways, their actual activity levels and outputs are however pure speculation when only based on a proteomics study. Thus, it can also not clearly be determined whether OXPHOS actually turns out to be a bottle neck.

5.1.3.4 Experimental approaches to confirm proposed axonal metabolic changes

Measurement of protein levels cannot give us information about the actual levels of metabolites and their flow, as protein levels do not always correlate directly with overall activity. Thus, to further unravel what actually happens in axonal mitochondria on the metabolic level it would be necessary to measure some of those metabolites. The very small amount of material, especially from the axonal compartment makes many of those experiments challenging or impossible, such as metabolite flux measurements or oxygen consumption with the oroboros system. Furthermore, direct comparisons of axon and WC compartment should be avoided for the discussed problems of normalisation. Rather it would be a good approach to inhibit or boost certain parts of the pathways and compare the relative changes of specific metabolite steady states before and after treatment, to see whether both compartments react differently. To investigate the usage of the ASS one could inhibit Got and the malate-aspartate shuttle, which is crucial for the exchange of metabolites between cytosol (urea cycle) and mitochondria (citric acid cycle) (Kauppinen, Sihra, and Nicholls 1987). As a result, one would expect an accumulation of oxaloacetate, that should be higher in axons than the WC, as in axons its assumed that ASS plays a bigger role for oxaloacetate processing than in the WC. It could also be tested whether such an inhibition of the ASS has an impact on more downstream readouts, like a change in ATP production, urea production, a reduction of axon growth or even increased axonal degeneration. Similar inhibitory strategies could also be attempted for fatty acid oxidation. Additionally, to investigate fatty acid oxidation activity, one could add radiolabelled fatty acids like [^{14}C]-palmitate specifically to the axonal compartment of a MFD culture and measure the release of radiolabelled CO_2 into the medium. Thereby, measuring axon specific fatty acid oxidation activity. With more time, the creation of KO out lines, targeting specific parts of the citric acid cycle, β -oxidation or urea cycle could also help to investigate their role in axonal maintenance.

5.1.4 Protein half-life, translation and mRNA levels do not majorly determine axonal enrichment on proteomic scale, but can be influential on pathway level

To find which possible mechanisms of protein level control come to play in case of the axonal enriched and depleted proteome, I have correlated my axonal enrichment data with other

datasets on axonal mRNA stability, axonal transcript enrichment, axonal translome and neuronal protein half-life. I have discovered that especially for mitochondrial proteins there is a very small positive correlation with mRNA stability and protein half-life, a slight negative correlation trend for axonal translation and no correlation with axonal transcript enrichment. For the whole proteome, the trend was similar, but with a weaker correlation to protein half-life and no correlation with translome and mRNA stability. Thus, from all these factors, the only one which shows at least a small positive correlation and could impact protein levels, seems to be the protein half-life. However, as the correlation is very low, it seems more likely that on this broad scale no one factor alone determines protein enrichment in axons.

It is in general important to note that all correlations I observed on a total or mitochondrial level were very low, with the highest correlation being of $r=0.223$. Thus, it could absolutely be argued that these results just show that there is no correlation of my protein enrichment data with any of the other studies. One reason for this is likely the fact that I am correlating data from different model systems, compartmentalisation methods, quantification methods and labs. The additional variabilities introduced by this situation make it more unlikely for me to find correlations of different factors like protein and transcript enrichment. The great influence of model, lab and method is easily illustrated by correlating datasets with the same kind of data, like *in vitro* neuronal protein half-life, where the average correlation is only $r=0.509$ (range: 0.231 to 0.815). This variability could also mean, that even though I do not find correlations with these datasets from other labs, if I would measure things like axonal transcriptome or translome in my model, I might actually find a strong correlation. At least for axonal transcript enrichment and neuronal protein half-life this seems however unlikely, as I am comparing to several independent studies, making those results more reliable. The second reason for the low correlations observed by me, could be that there simply are no meaningful correlations of these factors on the large scale of the total or even the mitochondrial proteome. With hundreds or thousands of proteins it may simply be unlikely or even impossible to find one regulating measure which alone could substantially explain the axonal protein enrichment. It seems much more likely to be a combination of factors with different influence on different protein groups and pathways, thus leading to low correlations with single factors. A perfect example providing evidence for this idea is the citric acid cycle. I found that when only looking at proteins of the citric acid cycle they correlated very well with protein-half live ($r=0.448$) and to a much higher level than the mitochondrial or total proteome. As a conclusion, rather than searching for one overall determining factor, for future and more in-depth analysis it would make more sense to divide the proteome by certain pathways and locations and see which of the regulating factors have the biggest influence on their axonal enrichment.

Putting my observations into the context of other studies, there are unfortunately only very few sources which measure the proteome regulating factors together in the same or similar samples. The advantage of such a study is that when everything comes from the same model and lab, variabilities will be smaller, leading to a higher chance of observing correlations. Zappulo et al. (2017) is to my knowledge the only study which have measured transcriptome, translome and proteome all together, however in neurites and not in axons. Within their study they actually found a positive correlation between neurite protein and transcriptome enrichment ($r=0.44$) and furthermore, found that those double enriched proteins were particularly increased in their translational activity. A different result comes from a study where also proteomics and transcriptomics were investigated but *in vivo* and with enrichment into growth cones. Neurons were isolated by a fluorescent label from mouse brains. I correlated their growth cone enrichment data of 955 measured proteins and transcripts and found no correlation ($r=0.023$) (Poulopoulos et al. 2019). Thus, even in studies correlating internal data it is not always clear to what extent mRNA enrichment is a mechanism of enriching proteins in neurites or growth cones. The difference between both studies could suggest a change in the relationship of mRNA and protein enrichment between developing and mature neurons or differences between neurites and growth cones in that sense. My data however aligned more with that from the mature neuronal growth cones. Another comparative study investigated axonal translome and transcript enrichment, but without proteome. They found transcript enrichment and translome to have no general correlation and for many mitochondrial genes even correlated negatively (Jung et al. 2022). This finding could explain why I found opposing trends for correlations of axonal enriched mitochondrial proteome with translome and transcript enrichment (Fig 7 A).

5.1.5 Mitochondrial morphology as a major determinant of protein composition

I have identified that the ratio of membrane associated to soluble proteins in mitochondria correlates very well with morphological differences between mitochondria in axons and around the soma. The very rounded shape of mitochondria in axons was connected to an almost four times higher ratio of soluble to membrane associated proteins, than in the elongated and complex shaped mitochondria closer to the soma. The obvious question is, which of these factors determines the other? Mitochondrial morphology and size are generally determined by fusion and fission activity, which are regulated by a group of fusion and fission factors (Misgeld and Schwarz 2017). And indeed, the morphological changes I observed, correlate well with the differential levels of the main fusion and fission factors. On the fusion side Opa1 (\log_2 fold change: -2.82) was significantly and substantially depleted from axons. Mfn1 and Mfn2 were only measured in one and two axonal samples, respectively and at much lower levels than in the WC, suggesting them to be drastically depleted or missing from axons. On the fission side Dnm11 (Drp1) and Mff were unchanged while Fis1 (-0.82) was significantly but only mildly

depleted from axons. Overall, in axons fusion factors were severely depleted while fission factors were mostly stable in level or only lightly depleted. This suggests much more mitochondrial fission than fusion to take place in axons, which would lead to the observed small and rounded mitochondria in axons. Thus, this data clearly confirms that the differential mitochondrial morphology was induced by the known fusion and fission factors, and this morphology in turn determined the overall proteome composition and ratio of soluble to membrane bound proteins.

The morphology might actually have a bigger influence on the axonal enriched proteome than some of the regulating factors like transcript enrichment, translation and protein half-life which were discussed before. The pathway which was in its totality most depleted from axons was OXPHOS, where almost all proteins which it is made up of are directly or indirectly bound to the mitochondrial IM. For the few pathways enriched or at least unchanged in their protein levels in axons, like parts of the citric acid cycle, the urea cycle and β -oxidation, they consist mostly of soluble proteins. This supports the conclusion that the mitochondrial morphology can greatly impact the relative protein composition and thus likely also their metabolic activity. This idea is also supported by reports that mitochondria close to synapses alter their morphology and ultrastructure depending on the synaptic performance (Cserép et al. 2018). Which means, at highly performing synapses, mitochondria do not just have a higher activity, but are larger and have a higher cristae density, likely to physically alter their protein content and allow for more OXPHOS components.

5.2 Relevance of CLUH for mechanisms of axonal mitochondrial maintenance

5.2.1 Failure to maintain the axonal mitochondrial proteome under KO of CLUH is not due to mitochondria transport

CLUH is an evolutionary conserved RBP specifically binding to NEM mRNAs and lack of CLUH leads to a characteristic clustering of mitochondria in many cell lines (Schatton et al. 2017; Gao et al. 2014). Mitochondria in CLUH KO primary motoneurons clearly show a biogenesis defect, which is reflected in the proteome as well as in a reduction of mitochondrial ATP production (Zaninello et al. 2024). Besides protein transport, the maintenance of the mitochondrial proteome in axons has been suggested to be mostly dependent on transport of mitochondria from the soma or on local translation of transported mRNAs (Schwarz 2013; Harbauer 2017). Therefore, it was an obvious choice to investigate a possible role of CLUH in these mechanisms. However, in the axons of primary motoneurons, motility and directionality of mitochondria trafficking was not affected by absence of CLUH, ruling out that replenishment

of axonal mitochondrial proteins via mitochondrial trafficking is suppressed by loss of CLUH and suggesting problems in local translation to be the cause of protein loss.

When putting the mitochondrial trafficking results in the context of other publications on mitochondria trafficking, the roughly 35% of motile mitochondria was in line with 10-40% reported in other published data (Schwarz 2013). However, I have detected a higher percentage of retrograde movement than anterograde movement. Bi-directional movement is typical, but usually the ratio of anterograde movement should be higher than retrograde, to achieve a net transport of mitochondria into the axon (Schwarz 2013). This readout suggests that the imaged axons were negatively affected in some way, leading to a retraction of some mitochondria, and potentially reducing the meaningfulness of this data. Possible reasons could have been the usage of MitoTracker or the stress of imaging the cells. The quality of the primary neurons is an unlikely reason, as axons clearly are containing many mitochondria, so movement must have been net anterograde before imaging.

5.2.2 mRNA transport is not affected by loss of CLUH in a way to reduce mRNA levels in axons

I also investigated local translation as the other major pathway of maintaining a functional mitochondrial protein pool in axons. For transcripts to be translated in axons, as a first step, they have to be transported there. RBPs like CLUH can play a major role in facilitating this transport by tethering RNAs to motor proteins or membranes of moving organelles. I studied the transport of CLUH target mRNAs in axons, but found no significant or substantial alteration, which would lead to a relevant reduction of axonal mRNA. Therefore, it seems unlikely that CLUH has any impact on local translation by affecting axonal mRNA transport.

For the fluorescent detection of a specific mRNA in a living cell I used a bacteriophage derived tether system. This system works by introducing a tag in form of RNA stem-loop structures (MS2) into the RNA sequence. These MS2 loops are then bound by the co-expressed MCP which is tagged with a HaloTag. Thus, when interpreting the results of my mRNA trafficking experiments it is important to note that I am detecting an overexpressed mRNA with additional sequences after its 3'UTR. There is no clear agreement on where to best insert the MS2 loops. In my case I inserted them downstream of the 3'UTR, but there are also some studies putting them in between coding sequence and 3'UTR (Cohen et al. 2022). Considering many RBPs bind in the 3'UTR (Eliscovich and Singer 2017), I wanted to keep CDS and 3'UTR together and therefore put the MS2 loops downstream of the 3'UTR. The addition of MS2 loops in the 3'UTR has been reported to destabilise some tagged mRNAs by activating the nonsense-mediated decay. This has however only been found for some mRNAs and *ActB* mRNA was one of the mRNAs not affected by this destabilisation (Li et al. 2022). Incomplete decay of mRNAs

with only their 3'UTR and MBS left has also been found to be a problem in some studies, leading to bigger blobs of fluorescence (Tutucci et al. 2018). However, I never observed such artifacts, which seem to arise if the constructs are expressed for a too extended time before imaging. By only waiting 24 hours before imaging, all mRNA spots were evenly sized and similar in fluorescence intensity, excluding the possibility of such decay fragments. Furthermore, to avoid an overload of the cell and obtain an expression level similar to the endogenous expression level, a weak Ubc promoter was used (Qin et al. 2010). The visualisation in this method comes from the binding of up to twelve complexes of stdMCP-stdHalo (around 100 kDa each) to the mRNA, which would mean an additional protein load of 1 MDa per mRNA. This additional weight has to however be put in the context with the many other RBPs bound to RNAs such as the ribosome complex at a total of 3.3 MDa (Gerstberger, Hafner, and Tuschl 2014; Mitchell and Parker 2014; Klinge et al. 2012). Lastly, the binding of CLUH to the overexpressed mRNA has not been proven. However, it is unlikely that CLUH binding to *Atp5a* or *Mdh2* mRNA was absent in the used constructs. The only logical case in which that could have happened is if CLUH binding would need a specific type of interaction between polyA sequence and some other part of the mRNA which are then too far separated by the insertion of the MBS. In general, it is important to note that the used method does not detect endogenous mRNA, and the additional bound proteins could potentially influence the behaviour of the RNA in the cell. For that reason, I was not only looking at one mRNA but had two CLUH target mRNAs (*Atp5a*, *Mdh2*) compared to the abundantly used control mRNA *ActB*, which were all tagged in the same way. Thereby, I controlled for possible artifacts introduced by the imaging method. Furthermore, the MS2-MCP and directly related methods like PP7-PCP method are the state of the art and most widely used methods in many studies on mRNA trafficking, localisation and translation (Wu, Chen, and Singer 2014; Wu et al. 2016; Yoon et al. 2016; Wu et al. 2015; Cohen et al. 2022; Harbauer et al. 2022; Hees, Wanderoy, et al. 2024; Hees, Segura, et al. 2024)

Alternatives to protein-based tools for mRNA tracking are fluorogenic RNA aptamers and small hybridising probes. In a similar fashion to the MS2-MCP system, fluorogenic RNA aptamers are specific mRNA sequences inserted somewhere into the target RNA. But instead of expressing a second protein which binds it, a cell permeable fluorophore is added. When bound to the RNA aptamer, it becomes highly fluorescent, as the structure of the aptamer rigidifies and the small molecule fluorophore is shaped into a fluorescently active state. The most recent examples of this system are called Broccoli, Corn, Mango II and Pepper (Li et al. 2020; Song et al. 2017; Cawte, Unrau, and Rueda 2020; Chen et al. 2019). Comparisons of the MS2-MCP and fluorogenic aptamer systems are mostly being published by groups developing the aptamers. They find MCP-EGFP and MCP-mCherry to work comparably good to Broccoli or

to be outperformed by Mango II and Pepper in live signal-to-noise ratio (Cawte, Unrau, and Rueda 2020; Chen et al. 2019; Li et al. 2020). However, some of these comparisons are irrelevant as they lack single-molecule resolution, and they are all comparing to the inferior MCP-mCherry or MCP-EGFP reporter instead of the superior MCP-HaloTag used by me. A very substantial improvement in mRNA live imaging could come from hybridisation-based probes or molecular beacons, which can detect endogenous RNA in a protein-independent way. They work by injecting a nucleic acid probe designed to hybridise with an RNA and have a fluorophore on one and a quencher on the other side. Once bound to the RNA the structure unfolds, fluorophore and quencher are separated, and fluorescence is turned on (Ma et al. 2017; Mao et al. 2020; Yang et al. 2022). No comparisons to the MS2-MCP system exist, but molecular beacons have been used to study trafficking of endogenous *ActB* mRNA in neurons (Turner-Bridger et al. 2018; Cioni et al. 2019). However, at this point signal quality does not look comparable to the MS2-MCP system.

5.2.3 mRNA localisation to endosomal translation hubs is not affected by CLUH KO in a way that suggests substantially increased mRNA decay

I found axonal mRNA transport to be unaffected by loss of CLUH. Nevertheless, it has been reported that CLUH target mRNAs (*Atp5a*, *Pink1*) are reduced in their axonal abundance under CLUH KO (Zaninello et al. 2024). Thus, there must be another explanation except of mRNA transport to explain why there are less NEM RNAs in axons when CLUH is absent. In MEFs it has been shown that CLUH slows down the decay of target mRNAs, so it can be assumed that a similar affect will also be present in neurons (Schatton et al. 2017). However, how exactly mRNA stability is affected remains elusive. The polarised nature of neurons created a chance to identify whether processes like mRNA localisation could be affected by CLUH and influence mRNA stability. Localisation of mRNA can greatly influence its translation activity and also the target localisation of the translated protein (Hüttelmaier et al. 2005; Dermitt et al. 2020; Gasparski et al. 2023). Furthermore, especially for mitochondrial proteins, localisation to the endolysosomal system in combination with the ER has been found to play a role in regulating translation and protein import (Hees, Segura, et al. 2024; Cioni et al. 2019; Schuhmacher et al. 2023). It could be hypothesised that detachment or mislocalisation from this system could lead to reduced protein translation combined with increased mRNA decay, for example by being less protected from systems of translational quality control like the no-go mRNA decay, where translation would be stalled due to the missing necessary chaperones and binding partners, leading to degradation of the nascent polypeptide, ribosome recycling and mRNA decay (Lykke-Andersen and Bennett 2014). I investigated whether CLUH plays an obvious role in this process, by checking on any effect the loss of CLUH may have on association of mRNA with late endosomes. I found an overall slightly decreased time of association and a seemingly

more unstable connection of late endosomes (marked with GFP-RAB7) with *Mdh2* and *ActB* mRNA in CLUH KO axons. These effects were however not of a magnitude to suggest they would induce mRNA decay, but rather suggest a general endosomal phenotype which could cause reduced tethering capability of late endosomes. Such a phenotype was however not visually obvious, as abundance and morphology of RAB7 positive vesicles in axons looked similar in WT and CLUH KO (Fig 14 A-E). Additional association studies with other types of endosomes and the ER could further elucidate whether CLUH KO has a relevant effect on association with the neuronal NEM protein translation pipeline proposed by current literature (Hees, Segura, et al. 2024).

By comparing my association results in axons of primary motoneurons to other similar studies I find some interesting similarities and differences. The colocalisation of endogenous *Mdh2* mRNA with early endosomes like in my pilot, has also been studied by another group. While they report no comparison to other types of endosomal markers, the 17% of colocalisation reported for *Mdh2* mRNA and EEA1 marked early endosomes compares quite well with my results, considering different methods and thresholds of analysis (Schuhmacher et al. 2023). One of the clearest take-aways from the neuronal pilot experiment was the much higher colocalisation of *Mdh2-MS2* mRNA with late endosomes (GFP-RAB7) than with mitochondria (MTS-GFP). A recent study performed a similar experiment on another NEM mRNA, *Cox7c*, showing the opposite result. There, endogenous *Cox7c* mRNA spots had a colocalisation of 60% with mitochondria and only 10% with late endosomes in axons of primary motoneurons. *Cox7c-CFP-MS2* even colocalised always with mitochondria and only about 25% of the spots also colocalised with lysosomes (Cohen et al. 2022). Thus, clearly not all mitochondrial mRNAs follow the same path of association in axons, but might even show opposing patterns, like *Mdh2* and *Cox7c*. It is interesting to see that also Cioni et al. (2019) have found that Cy3-RNA granules have a decreased movement speed when associated to GFP-Rab7a compared to when they are alone. This is a direct confirmation of the transition to a lower state-of-motion I found for *Mdh2-MS2* and *ActB-MS2* mRNA when they associated to GFP-RAB7. Furthermore, I observed that the vast majority of *Mdh2-MS2* and *ActB-MS2* mRNA was stationary or oscillatory when associated to GFP-RAB7 and only around 20% exhibited directed movement. These findings go well in line with what Cioni et al. (2019) report for general Cy3-RNA granules (28% directed) and endogenous *ActB* mRNA (20% directed). Therefore, I confirmed the idea that the function of mRNA tethering to endosomes is not mainly related to transport but rather to localisation to a specific spot, potentially important for protein translation, maturation and import.

In HeLa cells I replicated the finding from the primary motoneurons that CLUH KO did not affect the percentage of *Mdh2* or *ActB* mRNA colocalisation with RAB7. However, the

percentages of colocalisation were on very different levels, much higher in axons than HeLa. There likely were several reasons for this inconsistency. Firstly, I used different ways of analysis for both experiments: While HeLa cells were analysed for colocalisation in a very stringent and automated way, axons were analysed by manually assessed association. Secondly, there was likely an influence by looking at endogenous mRNA and RAB7 or overexpressed versions of both. Lastly, the HeLa cells visually had much less RAB7 signal than the neurons, likely due to the overexpression. Interestingly, in HeLa cells *Atp5a* had a significantly lower colocalisation to RAB7 than *ActB* mRNA. However, the percentages were very low for both mRNAs thus the relevance might not be very high. The much studied *ActB* mRNA has been found before to colocalise with early and late endosomes, as identified by imaging and co-IP in *Xenopus* axons (Cioni et al. 2019). No such data set exists for *Atp5a* and late endosomes, but only for another subunit of the ATP-Synthase, *Atp5b*, to be colocalising with early endosomes in axons of primary motoneurons (Schuhmacher et al. 2023). Thus, from the literature it seems likely that both mRNAs associate to some part of the endolysosomal system, but it is unclear whether *ActB* might have a slightly higher affinity to late endosomes than *Atp5a* mRNA.

5.2.4 CLUH acts on target mRNAs away from mitochondria and late endosomes

In the HeLa experiment I did not only investigate colocalisation of mRNAs with late endosomes in WT and CLUH KO, but also with mitochondria and CLUH itself. Colocalisation of mRNAs to mitochondria was equally unaffected by loss of CLUH as colocalisation to late endosomes. These results confirm previously published findings on *Atp5a* mRNA and mitochondria made with confocal imaging in MEFs (Schatton et al. 2017). Additional confirmation comes from Hémono, Haller, et al. (2022) who found that around 2% of *Atp5a* mRNA was localised to the crude mitochondrial fraction of HCT116 cells and this percentage was not changed in CLUH KO. In this study they look at nine other CLUH target mRNAs of which four are unaffected in their mitochondrial localisation, while the other five actually exhibit an increased presence in the crude mitochondrial fraction of CLUH KO. Therefore, localisation of CLUH target mRNAs to mitochondria may depend on the specific mRNA.

I have also identified a specific colocalisation between CLUH and *Atp5a* mRNA with 10% of the *Atp5a* mRNA spots, which was neither found on mitochondria nor late endosomes. Thus, I have presented the first imaging-based confirmation of the preferential interaction between a target mRNA and CLUH, which is however not happening on mitochondria or late endosomes. These results stand in contrast to some previous data from the lab, observing a specific colocalisation of CLUH to target mRNAs *Hadha* and *Pcx* under HBSS starvation in distinct granules but not in basal conditions (Pla-Martín et al. 2020). These granules were absent from my cells under basal conditions. The reason for the different observations could be the use of

another cell line (Hepatocytes and HeLa), the mRNAs checked, and the FISH method used. Another big impact was likely the lower resolution of confocal limited microscopy, which was used in the previous study and potentially prevented any detailed analysis of the busy cytosolic CLUH signal. A similar report of CLUH and mRNA co-localisation only in specific granules comes from a new preprint using *Drosophila* ovaries, which finds Clu granules next to mitochondria, which are dissolved upon RNase treatment, suggesting those granules to contain RNA (Miller-Fleming et al. 2024).

The Cluh target mRNA *Mdh2* exhibited a different localisation than *Atp5a*, as it showed no preferential colocalisation to CLUH over *ActB*. One of the reasons for this difference could be that CLUH interaction with its target mRNAs is dynamic, i.e. CLUH does not interact with all of them all the time. ATP5a is a subunit of the ATP-synthase, which is part of OXPHOS, while MDH2 is part of the citric acid cycle. As presence of CLUH negatively regulates mRNA and protein level, it could be hypothesised that the binding of CLUH is dependent on the specific metabolic needs of the cell in the current condition. The active translation of mRNAs has for example been found to be a requirement for CLUH binding to some target mRNAs (Hémono, Haller, et al. 2022). Specific treatments of the cell, like blocking (Antimycin A inhibits complex III and Oligomycin inhibits complex V) or boosting OXPHOS (Galactose media prevents glycolysis) could help to identify whether demand of a certain pathway like OXPHOS, influences the binding of CLUH to related and unrelated mRNAs. Another possible reason for the difference between *Mdh2* and *Atp5a* mRNA is the overall low number of spots per cell detected for *Mdh2*, with less than half of the *Atp5a* mRNA. With only 5.7 spots per cell in CLUH KO, any observations for *Mdh2* were therefore substantially more susceptible to influences by artifactually signal. Such off-target signal is generally unlikely due to high specificity of the FISH probes and is usually mostly found in the nucleus, which was excluded from analysis, but can also occur in rare occasions in the cytosol.

5.2.5 Diminished local translation is likely the cause for the failure to maintain the axonal mitochondrial proteome under KO of CLUH

In general, local translation in axons of primary motoneurons does appear to be affected by loss of CLUH, but not at the steps investigated by me. Local translation is likely the cause of diminished mitochondrial protein levels in axons, as it was identified that abundance of CLUH target mRNAs (*Atp5a*, *Pink1*) is reduced in CLUH KO and general axonal translation is abolished (Zaninello et al. 2024). I found that the reduced axonal transcript abundance is likely not caused by mRNA transport or localisation of mRNA to late endosomal translation hubs. Instead, the cause is most probably due a decreased mRNA stability similar to what has been found in CLUH KO MEF cells (Schatton et al. 2017).

One possible pathway affecting mRNA stability that has not been greatly explored yet is the co-translational quality control, which makes sure defective translation complexes with problematic transcripts, nascent polypeptides or translation machinery are resolved (Lykke-Andersen and Bennett 2014). A strong hint towards this direction also came from our most recent publication which found overexpression of the ribosome recycling factor ABCE1 to rescue mRNA and translation defects, and growth cone size in CLUH KO neurons (Zaninello et al. 2024). This sparked the idea that translation may be stalled on CLUH target mRNAs in axons, triggering quality control mechanisms like the stalling dependent no-go decay or ribosome associated protein quality control (Brandman and Hegde 2016; Joazeiro 2019; Lykke-Andersen and Bennett 2014). The following degradation of mRNA, nascent polypeptide, and ribosomes, then diminishes overall axonal translation due to lack of ribosomes. By enhancing the ribosomes recycling process with ABCE1 overexpression, overall translation was rescued and even the CLUH target transcript decay was prevented. Whether the ABCE1 overexpression really prevents a possible stalling caused by CLUH deficiency and protein levels of target encoded proteins are equally rescued is currently unknown. Therefore, to provide more evidence for this hypothesis it would be good to further investigate whether CLUH deficiency actually triggers some sort of stalling or similar on CLUH target mRNAs, in combination with the recruitment of proteins of the co-translational quality control. This could for example be achieved by utilising the MS2-MCP constructs for an IP rather than imaging (Tsai et al. 2011; Slobodin and Gerst 2010; Eliscovich and Singer 2017). Such an experiment is only realistic in a simpler model like HeLa cells, but an IP of mRNAs in WT and CLUH KO condition could help to identify whether the interactors of these mRNAs change in some way, like by recruiting more proteins related to pathways like the no-go mediated decay. Assuming that the CLUH target specific effects are detectable on a systemic level, one could also explore a general increase in stalling by measuring eIF2 α and GCN2 phosphorylation or a polysome profiling after RNase digest (Wu et al. 2020) and as a part of the co-translational quality control pathways an increase in ubiquitylation of nascent polypeptides and ribosomes in CLUH KO (Lykke-Andersen and Bennett 2014).

In addition to an approach targeted at the assumed cause for reduced local translation, it is also necessary to more directly prove the influence of CLUH on local translation of target mRNAs. On an omics level one could feed the cells with a methionine analogue or a pulse of SILAC medium to detect newly synthesised peptides in MS (Zappulo et al. 2017). Putting this data in relation to the local transcriptome in WT and CLUH KO would give a general overview of the effect of CLUH on translation activity on specific transcripts. A more specific way could be to use imaging to explore the translation activity of mRNAs in axons or when localised to late endosomes in a WT and CLUH KO background. This could be done by combining my MS2-

MCP constructs with an additional Sun-Tag, that allows to visualise newly synthesised proteins in live (Wu et al. 2016). Alternatively, similar information could be achieved by a Puro- or FUNCAT-PLA approach, where specific newly synthesised proteins are visualised by a proximity ligation between an antibody of a specific protein and newly synthesised peptides (Tom Dieck et al. 2015). Assuming the base CLUH functions are conserved between HeLa and neurons, one could also repeat the mRNA and CLUH colocalisation experiment in HeLa cells, but with blocking (Homoharringtonine, Puromycin and Cycloheximide block elongation, Rapamycin inhibits mTOR) or boosting of translation (Insulin stimulates mTOR), to see how the presence of translation influences CLUH preferential binding to *Atp5a* mRNA.

5.3 Limitations of the experimental models

5.3.1 Primary moto neurons

For all experiments on neurons, I have used primary motoneuron cultures. It is important to note that those were embryonic, developing neurons, without functional synaptic connections, no myelination and much shorter length than *in vivo*. Thus, observations from my model may not align with observations *in vivo* and may also not be directly translatable to humans. For example, the axonal mitochondrial proteome changes, like the loss of OXPHOS and citric acid cycle proteins, may be caused by the usage of developing axons with no meaningful synapses and thus action potentials to process. It is entirely possible that in mature axons mitochondria change their proteome by upregulation of translation and mRNA transport of those pathways. Using a MFDs with a third chamber, so primary motoneurons are co-cultured with myoblasts to create neuro muscular junctions and culturing the neurons for longer times, could be an approach to counteract these shortcomings of my model. Using *in vivo* post-natal neurons and an approach where the whole axonal proteome, including mitochondria can be analysed, would be another solution.

Another thing to consider in the culture of neurons in the MFD, is the lack of glia cells on the axonal side and its possible impact on proteomic changes. They may have only been few astrocytes in the WC compartment but contact to those could still change metabolic needs of those neurons. For example, astrocytic mitochondria have been shown to more efficiently metabolise fatty acids than neurons (Fecher et al. 2019) and astrocytes can provide lactate to neurons, which is transformed to pyruvate for the citric acid cycle (Bélanger, Allaman, and Magistretti 2011).

Primary cultures especially of neurons usually suffer from large variability between cultures, caused by the different source individuals and the preparation quality. Furthermore, the high variability comes in combination with limited availability. Thereby, leading to often times low

numbers of N with high standard deviation and decreasing the chance of identifying smaller differences between samples. Additionally, doing imaging studies where only a small sub population of the post-mitotic neurons is transfected, the number of axons available for imaging ends up very low.

5.3.2 HeLa cells

HeLa cells are an immortal cell line, sourced from a cervical cancer of woman called Henrietta Lacks. They were used by me in the super resolution imaging of mRNA, CLUH and organelles. As a human cancer cell line, results from these cells cannot always be directly translated to other models and even the human, due to their genetic changes, such as mutations and karyotype changes. However, the association of the RNA binding protein CLUH to target mRNA can be assumed to be a conserved molecular mechanism. It is also important to note that the knockout of CLUH from the HeLa cells was done by CRISPR/Cas, followed by clonal selection. It is therefore possible that the surviving clones developed adaptations to the loss of CLUH which could create differences compared to an acute depletion.

Appendix

Table S1: Proteome of mitochondrial proteins in axons and the whole cell. Proteins sorted by Log₂ fold change from highest to lowest.

PG. Genes	PG. Protein Groups	Sub Mito Localisation	Cluh target	Significant (Ax-WC)	q-value (Ax-WC)	-Log10 p-value (Ax-WC)	Log2 fold change (Ax-WC)	Median AX	Median WC
Coq6	Q8R1S0	MIM	+	+	0.00	3.06	6.24	-5.19	-13.40
Mrps25	Q9D125	Matrix		+	0.00	6.12	6.18	-2.67	-9.65
Otc	P11725	Matrix		+	0.00	6.25	5.92	-8.90	-15.12
Aldh1a7	O35945	unknown		+	0.00	3.50	4.55	-11.60	-17.23
Ckmt2	Q6P8J7	MIM		+	0.00	2.63	4.36	-11.56	-15.00
Decr1	Q9CQ62	Matrix	+	+	0.00	8.06	3.95	-7.90	-11.74
Slc25a31	Q3V132	MIM		+	0.00	4.26	3.50	-12.66	-15.67
Cps1	Q8C196	Matrix	+	+	0.00	6.48	3.49	-11.88	-15.08
Acss3	Q14DH7	Matrix		+	0.00	2.86	3.35	-14.34	-17.55
Rpia	P47968	Matrix		+	0.00	2.07	3.19	-11.34	-14.76
Coq8a	Q60936	MIM			0.08	0.74	2.96	-12.04	-16.32
Trmt10c	Q3UFY8	Matrix	+	+	0.00	5.67	2.86	-11.02	-13.70
Acad12	D3Z7X0	Matrix		+	0.00	1.83	2.52	-13.57	-14.84
Mthfd2	P18155	Matrix		+	0.00	4.10	2.51	-11.14	-13.78
Tomm22	Q9CPQ3	MOM		+	0.00	3.13	2.49	-8.75	-11.48
Aldh2	P47738	Matrix	+	+	0.00	5.93	2.35	-6.56	-8.74
Adhfe1	Q8R0N6	Matrix		+	0.00	5.32	2.17	-9.53	-11.66
Cat	P24270	IMS		+	0.00	6.06	2.16	-6.61	-8.93
Crot	Q9DC50	unknown		+	0.00	1.92	2.14	-11.93	-13.26
Hspd1	P63038	Matrix	+	+	0.00	4.97	1.89	-4.59	-6.45
Acaa2	Q8BWT1	Matrix	+	+	0.00	4.95	1.89	-8.55	-10.17
Acaa1a	Q921H8	Matrix		+	0.00	3.86	1.74	-9.57	-11.34
Sdha	Q8K2B3	MIM	+	+	0.00	5.83	1.58	-6.74	-7.94
Tst	P52196	Matrix	+	+	0.03	1.02	1.48	-12.27	-13.70
Pycr2	Q922Q4	Matrix		+	0.00	1.82	1.41	-9.96	-11.29
Txnrd2	Q9JLT4	Matrix	+	+	0.03	1.01	1.41	-14.30	-15.03
Echs1	Q8BH95	Matrix	+	+	0.00	4.15	1.32	-7.95	-9.25
Cpox	P36552	MIM	+		0.13	0.65	1.27	-12.03	-15.04
Cryz	P47199	Matrix		+	0.00	3.61	1.23	-10.07	-11.35
Dnajc11	Q5U458	MOM		+	0.00	3.02	1.15	-9.42	-10.93
Hadh	Q61425	Matrix		+	0.00	2.60	1.10	-9.01	-10.07
Slc25a13	Q9QXX4	MIM			0.26	0.47	1.09	-13.85	-14.72
Ccdc51	Q3URS9	MIM	+	+	0.04	0.99	1.09	-12.53	-14.16
Lypla1	P97823	unknown		+	0.00	3.48	1.08	-9.47	-10.59
Aldh9a1	Q9JLJ2	Matrix	+	+	0.02	1.14	1.07	-9.45	-10.25

Acadl	P51174	MIM	+		0.13	0.68	1.06	-10.21	-9.94
Park7	Q99LX0	MOM		+	0.00	3.11	0.90	-7.82	-8.75
Pcca	Q91ZA3	Matrix	+	+	0.00	2.61	0.85	-10.52	-11.32
Shmt2	Q9CZN7	Matrix			0.18	0.60	0.84	-11.53	-12.68
Ethel	Q9DCM0	Matrix		+	0.00	2.47	0.82	-9.55	-10.37
Ppif	Q99KR7	Matrix	+	+	0.00	2.27	0.76	-11.56	-12.14
Hdhd5	Q91WM2	Matrix			0.15	0.67	0.73	-13.75	-14.34
Mpc1	P63030	MIM			0.46	0.30	0.71	-11.98	-13.02
Fdps	Q920E5	MIM		+	0.01	1.80	0.65	-6.29	-6.82
Atp5mf	P56135	MIM		+	0.00	3.22	0.64	-6.39	-7.00
Slc25a4	P48962	MIM		+	0.00	3.59	0.61	-5.25	-6.01
Slc25a5	P51881	MIM		+	0.01	1.93	0.61	-5.31	-6.32
Timm8a1	Q9WVA2	MIM			0.17	0.68	0.60	-9.84	-10.25
Fastkd2	Q922E6	Matrix			0.48	0.29	0.56	-15.10	-15.21
Atp5if1	O35143	Matrix		+	0.02	1.67	0.55	-7.51	-7.95
Acot7	Q91V12	Matrix		+	0.03	1.43	0.50	-5.97	-6.67
Acly	Q91V92	Matrix			0.06	1.22	0.48	-7.66	-7.97
Mt-Cyb	P00158	MIM			0.49	0.29	0.44	-11.92	-12.40
Hspa9	P38647	Matrix	+		0.10	1.11	0.38	-6.96	-7.36
Mdh2	P08249	Matrix	+		0.15	0.88	0.37	-5.48	-5.42
Ak2	Q9WTP6	IMS			0.53	0.26	0.37	-9.74	-9.59
Mtco2	P00405	MIM			0.12	1.02	0.35	-7.83	-8.04
Slc25a46	Q9CQS4	MOM			0.68	0.15	0.34	-11.40	-12.52
Acs11	P41216	MOM			0.64	0.18	0.33	-13.06	-12.31
Trap1	Q9CQN1	Matrix			0.36	0.49	0.29	-6.17	-6.45
Cs	Q9CZU6	Matrix			0.18	1.05	0.25	-6.80	-6.99
Ldhb	P16125	unknown			0.44	0.39	0.24	-6.21	-6.65
Hspe1	Q64433	Matrix			0.40	0.47	0.24	-5.67	-6.16
Prdx2	Q61171	unknown			0.57	0.28	0.17	-5.46	-5.95
Mrps16	Q9CPX7	Matrix			0.53	0.35	0.17	-11.30	-11.31
Hint3	Q9CPS6	unknown			0.78	0.11	0.16	-12.74	-12.63
Mpc2	Q9D023	MIM			0.85	0.07	0.16	-11.12	-11.30
Nipsnap3									
b	Q9CQE1	Matrix			0.76	0.13	0.14	-9.16	-9.19
Prkaca	P05132	MIM			0.67	0.21	0.13	-11.93	-12.24
Prdx5	P99029	Matrix			0.79	0.14	0.07	-7.31	-7.27
Slc25a3	Q8VEM8	MIM			0.77	0.17	0.06	-6.48	-6.76
Acot13	Q9CQR4	Matrix			0.94	0.03	0.05	-11.04	-10.67
Dld	O08749	Matrix	+		0.93	0.03	0.04	-10.88	-10.72
Fh	P97807	Matrix	+		0.97	0.02	0.01	-8.15	-8.27
Atp5f1b	P56480	MIM			0.94	0.04	-0.01	-4.87	-4.83
Ndufa4	Q62425	MIM			0.92	0.06	-0.02	-6.43	-6.35
Ndufa12	Q7TMF3	MIM			0.90	0.06	-0.03	-9.60	-9.49
Gars1	Q9CZD3	Matrix			0.89	0.06	-0.05	-8.70	-8.83
Idi1	P58044	Matrix			0.81	0.11	-0.07	-9.29	-9.27
Cox7b	P56393	MIM			0.86	0.07	-0.08	-9.32	-8.82
Aifm1	Q9Z0X1	MIM	+		0.86	0.07	-0.09	-10.62	-10.36

Sod1	P08228	IMS		0.80	0.10	-0.12	-11.16	-10.56
Phb1	P67778	MIM		0.71	0.18	-0.12	-7.58	-7.61
Nif3l1	Q9EQ80	Matrix		0.62	0.28	-0.12	-11.85	-11.85
Eci1	P42125	Matrix		0.90	0.04	-0.12	-10.93	-11.18
Got2	P05202	MIM		0.49	0.50	-0.13	-6.53	-6.27
Hint1	P70349	unknown		0.72	0.16	-0.13	-5.97	-6.22
Mtfr1l	Q9CWE0	unknown		0.84	0.07	-0.15	-12.63	-13.31
Fam210a	Q8BGY7	MIM	+	0.78	0.11	-0.16	-12.85	-11.94
Dbt	P53395	Matrix	+	0.53	0.35	-0.16	-12.17	-11.79
Atp5f1a	Q03265	MIM	+	0.33	0.84	-0.17	-4.63	-4.40
Casp3	P70677	IMS		0.61	0.24	-0.17	-8.42	-8.28
Phb2	O35129	MIM		0.43	0.51	-0.18	-7.50	-7.20
Cox7c	P17665	MIM		0.33	0.65	-0.21	-7.49	-7.32
Mtnd5	P03921	MIM		0.75	0.12	-0.22	-13.33	-13.38
Guk1	Q64520	Matrix		0.46	0.37	-0.24	-10.95	-10.75
Csl	Q80X68	Matrix		0.11	1.56	-0.25	-7.03	-6.95
Vdac1	Q60932	MOM		0.25	0.77	-0.25	-6.24	-5.94
Mff	Q6PCP5	MOM		0.50	0.32	-0.25	-10.22	-10.24
Cmc1	Q9CPZ8	IMS		0.46	0.36	-0.26	-10.97	-11.06
Bcl2l13	P59017	MOM		0.38	0.47	-0.28	-11.01	-10.68
Fasn	P19096	IMS		0.31	0.58	-0.28	-8.95	-8.48
Aco2	Q99KI0	Matrix	+	0.22	0.78	-0.30	-6.96	-6.60
Cox20	Q9D7J4	MIM		0.68	0.16	-0.31	-12.14	-11.15
Cycs	P62897	IMS		0.12	1.09	-0.32	-6.57	-6.33
Arl2	Q9D0J4	IMS		0.52	0.28	-0.32	-10.18	-9.79
Atp5f1e	P56382	MIM		0.16	0.90	-0.33	-7.19	-6.87
Prdx6	O08709	unknown		0.40	0.40	-0.34	-8.60	-8.03
Tomm5	B1AXP6	MOM		0.28	0.57	-0.34	-8.95	-8.60
Atp5f1c	Q91VR2	MIM		0.06	1.47	-0.35	-6.82	-6.27
Sdhc	Q9CZB0	MIM	+	0.33	0.48	-0.37	-11.50	-11.53
Pccb	Q99MN9	Matrix	+	0.43	0.36	-0.37	-11.55	-11.82
Ndufs4	Q9CXZ1	MIM		0.22	0.66	-0.40	-10.98	-10.49
Atp5mk	Q78IK2	MIM	+	0.03	1.71	-0.44	-6.72	-6.28
Nsun2	Q1HFZ0	Matrix		0.52	0.26	-0.44	-11.55	-11.46
Etfb	Q9DCW4	Matrix		0.41	0.37	-0.44	-9.31	-8.45
Ndufb6	Q3UIU2	MIM		0.13	0.86	-0.46	-11.75	-11.12
Dnm1l	Q8K1M6	MOM		0.10	0.96	-0.46	-9.26	-8.90
Ndufb1l	O09111	MIM	+	0.02	1.90	-0.46	-9.55	-8.99
Atp5po	Q9DB20	MIM	+	0.02	1.80	-0.46	-6.89	-6.41
Vdac3	Q60931	MOM	+	0.01	1.99	-0.48	-6.90	-6.30
Ndufs7	Q9DC70	MIM	+	0.43	0.34	-0.49	-11.62	-10.07
Cox6c	Q9CPQ1	MIM	+	0.02	1.64	-0.49	-6.22	-5.90
Qdpr	Q8BVI4	Matrix		0.05	1.21	-0.51	-9.81	-9.11
Vdac2	Q60930	MOM	+	0.01	2.22	-0.52	-6.83	-6.41
Atp5pf	P97450	MIM	+	0.01	1.84	-0.53	-7.48	-6.85
Idh2	P54071	Matrix	+	0.44	0.32	-0.54	-11.13	-10.15
Poldip2	Q91VA6	Matrix	+	0.55	0.23	-0.56	-11.35	-12.15

Prdx3	P20108	Matrix	+	+	0.00	2.30	-0.56	-8.93	-8.39
Ndufa3	Q9CQ91	MIM			0.20	0.62	-0.56	-9.92	-9.78
Snap29	Q9ERB0	IMS			0.12	0.80	-0.59	-11.19	-10.25
Ghitm	Q91VC9	MIM	+		0.07	1.02	-0.60	-11.00	-10.90
Cox6a1	P43024	MIM			0.44	0.32	-0.61	-11.64	-11.48
Mccc1	Q99MR8	Matrix	+		0.36	0.39	-0.62	-13.81	-12.23
Atp5pd	Q9DCX2	MIM		+	0.00	2.60	-0.63	-6.91	-6.36
Auh	Q9JLZ3	Matrix	+	+	0.02	1.42	-0.64	-11.07	-10.46
Acadm	P45952	Matrix	+		0.25	0.52	-0.64	-10.65	-9.93
Hibadh	Q99L13	Matrix	+		0.06	1.02	-0.67	-11.42	-11.11
Slc25a1	Q8JZU2	MIM		+	0.01	1.57	-0.68	-9.27	-8.82
Mrrf	Q9D6S7	Matrix		+	0.00	2.42	-0.70	-12.53	-11.77
Paics	Q9DCL9	Matrix			0.10	0.84	-0.70	-9.98	-9.38
Sucla2	Q9Z2I9	Matrix		+	0.00	2.06	-0.70	-9.33	-8.60
Tbrg4	Q91YM4	Matrix			0.17	0.63	-0.71	-12.26	-12.05
Cox7a2	P48771	MIM		+	0.00	3.32	-0.71	-7.55	-6.66
Cox6b1	P56391	MIM		+	0.00	2.11	-0.71	-8.38	-7.53
Glr5	Q80Y14	Matrix		+	0.03	1.24	-0.72	-10.89	-10.27
Naxe	Q8K4Z3	Matrix		+	0.01	1.56	-0.73	-11.42	-10.80
Cyb5r3	Q9DCN2	MOM		+	0.00	2.27	-0.73	-8.87	-8.33
Oxct1	Q9D0K2	Matrix	+	+	0.00	3.54	-0.73	-8.31	-7.56
Suclg2	Q9Z2I8	Matrix			0.10	0.83	-0.73	-12.64	-12.06
Cox4i1	P19783	MIM		+	0.01	1.72	-0.75	-7.55	-7.01
Ndufb3	Q9CQZ6	MIM		+	0.01	1.84	-0.75	-10.08	-9.16
Timm22	Q9CQ85	MIM			0.08	0.88	-0.76	-11.51	-11.50
Tufm	Q8BFR5	Matrix		+	0.00	2.26	-0.76	-8.65	-8.02
Idh3a	Q9D6R2	Matrix		+	0.00	3.48	-0.76	-8.14	-7.54
Slc25a11	Q9CR62	MIM		+	0.00	5.01	-0.77	-9.64	-8.81
Armc10	Q9D0L7	MOM		+	0.03	1.22	-0.79	-11.79	-11.03
Sfxn1	Q99JR1	MIM			0.07	0.91	-0.81	-9.04	-8.85
Timm17b	Q9Z0V7	MIM			0.10	0.80	-0.82	-11.60	-11.34
Fis1	Q9CQ92	MOM		+	0.00	2.15	-0.82	-11.19	-10.26
Gatm	Q9D964	Matrix	+	+	0.00	2.69	-0.84	-12.23	-11.22
Acat1	Q8QZT1	Matrix	+	+	0.01	1.65	-0.86	-8.29	-7.61
Fahd2	Q3TC72	Matrix			0.10	0.79	-0.86	-12.72	-11.77
Ndufs8	Q8K3J1	MIM		+	0.01	1.57	-0.88	-9.87	-9.24
Etfdh	Q921G7	MIM	+		0.37	0.36	-0.88	-13.99	-11.22
Fundc2	Q9D6K8	MOM		+	0.00	1.84	-0.89	-10.68	-10.00
Nme3	Q9WV85	MOM			0.18	0.59	-0.91	-11.58	-11.30
Atp5pb	Q9CQQ7	MIM		+	0.01	1.63	-0.92	-7.75	-7.14
Mtstp8	P03930	MIM		+	0.00	3.39	-0.93	-7.49	-6.67
Apoo	Q9DCZ4	MIM		+	0.00	3.17	-0.93	-10.38	-9.70
Mtnd4	P03911	MIM		+	0.00	3.64	-0.94	-10.76	-9.93
Dcakd	Q8BHC4	Membrane		+	0.00	2.77	-0.95	-10.06	-9.08
Timm44	O35857	MIM		+	0.03	1.10	-0.96	-11.58	-11.16
Glod4	Q9CPV4	Matrix		+	0.00	2.38	-0.96	-10.05	-9.05
Sdhb	Q9CQA3	MIM	+	+	0.00	4.30	-0.97	-9.65	-8.64

Dlst	Q9D2G2	Matrix	+	+	0.00	3.46	-0.97	-9.40	-8.43
Uqerc2	Q9DB77	MIM	+	+	0.00	2.20	-0.97	-8.61	-7.79
Timm10	P62073	MIM		+	0.00	2.79	-0.98	-9.46	-8.40
Agk	Q9ESW4	MIM	+	+	0.00	2.04	-0.98	-10.41	-9.64
Ndufs3	Q9DCT2	MIM		+	0.02	1.27	-0.99	-9.04	-8.47
Mrps17	Q9CQE3	Matrix		+	0.01	1.50	-1.00	-12.10	-11.05
Grpel1	Q99LP6	Matrix		+	0.00	2.40	-1.03	-10.31	-9.44
Armex2	Q6A058	Membrane			0.06	0.91	-1.05	-14.79	-13.40
Akr7a2	Q8CG76	Matrix		+	0.01	1.54	-1.07	-12.97	-11.45
Ndufb5	Q9CQH3	MIM		+	0.00	4.28	-1.08	-10.12	-9.00
Tomm40	Q9QYA2	MOM		+	0.00	4.72	-1.08	-10.68	-9.79
Bax	Q07813	MOM		+	0.00	2.47	-1.08	-9.67	-8.64
Ndufa2	Q9CQ75	MIM		+	0.00	2.05	-1.10	-10.61	-9.39
Pdhb	Q9D051	Matrix	+	+	0.00	4.41	-1.10	-8.83	-7.64
Samm50	Q8BGH2	MOM		+	0.00	2.99	-1.11	-11.41	-10.23
Atp5mg	Q9CPQ8	MIM		+	0.00	1.64	-1.12	-9.44	-8.16
Ndufb8	Q9D6J5	MIM		+	0.04	1.01	-1.14	-11.49	-10.15
Mrps9	Q9D7N3	Matrix		+	0.01	1.30	-1.15	-14.40	-13.51
Txnrd1	Q9JMH6	unknown		+	0.00	1.94	-1.15	-11.95	-10.89
Gdap1	O88741	MOM		+	0.02	1.20	-1.16	-10.14	-9.44
Ndufb9	Q9CQJ8	MIM		+	0.01	1.47	-1.16	-13.09	-11.52
Uqerc1	Q9CZ13	MIM		+	0.00	3.69	-1.18	-9.27	-8.26
Acadv1	P50544	MIM	+		0.20	0.54	-1.19	-13.06	-11.68
Acadsb	Q9DBL1	Matrix	+	+	0.00	5.91	-1.20	-11.50	-10.20
Timm9	Q9WV98	MIM		+	0.00	1.67	-1.20	-9.07	-8.28
Nfs1	Q9Z1J3	Matrix	+	+	0.01	1.53	-1.20	-13.21	-12.44
Atp5me	Q06185	MIM		+	0.00	4.51	-1.22	-7.47	-6.23
Slc25a12	Q8BH59	MIM		+	0.00	2.36	-1.24	-9.24	-8.23
Bdh1	Q80XN0	MIM	+	+	0.00	5.38	-1.24	-9.13	-7.86
Coa3	Q9D2R6	MIM		+	0.00	3.90	-1.24	-10.41	-9.25
Aldh4a1	Q8CHT0	Matrix	+	+	0.00	2.02	-1.25	-13.06	-11.21
Ogdh	Q60597	Matrix	+	+	0.00	2.99	-1.25	-10.72	-9.25
Atad3	Q925I1	MIM		+	0.00	1.85	-1.26	-11.85	-10.21
Glud1	P26443	Matrix	+	+	0.00	6.58	-1.27	-8.70	-7.46
Immt	Q8CAQ8	MIM	+	+	0.00	3.96	-1.27	-9.87	-8.42
Mrpl21	Q9D1N9	Matrix			0.09	0.76	-1.27	-11.77	-11.78
Atp5f1d	Q9D3D9	MIM		+	0.00	4.36	-1.27	-7.81	-6.80
Suclg1	Q9WUM5	Matrix		+	0.00	1.78	-1.30	-9.09	-8.26
Hadha	Q8BMS1	MIM	+		0.11	0.71	-1.30	-11.30	-10.00
Mrpl28	Q9D1B9	Matrix		+	0.00	1.87	-1.31	-13.30	-11.26
Ndufab1	Q9CR21	MIM	+	+	0.01	1.49	-1.31	-10.68	-9.14
Gfm1	Q8K0D5	Matrix	+		0.06	0.85	-1.32	-13.57	-12.24
Pmpcb	Q9CXT8	Matrix		+	0.00	1.53	-1.32	-12.48	-11.32
Tomm70	Q9CZW5	MOM		+	0.00	1.91	-1.35	-10.52	-9.13
Aldh6a1	Q9EQ20	MIM	+	+	0.00	1.71	-1.36	-12.49	-11.26
Ociad1	Q9CRD0	MOM		+	0.00	4.42	-1.36	-10.82	-9.37
Mrpl12	Q9DB15	Matrix		+	0.00	4.95	-1.38	-9.69	-8.27

Uqcrq	Q9CQ69	MIM		+	0.00	7.07	-1.39	-9.67	-8.31
Timm50	Q9D880	MIM		+	0.00	2.12	-1.40	-11.05	-10.04
Hccs	P53702	IMS		+	0.00	2.29	-1.43	-13.30	-11.28
Sfxn3	Q91V61	MIM		+	0.00	4.81	-1.43	-10.67	-9.18
Nrdc	Q8BHG1	Matrix		+	0.00	3.86	-1.44	-12.82	-11.16
Myg1	Q9JK81	Matrix		+	0.00	4.99	-1.46	-12.89	-11.26
Ndufb4	Q9CQC7	MIM		+	0.00	2.54	-1.47	-8.87	-8.02
Ndufa5	Q9CPP6	MIM		+	0.00	4.45	-1.48	-10.21	-8.73
Gls	D3Z7P3	MIM	+	+	0.00	1.81	-1.49	-13.10	-11.31
Ndufs5	Q99LY9	MIM		+	0.00	1.85	-1.50	-10.70	-8.77
Gsr	P47791	Matrix		+	0.00	1.67	-1.50	-11.31	-10.29
Ndufa8	Q9DCJ5	MIM		+	0.00	3.69	-1.52	-9.21	-7.87
Clpp	O88696	Matrix	+	+	0.00	2.33	-1.53	-13.12	-11.36
Pdhx	Q8BKZ9	Matrix	+	+	0.00	2.98	-1.53	-12.80	-10.86
Prxl2a	Q9CYH2	Membrane		+	0.01	1.47	-1.54	-11.56	-10.21
Mrps28	Q9CY16	Matrix		+	0.00	1.77	-1.55	-11.81	-10.64
Tmem126a	Q9D8Y1	MIM		+	0.00	5.76	-1.56	-11.80	-10.39
EtfA	Q99LC5	Matrix	+	+	0.00	1.51	-1.57	-10.48	-9.55
Ndufs1	Q91VD9	MIM	+	+	0.00	3.57	-1.57	-10.37	-8.65
Sod2	P09671	Matrix		+	0.00	3.06	-1.58	-10.60	-9.25
Aldh5a1	Q8BWF0	Matrix	+	+	0.00	3.53	-1.58	-10.59	-9.11
Aldh1b1	Q9CZS1	Matrix	+	+	0.00	3.62	-1.58	-13.57	-11.86
Coasy	Q9DBL7	Matrix		+	0.00	3.49	-1.58	-13.11	-11.64
Mgst3	Q9CPU4	MOM		+	0.00	3.89	-1.59	-10.87	-9.25
Aldh7a1	Q9DBF1	Matrix	+	+	0.00	3.15	-1.59	-12.47	-11.42
Hsd17b4	P51660	unknown		+	0.00	6.71	-1.65	-11.04	-9.41
Slc25a18	Q9DB41	MIM		+	0.00	5.96	-1.65	-10.73	-9.46
Chchd3	Q9CRB9	MIM		+	0.00	3.02	-1.67	-10.40	-8.34
Afg3l2	Q8JZQ2	MIM		+	0.00	4.12	-1.67	-12.87	-10.95
Dnaja3	Q99M87	Matrix		+	0.00	3.77	-1.69	-12.60	-11.13
Nudt2	P56380	Matrix		+	0.00	2.65	-1.71	-11.55	-9.97
Uqcrfs1	Q9CR68	MIM	+	+	0.00	3.55	-1.72	-9.55	-7.61
Ecsit	Q9QZH6	MIM		+	0.00	6.14	-1.73	-13.76	-12.20
Nudt5	Q9JKX6	unknown		+	0.00	2.22	-1.73	-13.07	-11.46
Gcat	O88986	unknown		+	0.00	1.63	-1.73	-14.18	-12.27
Rdh14	Q9ERI6	Membrane		+	0.00	3.11	-1.73	-14.01	-12.06
Nln	Q91YP2	Matrix		+	0.00	4.52	-1.73	-11.87	-10.24
Mtch2	Q791V5	MOM		+	0.00	4.84	-1.73	-10.31	-8.68
Dlat	Q8BMF4	Matrix	+	+	0.00	5.37	-1.76	-10.91	-9.34
Slc25a25	A2ASZ8	MIM		+	0.00	3.28	-1.77	-12.97	-11.16
Mmut	P16332	Matrix		+	0.00	2.03	-1.77	-14.43	-12.14
Echdc1	Q9D9V3	unknown		+	0.00	3.06	-1.77	-13.17	-11.94
Slirp	Q9D8T7	Matrix		+	0.00	3.25	-1.79	-12.12	-10.76
Hadhb	Q99JY0	MIM	+	+	0.04	0.90	-1.81	-13.23	-10.19
Slc25a20	Q9Z2Z6	MIM		+	0.00	2.73	-1.81	-11.92	-10.41
Pam16	Q9CQV1	MIM		+	0.00	3.52	-1.83	-12.78	-11.03

Comt	O88587	Membrane		+	0.00	7.51	-1.83	-13.28	-11.54
Dap3	Q9ER88	Matrix		+	0.01	1.33	-1.84	-14.04	-11.06
Oat	P29758	Matrix	+	+	0.00	5.78	-1.86	-11.59	-9.86
Synj2bp	Q9D6K5	MOM		+	0.00	2.00	-1.87	-12.50	-10.96
Ndufv1	Q91YT0	MIM	+	+	0.00	3.78	-1.87	-10.91	-8.60
Acot9	Q9R0X4	MIM		+	0.00	4.46	-1.87	-12.36	-10.28
Ppa2	Q91VM9	Matrix	+	+	0.00	3.18	-1.89	-12.96	-10.50
Apool	Q78IK4	MIM		+	0.00	2.16	-1.90	-13.09	-10.84
Ndufa9	Q9DC69	MIM	+	+	0.02	1.13	-1.91	-12.81	-10.58
Plpbp	Q9Z2Y8	Matrix		+	0.00	3.25	-1.91	-12.29	-10.62
Plgrkt	Q9D3P8	Membrane		+	0.00	7.50	-1.94	-12.21	-10.36
Gatd3	Q9D172	Matrix		+	0.00	2.54	-1.95	-12.50	-10.08
Mrps23	Q8VE22	Matrix		+	0.00	3.53	-1.95	-11.88	-9.99
Ndufa10	Q99LC3	MIM	+	+	0.00	3.55	-1.96	-11.15	-9.27
Mrps22	Q9CXW2	Matrix		+	0.00	1.66	-1.97	-12.05	-11.11
Tmem65	Q4VAE3	MIM		+	0.00	5.80	-1.99	-11.73	-9.93
Uqcrh	P99028	MIM		+	0.00	4.86	-2.00	-9.66	-7.77
Pdha1	P35486	Matrix	+	+	0.00	5.57	-2.03	-9.23	-6.99
Atad1	Q9D5T0	MOM		+	0.00	4.25	-2.04	-12.34	-10.13
Nt5dc3	Q3UHB1	Matrix		+	0.00	3.15	-2.04	-12.31	-10.73
Ndufs2	Q91WD5	MIM	+	+	0.00	3.25	-2.07	-10.47	-8.82
Grsf1	Q8C5Q4	Matrix		+	0.00	3.89	-2.08	-13.88	-11.78
Oxa11	Q8BGA9	MIM	+	+	0.00	3.99	-2.08	-13.06	-10.70
Marchf5	Q3KNM2	MOM		+	0.00	5.57	-2.08	-12.68	-10.92
Arf5	P84084	unknown		+	0.00	4.27	-2.10	-11.55	-9.11
Cyc1	Q9D0M3	MIM		+	0.00	1.73	-2.10	-11.05	-9.99
Tsfm	Q9CZR8	Matrix	+	+	0.00	4.75	-2.10	-13.87	-11.30
Apex1	P28352	Matrix		+	0.02	1.11	-2.12	-10.35	-9.42
Lap3	Q9CPY7	Matrix		+	0.00	2.59	-2.15	-13.46	-10.94
Tfam	P40630	Matrix	+	+	0.00	3.78	-2.19	-13.23	-11.47
Mrpl55	Q9CZ83	Matrix		+	0.00	2.58	-2.20	-14.07	-12.33
Pmpca	Q9DC61	Matrix	+	+	0.00	5.43	-2.22	-13.71	-10.89
Abcb7	Q61102	MIM	+	+	0.00	6.41	-2.23	-14.36	-12.33
Mrpl22	Q8BU88	Matrix	+	+	0.00	5.38	-2.23	-13.33	-10.87
Slc30a9	Q5IRJ6	MIM	+	+	0.00	5.04	-2.25	-14.36	-12.24
Ogdhl	E9Q7L0	Matrix	+	+	0.00	2.37	-2.26	-14.52	-11.83
Bola1	Q9D8S9	Matrix		+	0.00	3.04	-2.27	-12.20	-10.08
Ndufa7	Q9Z1P6	MIM		+	0.00	4.11	-2.29	-10.77	-8.21
Timm8b	P62077	MIM		+	0.00	2.22	-2.29	-11.76	-9.46
Ndufb10	Q9DCS9	MIM		+	0.00	4.30	-2.29	-11.54	-9.35
Hibch	Q8QZS1	Matrix	+	+	0.00	2.35	-2.33	-14.11	-11.30
Scp2	P32020	MIM		+	0.00	1.91	-2.36	-11.76	-10.12
Mtch1	Q791T5	MOM		+	0.00	3.61	-2.39	-11.58	-9.16
Stoml2	Q99JB2	MIM		+	0.00	2.64	-2.41	-12.08	-10.17
Letm1	Q9Z2I0	MIM	+	+	0.00	5.08	-2.42	-12.99	-10.68
Ndufv2	Q9D6J6	MIM		+	0.00	4.59	-2.42	-12.39	-9.77
Lonp1	Q8CGK3	Matrix	+	+	0.00	3.87	-2.43	-13.23	-10.98

Ivd	Q9JHI5	Matrix		+	0.00	1.59	-2.44	-14.13	-9.94
Spyrd4	Q91WK1	Matrix	+	+	0.00	4.64	-2.46	-13.89	-11.52
Them4	Q3UUI3	MIM		+	0.00	3.16	-2.50	-14.20	-11.43
Ptges2	Q8BWM0	MIM		+	0.00	4.42	-2.51	-14.36	-11.79
Mtnd1	P03888	MIM		+	0.00	2.65	-2.51	-11.75	-8.34
Ndufs6	P52503	MIM		+	0.00	3.13	-2.53	-10.94	-9.28
Hsd1l	Q8BTX9	unknown		+	0.00	4.11	-2.56	-12.32	-9.74
Pgam5	Q8BX10	MOM		+	0.00	5.92	-2.58	-12.37	-9.93
Ckmt1	P30275	MIM		+	0.00	1.90	-2.61	-11.98	-9.69
Dhx30	Q99PU8	Matrix		+	0.00	2.59	-2.64	-14.03	-11.79
Abat	P61922	Matrix		+	0.00	6.66	-2.67	-11.31	-8.85
Naxd	Q9CZ42	MIM		+	0.00	2.53	-2.68	-13.06	-10.47
Ahcy1l	Q80SW1	MOM		+	0.00	5.35	-2.70	-12.16	-9.44
Acaca	Q5SWU9	Matrix		+	0.00	4.02	-2.70	-14.05	-11.46
Mtx2	O88441	MOM		+	0.00	4.84	-2.70	-13.14	-10.32
Nfu1	Q9QZ23	Matrix		+	0.00	4.56	-2.72	-12.44	-9.81
Rhot1	Q8BG51	MOM		+	0.00	3.69	-2.77	-12.83	-10.22
Mrps34	Q9JIK9	Matrix		+	0.00	3.34	-2.80	-12.81	-10.78
Dhrs1	Q99L04	MIM		+	0.00	9.27	-2.80	-12.77	-9.91
Maoa	Q64133	MOM		+	0.00	5.82	-2.81	-13.32	-10.61
Opa1	P58281	MIM	+	+	0.00	4.70	-2.82	-13.46	-10.52
Acad9	Q8JZN5	MIM	+	+	0.00	5.01	-2.82	-13.11	-10.46
Idh3g	P70404	Matrix		+	0.00	6.03	-2.84	-12.07	-9.53
Pnpla8	Q8K1N1	MIM		+	0.00	8.89	-2.88	-14.92	-12.12
Aldh18a1	Q9Z110	Matrix	+	+	0.00	4.35	-2.96	-13.48	-10.88
Slc25a22	Q9D6M3	MIM		+	0.00	6.17	-3.02	-12.29	-9.25
Ak3	Q9WTP7	Matrix		+	0.02	1.05	-3.13	-10.97	-10.22
Mrps5	Q99N87	Matrix		+	0.00	4.97	-3.15	-13.78	-11.27
Clpx	Q9JHS4	Matrix		+	0.00	6.32	-3.18	-15.11	-11.98
Idh3b	Q91VA7	Matrix		+	0.00	5.01	-3.26	-12.24	-8.42
Aldh112	Q8K009	Matrix	+	+	0.00	5.65	-3.30	-13.69	-10.97
Mcu	Q3UMR5	MIM		+	0.00	4.49	-3.31	-15.04	-11.84
Lrpprc	Q6PB66	Matrix	+	+	0.00	6.79	-3.34	-13.06	-9.71
Abcd3	P55096	Membrane		+	0.00	6.96	-3.34	-13.64	-10.57
Chchd6	Q91VN4	MIM		+	0.00	4.21	-3.61	-13.18	-9.63
Kars1	Q99MN1	Matrix		+	0.00	3.44	-3.63	-13.41	-9.16
Acs16	Q91WC3	MOM		+	0.00	3.09	-3.73	-14.11	-10.84
Mrps7	Q80X85	Matrix		+	0.00	8.17	-3.84	-14.93	-11.32
Snd1	Q78PY7	unknown		+	0.00	2.72	-3.86	-14.07	-9.17
Dbi	P31786	unknown		+	0.00	3.36	-4.07	-10.62	-6.95
Ndufc2	Q9CQ54	MIM		+	0.00	1.45	-4.34	-12.01	-10.49
Tomm20	Q9DCC8	MOM		+	0.00	1.46	-4.49	-18.89	-14.15
Atp5mj	P56379	MIM		+	0.00	1.95	-4.87	-11.31	-9.50
Ssbp1	Q9CYR0	Matrix		+	0.00	1.70	-5.30	-13.04	-10.61
Timm13	P62075	MIM		+	0.00	2.46	-5.32	-13.81	-9.59
Cisd1	Q91WS0	MOM		+	0.00	2.34	-5.50	-11.76	-8.13
Ndufb7	Q9CR61	MIM		+	0.00	2.54	-6.91	-16.61	-9.44

Rfk	Q8CFV9	Matrix	+	0.00	3.79	-7.68	-21.13	-11.59
Uqcc2	Q9CQY6	MIM	+	0.00	3.17	-7.92	-21.62	-11.25
mt-Co3	P00416	MIM	+	0.00	3.56	-7.99	-20.13	-9.15

Table S2: Lists of OXPHOS proteins from proteomics of mitochondrial proteins as in Table S1. Proteins sorted by Log₂ fold change from highest to lowest.

PG. Genes	Significant (Ax-WC)	Log10 p-value (Ax-WC)	q-value (Ax-WC)	Log2 fold change (Ax-WC)	PG. Genes	Significant (Ax-WC)	Log10 p-value (Ax-WC)	q-value (Ax-WC)	Log2 fold change (Ax-WC)
Sdha	+	5.83	0.00	1.58	Uqcrc2	+	2.20	0.00	-0.97
Atp5mf	+	3.22	0.00	0.64	Ndufs3	+	1.27	0.02	-0.99
Atp5if1	+	1.67	0.02	0.55	Ndufb5	+	4.28	0.00	-1.08
Mt-Cyb		0.29	0.49	0.44	Ndufa2	+	2.05	0.00	-1.10
Mtco2		1.02	0.12	0.35	Atp5mg	+	1.64	0.00	-1.12
Atp5flb		0.04	0.94	-0.01	Ndufb8	+	1.01	0.04	-1.14
Ndufa4		0.06	0.92	-0.02	Ndufb9	+	1.47	0.01	-1.16
Ndufa12		0.06	0.90	-0.03	Uqcrc1	+	3.69	0.00	-1.18
Cox7b		0.07	0.86	-0.08	Atp5me	+	4.51	0.00	-1.22
Aifm1		0.07	0.86	-0.09	Coa3	+	3.90	0.00	-1.24
Atp5fla		0.84	0.33	-0.17	Atp5fld	+	4.36	0.00	-1.27
Cox7c		0.65	0.33	-0.21	Ndufab1	+	1.49	0.01	-1.31
Mtnd5		0.12	0.75	-0.22	Uqcrq	+	7.07	0.00	-1.39
Cmc1		0.36	0.46	-0.26	Hccs	+	2.29	0.00	-1.43
Cox20		0.16	0.68	-0.31	Ndufb4	+	2.54	0.00	-1.47
Cycs		1.09	0.12	-0.32	Ndufa5	+	4.45	0.00	-1.48
Atp5fle		0.90	0.16	-0.33	Ndufs5	+	1.85	0.00	-1.50
Atp5flc		1.47	0.06	-0.35	Ndufa8	+	3.69	0.00	-1.52
Sdhc		0.48	0.33	-0.37	Tmem126a	+	5.76	0.00	-1.56
Ndufs4		0.66	0.22	-0.40	Ndufs1	+	3.57	0.00	-1.57
Atp5mk	+	1.71	0.03	-0.44	Uqcrrs1	+	3.55	0.00	-1.72
Ndufb6		0.86	0.13	-0.46	Ecsit	+	6.14	0.00	-1.73
Ndufb11	+	1.90	0.02	-0.46	Ndufv1	+	3.78	0.00	-1.87
Atp5po	+	1.80	0.02	-0.46	Ndufa9	+	1.13	0.02	-1.91
Ndufs7		0.34	0.43	-0.49	Ndufa10	+	3.55	0.00	-1.96
Cox6c	+	1.64	0.02	-0.49	Uqcrrh	+	4.86	0.00	-2.00
Atp5pf	+	1.84	0.01	-0.53	Ndufs2	+	3.25	0.00	-2.07
Ndufa3		0.62	0.20	-0.56	Cyc1	+	1.73	0.00	-2.10
Cox6a1		0.32	0.44	-0.61	Ndufa7	+	4.11	0.00	-2.29
Atp5pd	+	2.60	0.00	-0.63	Ndufb10	+	4.30	0.00	-2.29
Cox7a2	+	3.32	0.00	-0.71	Ndufv2	+	4.59	0.00	-2.42
Cox6b1	+	2.11	0.00	-0.71	Mtnd1	+	2.65	0.00	-2.51
Cox4i1	+	1.72	0.01	-0.75	Ndufs6	+	3.13	0.00	-2.53
Ndufb3	+	1.84	0.01	-0.75	Acad9	+	5.01	0.00	-2.82
Ndufs8	+	1.57	0.01	-0.88	Ndufc2	+	1.45	0.00	-4.34
Atp5pb	+	1.63	0.01	-0.92	Atp5mj	+	1.95	0.00	-4.87
Mtstp8	+	3.39	0.00	-0.93	Ndufb7	+	2.54	0.00	-6.91
Mtnd4	+	3.64	0.00	-0.94	Uqcc2	+	3.17	0.00	-7.92
Sdhb	+	4.30	0.00	-0.97	mt-Co3	+	3.56	0.00	-7.99

Table S3: Lists of citric acid cycle and related pyruvate metabolism proteins from proteomics of mitochondrial proteins as in Table S1. Proteins sorted by Log₂ fold change from highest to lowest.

PG.Genes	Signifi- cant (Ax- WC)	-Log10 p-value (Ax- WC)	q-value (Ax- WC)	Log2 fold change (Ax-WC)	Valid values Ax	Valid values WC
Idh3b	+	5.01	0.00	-3.26	7	9
Idh3g	+	6.03	0.00	-2.84	8	9
Ogdhl	+	2.99	0.00	-2.26	4	9
Suclg1	+	1.78	0.00	-1.30	9	9
Ogdh	+	2.99	0.00	-1.25	9	9
Dlst	+	3.46	0.00	-0.97	9	9
Sdhb	+	4.30	0.00	-0.97	8	9
Idh3a	+	3.48	0.00	-0.76	9	9
Suclg2		0.83	0.10	-0.73	5	9
Sucla2	+	2.06	0.00	-0.70	8	9
Idh2		0.32	0.44	-0.54	8	9
Sdhc		0.48	0.33	-0.37	6	9
Aco2		0.78	0.22	-0.30	9	9
Fh		0.02	0.97	0.01	9	9
Dld		0.03	0.93	0.04	8	9
Cs		1.05	0.18	0.25	9	9
Mdh2		0.88	0.15	0.37	9	9
Sdha	+	5.83	0.00	1.58	9	9
Pyruvate Metabolism						
Mpc2		0.07	0.85	0.16	4	9
Mpc1		0.30	0.46	0.71	3	8
Pdhb	+	4.41	0.00	-1.10	9	9
Dlat	+	5.37	0.00	-1.76	8	9
Dld		0.03	0.93	0.04	8	9

Table S4: Lists of fatty acid oxidation proteins from proteomics of mitochondrial proteins as in Table S1. Proteins sorted by Log₂ fold change from highest to lowest.

PG. Genes	Significant (Ax-WC)	-Log ₁₀ p-value (Ax-WC)	q-value (Ax-WC)	Log ₂ fold change (Ax-WC)
Acad12	+	1.83	0.00	2.52
Acaa2	+	4.95	0.00	1.89
Acaa1a	+	3.86	0.00	1.74
Echs1	+	4.15	0.00	1.32
Hadh	+	2.60	0.00	1.10
Acadl		0.68	0.13	1.06
Acadm		0.52	0.25	-0.64
Acat1	+	1.65	0.01	-0.86
Acadv1		0.54	0.20	-1.19
Acadsb	+	5.91	0.00	-1.20
Hadha		0.71	0.11	-1.30
Hsd17b4	+	6.71	0.00	-1.65
Hadhb	+	0.90	0.04	-1.81

Table S5: Lists of Urea cycle related proteins from proteomics of mitochondrial proteins as in Table S1 and of the total proteomics.

PG. Genes	Significant (Ax-WC) Mitochondrial	Significant (Ax-WC) Total	Log ₂ fold change (Ax-WC)		N Ax	N WC
			Mitochondrial	Total		
Cps1	+	+	3.49	3.21	9	9
Otc	+	+	5.92	5.68	9	8
Ass1		+		1.79	3	9
Asl		+		3.27	9	9
Arg1				3.78	6	1
Arg2			-1.59	-1.85	1	9
Slc25a15					0	7
Got1				-0.38	8	9
Got2			-0.13	0.28	9	9
Oat	+	+	-1.86	-2.11	9	9
Pycr2	+		1.41		4	9
Gls	+	+	-1.49	-1.76	7	9
Glul		+		-4	5	9
Glud1	+	+	-1.27	-1.47	9	9
Nos1		+		1.73	6	9

References

- Abraham, Zachary, Emma Hawley, Daniel Hayosh, Victoria A. Webster-Wood, and Ozan Akkus. 2018. 'Kinesin and Dynein Mechanics: Measurement Methods and Research Applications', *J. Biomech. Eng.*, 140.
- Alexander, C., M. Votruba, U. E. A. Pesch, D. L. Thiselton, S. Mayer, A. Moore, M. Rodriguez, U. Kellner, B. Leo-Kottler, G. Auburger, S. S. Bhattacharya, and B. Wissinger. 2000. 'OPA1, encoding a dynamin-related GTPase, is mutated in autosomal dominant optic atrophy linked to chromosome 3q28', *Nature Genetics*, 26: 211-15.
- Änkö, Minna-Liisa, and Karla M. Neugebauer. 2012. 'RNA–protein interactions in vivo: global gets specific', *Trends in Biochemical Sciences*, 37: 255-62.
- Antonicka, Hana, Zhen-Yuan Lin, Alexandre Janer, Mari J. Aaltonen, Woranontee Weraarpachai, Anne-Claude Gingras, and Eric A. Shoubridge. 2020. 'A High-Density Human Mitochondrial Proximity Interaction Network', *Cell Metabolism*, 32: 479-97.e9.
- Aschrafi, Armaz, Amar N. Kar, Jenna R. Gale, Abdel G. Elkahoun, Jose Noberto S. Vargas, Naomi Sales, Gabriel Wilson, Miranda Tompkins, Anthony E. Gioio, and Barry B. Kaplan. 2016. 'A heterogeneous population of nuclear-encoded mitochondrial mRNAs is present in the axons of primary sympathetic neurons', *Mitochondrion*, 30: 18–23.
- Basu, Himanish, Lai Ding, Gulcin Pekkurnaz, Michelle Cronin, and Thomas L. Schwarz. 2020. 'Kymolyzer, a Semi-Autonomous Kymography Tool to Analyze Intracellular Motility', *Current Protocols in Cell Biology*, 87: e107.
- Bean, Bruce P. 2007. 'The action potential in mammalian central neurons', *Nature Reviews Neuroscience*, 8: 451-65.
- Bélanger, Mireille, Igor Allaman, and Pierre J Magistretti. 2011. 'Brain Energy Metabolism: Focus on Astrocyte-Neuron Metabolic Cooperation', *Cell Metabolism*, 14: 724-38.
- Bertrand, Edouard, Pascal Chartrand, Matthias Schaefer, Shailesh M. Shenoy, Robert H. Singer, and Roy M. Long. 1998. 'Localization of ASH1 mRNA Particles in Living Yeast', *Mol. Cell*, 2: 437–45.
- Besse, Florence, and Anne Ephrussi. 2008. 'Translational control of localized mRNAs: restricting protein synthesis in space and time', *Nat. Rev. Mol. Cell Biol.*, 9: 971–80.
- Billups, Brian, and Ian D. Forsythe. 2002. 'Presynaptic Mitochondrial Calcium Sequestration Influences Transmission at Mammalian Central Synapses', *J. Neurosci.*, 22: 5840–47.
- Bolam, J. Paul, and Eleftheria K. Pissadaki. 2012. 'Living on the edge with too many mouths to feed: Why dopamine neurons die', *Movement Disorders*, 27: 1478-83.
- Bourke, Ashley M., Andre Schwarz, and Erin M. Schuman. 2023. 'De-centralizing the Central Dogma: mRNA translation in space and time', *Molecular Cell*, 83: 452-68.
- Brandman, Onn, and Ramanujan S. Hegde. 2016. 'Ribosome-associated protein quality control', *Nature Structural & Molecular Biology*, 23: 7-15.
- Brickley, Kieran, and F. Anne Stephenson. 2011. 'Trafficking Kinesin Protein (TRAK)-mediated Transport of Mitochondria in Axons of Hippocampal Neurons*', *Journal of Biological Chemistry*, 286: 18079-92.
- Briese, M., L. Saal, S. Appenzeller, M. Moradi, A. Baluapuri, and M. Sendtner. 2016a. 'Whole transcriptome profiling reveals the RNA content of motor axons', *Nucleic Acids Res*, 44: e33.
- Briese, Michael, Lena Saal, Silke Appenzeller, Mehri Moradi, Apoorva Baluapuri, and Michael Sendtner. 2016b. 'Whole transcriptome profiling reveals the RNA content of motor axons', *Nucleic Acids Res.*, 44: e33–e33.
- Burke, Robert E., and Karen O'Malley. 2013. 'Axon degeneration in Parkinson's disease', *Experimental Neurology*, 246: 72-83.

- Buxbaum, Adina R., Gal Haimovich, and Robert H. Singer. 2014. 'In the right place at the right time: visualizing and understanding mRNA localization', *Nat. Rev. Mol. Cell Biol.*, 16: 95–109.
- Cagnetta, Roberta, Christian K. Frese, Toshiaki Shigeoka, Jeroen Krijgsveld, and Christine E. Holt. 2018. 'Rapid Cue-Specific Remodeling of the Nascent Axonal Proteome', *Neuron*, 99: 29–46.e4.
- Cajigas, Iván J., Georgi Tushev, Tristan J. Will, Susanne Tom Dieck, Nicole Fuerst, and Erin M. Schuman. 2012. 'The Local Transcriptome in the Synaptic Neuropil Revealed by Deep Sequencing and High-Resolution Imaging', *Neuron*, 74: 453–66.
- Carey, E. M. 1975. 'A COMPARATIVE STUDY OF THE METABOLISM OF DE NOVO SYNTHESIZED FATTY ACIDS FROM ACETATE AND GLUCOSE, AND EXOGENOUS FATTY ACIDS, IN SLICES OF RABBIT CEREBRAL CORTEX DURING DEVELOPMENT', *Journal of Neurochemistry*, 24: 237–44.
- Casari, Giorgio, Maurizio De Fusco, Sonia Ciarmatori, Massimo Zeviani, Marina Mora, Patricio Fernandez, Giuseppe De Michele, Alessandro Filla, Sergio Coccozza, Roberto Marconi, Alexandre Dürr, Bertrand Fontaine, and Andrea Ballabio. 1998. 'Spastic Paraplegia and OXPHOS Impairment Caused by Mutations in Paraplegin, a Nuclear-Encoded Mitochondrial Metalloprotease', *Cell*, 93: 973–83.
- Cassereau, Julien, Arnaud Chevrollier, Naïg Gueguen, Valérie Desquirit, Christophe Verny, Guillaume Nicolas, Frédéric Dubas, Patrizia Amati-Bonneau, Pascal Reynier, Dominique Bonneau, and Vincent Procaccio. 2011. 'Mitochondrial dysfunction and pathophysiology of Charcot–Marie–Tooth disease involving GDAP1 mutations', *Exp. Neurol.*, 227: 31–41.
- Cavarischia-Rega, Claudia, Karan Sharma, Julia C. Fitzgerald, and Boris Macek. 2024. 'Proteome Dynamics in iPSC-Derived Human Dopaminergic Neurons', *Molecular & Cellular Proteomics*, 23: 100838.
- Cawte, Adam D., Peter J. Unrau, and David S. Rueda. 2020. 'Live cell imaging of single RNA molecules with fluorogenic Mango II arrays', *Nat. Commun.*, 11: 1–11.
- Chen, Weixuan, Johanna M. Smeekens, and Ronghu Wu. 2016. 'Systematic study of the dynamics and half-lives of newly synthesized proteins in human cells', *Chem. Sci.*, 7: 1393–400.
- Chen, Xianjun, Dasheng Zhang, Ni Su, Bingkun Bao, Xin Xie, Fangting Zuo, Lipeng Yang, Hui Wang, Li Jiang, Qiuning Lin, Mengyue Fang, Ningfeng Li, Xin Hua, Zhengda Chen, Chunyan Bao, Jinjin Xu, Wenli Du, Lixin Zhang, Yuzheng Zhao, Linyong Zhu, Joseph Loscalzo, and Yi Yang. 2019. 'Visualizing RNA dynamics in live cells with bright and stable fluorescent RNAs', *Nature Biotechnology*, 37: 1287–93.
- Chuang, Chih-Fan, Chih-En King, Bo-Wei Ho, Kun-Yi Chien, and Yen-Chung Chang. 2018. 'Unbiased Proteomic Study of the Axons of Cultured Rat Cortical Neurons', *J. Proteome Res.*, 17: 1953–66.
- Chung, Hui-Wen, Ju-Chen Weng, Chih-En King, Chih-Fan Chuang, Wei-Yuan Chow, and Yen-Chung Chang. 2019. 'BDNF elevates the axonal levels of hnRNPs Q and R in cultured rat cortical neurons', *Mol. Cell. Neurosci.*, 98: 97–108.
- Cioni, Jean-Michel, Julie Qiaojin Lin, Anne V. Holtermann, Max Koppers, Maximilian A. H. Jakobs, Afnan Azizi, Benita Turner-Bridger, Toshiaki Shigeoka, Kristian Franze, William A. Harris, and Christine E. Holt. 2019. 'Late Endosomes Act as mRNA Translation Platforms and Sustain Mitochondria in Axons', *Cell*, 176: 56–72.e15.
- Cohen, Bar, Topaz Altman, Adi Golani-Armon, Anca F. Savulescu, Amjd Ibraheem, Musa M. Mhlanga, Eran Perlson, and Yoav S. Arava. 2022. 'Co-transport of the nuclear-encoded Cox7c mRNA with mitochondria along axons occurs through a coding-region-dependent mechanism', *Journal of Cell Science*, 135.

- Cohen, Laurie D., and Noam E. Ziv. 2019. 'Neuronal and synaptic protein lifetimes', *Current Opinion in Neurobiology*, 57: 9-16.
- Cohen, Laurie D., Rina Zuchman, Oksana Sorokina, Anke Müller, Daniela C. Dieterich, J. Douglas Armstrong, Tamar Ziv, and Noam E. Ziv. 2013. 'Metabolic Turnover of Synaptic Proteins: Kinetics, Interdependencies and Implications for Synaptic Maintenance', *PLoS One*, 8: e63191.
- Cosker, Katharina E., Sara J. Fenstermacher, Maria F. Pazyra-Murphy, Hunter L. Elliott, and Rosalind A. Segal. 2016. 'The RNA-binding protein SFPQ orchestrates an RNA regulon to promote axon viability', *Nat. Neurosci.*, 19: 690–96.
- Cox, Rachel T., and Allan C. Spradling. 2009. 'clueless, a conserved Drosophila gene required for mitochondrial subcellular localization, interacts genetically with parkin', *Disease Models & Mechanisms*, 2: 490-99.
- Cserép, Csaba, Balázs Pósfai, Anett Dóra Schwarcz, and Ádám Dénes. 2018. 'Mitochondrial Ultrastructure Is Coupled to Synaptic Performance at Axonal Release Sites', *eneuro*, 5: ENEURO.0390-17.2018.
- Das, Sulagna, Maria Vera, Valentina Gandin, Robert H. Singer, and Evelina Tutucci. 2021. 'Intracellular mRNA transport and localized translation', *Nat. Rev. Mol. Cell Biol.*, 22: 483–504.
- De Pace, Raffaella, Saikat Ghosh, Veronica H. Ryan, Mira Sohn, Michal Jarnik, Paniz Rezvan Sangsari, Nicole Y. Morgan, Ryan K. Dale, Michael E. Ward, and Juan S. Bonifacino. 2024. 'Messenger RNA transport on lysosomal vesicles maintains axonal mitochondrial homeostasis and prevents axonal degeneration', *Nat. Neurosci.*, 27: 1087–102.
- Delettre, C., G. Lenaers, J. M. Griffoin, N. Gigarel, C. Lorenzo, P. Belenguer, L. Pelloquin, J. Grosgeorge, C. Turc-Carel, E. Perret, C. Astarie-Dequeker, L. Lasquelles, B. Arnaud, B. Ducommun, J. Kaplan, and C. P. Hamel. 2000. 'Nuclear gene OPA1, encoding a mitochondrial dynamin-related protein, is mutated in dominant optic atrophy', *Nature Genetics*, 26: 207-10.
- Dermitt, Maria, Martin Dodel, Flora C. Y. Lee, Muhammad S. Azman, Hagen Schwenzer, J. Louise Jones, Sarah P. Blagden, Jernej Ule, and Faraz K. Mardakheh. 2020. 'Subcellular mRNA Localization Regulates Ribosome Biogenesis in Migrating Cells', *Dev. Cell*, 55: 298–313.e10.
- Donovan, Eavan J., Anamika Agrawal, Nicole Liberman, Jordan I. Kalai, Avi J. Adler, Adam M. Lamper, Hailey Q. Wang, Nicholas J. Chua, Elena F. Koslover, and Erin L. Barnhart. 2024. 'Dendrite architecture determines mitochondrial distribution patterns in vivo', *Cell Reports*, 43.
- Dörrbaum, Aline R., Lisa Kochen, Julian D. Langer, and Erin M. Schuman. 2018. 'Local and global influences on protein turnover in neurons and glia', *Elife*.
- Dotti, C. G., C. A. Sullivan, and G. A. Banker. 1988. 'The establishment of polarity by hippocampal neurons in culture', *J. Neurosci.*, 8: 1454–68.
- Duff, Claire, and Julien Baruteau. 2022. 'Modelling urea cycle disorders using iPSCs', *npj Regenerative Medicine*, 7: 56.
- Dumrongprechachan, Vasin, Ryan B. Salisbury, Lindsey Butler, Matthew L. MacDonald, and Yevgenia Kozorovitskiy. 2022. 'Dynamic proteomic and phosphoproteomic atlas of corticostriatal axons in neurodevelopment', *Elife*, 11: e78847.
- Edmond, J., R. A. Robbins, J. D. Bergstrom, R. A. Cole, and J. de Vellis. 1987. 'Capacity for substrate utilization in oxidative metabolism by neurons, astrocytes, and oligodendrocytes from developing brain in primary culture', *Journal of Neuroscience Research*, 18: 551-61.
- El Zawily, Amr M., Markus Schwarzländer, Iris Finkemeier, Iain G. Johnston, Abdelilah Benamar, Yongguo Cao, Clémence Gissot, Andreas J. Meyer, Ken Wilson, Raju Datla, David Macherel, Nick S. Jones, and David C. Logan. 2014. 'FRIENDLY Regulates

- Mitochondrial Distribution, Fusion, and Quality Control in Arabidopsis', *Plant Physiology*, 166: 808-28.
- Eliscovich, Carolina, and Robert H. Singer. 2017. 'RNP transport in cell biology: the long and winding road', *Curr. Opin. Cell Biol.*, 45: 38–46.
- Eliyahu, Erez, Lilach Pnueli, Daniel Melamed, Tanja Scherrer, André P. Gerber, Ophry Pines, Doron Rapaport, and Yoav Arava. 2010. 'Tom20 Mediates Localization of mRNAs to Mitochondria in a Translation-Dependent Manner', *Molecular and Cellular Biology*, 30: 284-94.
- Eom, Taesun, Laura N. Antar, Robert H. Singer, and Gary J. Bassell. 2003. 'Localization of a β -Actin Messenger Ribonucleoprotein Complex with Zipcode-Binding Protein Modulates the Density of Dendritic Filopodia and Filopodial Synapses', *Journal of Neuroscience*, 23: 10433-44.
- Faitg, Julie, Clay Lacefield, Tracey Davey, Kathryn White, Ross Laws, Stylianos Kosmidis, Amy K. Reeve, Eric R. Kandel, Amy E. Vincent, and Martin Picard. 2021. '3D neuronal mitochondrial morphology in axons, dendrites, and somata of the aging mouse hippocampus', *Cell Reports*, 36: 109509.
- Fecher, Caroline, Laura Trovò, Stephan A. Müller, Nicolas Snaidero, Jennifer Wettmarshausen, Sylvia Heink, Oskar Ortiz, Ingrid Wagner, Ralf Kühn, Jana Hartmann, Rosa Maria Karl, Arthur Konnerth, Thomas Korn, Wolfgang Wurst, Doron Merkler, Stefan F. Lichtenthaler, Fabiana Perocchi, and Thomas Misgeld. 2019. 'Cell-type-specific profiling of brain mitochondria reveals functional and molecular diversity', *Nat. Neurosci.*, 22: 1731–42.
- Fields, Stephen D., Michael N. Conrad, and Margaret Clarke. 1998. 'The *S. cerevisiae* CLU1 and *D. discoideum* cluA genes are functional homologues that influence mitochondrial morphology and distribution', *Journal of Cell Science*, 111: 1717-27.
- Fornasiero, Eugenio F., Sunit Mandad, Hanna Wildhagen, Mihai Alevra, Burkhard Rammner, Sarva Keihani, Felipe Opazo, Inga Urban, Till Ischebeck, M. Sadman Sakib, Maryam K. Fard, Koray Kirli, Tonatiuh Pena Centeno, Ramon O. Vidal, Raza-Ur Rahman, Eva Benito, André Fischer, Sven Dennerlein, Peter Rehling, Ivo Feussner, Stefan Bonn, Mikael Simons, Henning Urlaub, and Silvio O. Rizzoli. 2018. 'Precisely measured protein lifetimes in the mouse brain reveal differences across tissues and subcellular fractions', *Nature Communications*, 9: 4230.
- Friedman, Jonathan R., and Jodi Nunnari. 2014. 'Mitochondrial form and function', *Nature*, 505: 335-43.
- Fukuda, Yusuke, Maria F. Pazyra-Murphy, Elizabeth S. Silagi, Ozge E. Tasdemir-Yilmaz, Yihang Li, Lillian Rose, Zoe C. Yeoh, Nicholas E. Vangos, Ezekiel A. Geffken, Hyuk-Soo Seo, Guillaume Adelmant, Gregory H. Bird, Loren D. Walensky, Jarrod A. Marto, Sirano Dhe-Paganon, and Rosalind A. Segal. 2021. 'Binding and transport of SFPQ-RNA granules by KIF5A/KLC1 motors promotes axon survival', *J. Cell Biol.*, 220.
- Gao, Jie, Désirée Schatton, Paola Martinelli, Henriette Hansen, David Pla-Martin, Esther Barth, Christian Becker, Janine Altmueller, Peter Frommolt, Marco Sardiello, and Elena I. Rugarli. 2014. 'CLUH regulates mitochondrial biogenesis by binding mRNAs of nuclear-encoded mitochondrial proteins', *J. Cell Biol.*, 207: 213–23.
- García-Rodríguez, Luis J., Anna Card Gay, and Liza A. Pon. 2007. 'Puf3p, a Pumilio family RNA binding protein, localizes to mitochondria and regulates mitochondrial biogenesis and motility in budding yeast', *Journal of Cell Biology*, 176: 197-207.
- Gasparski, Alexander N., Konstadinos Moissoglou, Sandeep Pallikkuth, Sezen Meydan, Nicholas R. Guydosh, and Stavroula Mili. 2023. 'mRNA location and translation rate determine protein targeting to dual destinations', *Molecular Cell*, 83: 2726-38.e9.
- Gerstberger, Stefanie, Markus Hafner, and Thomas Tuschl. 2014. 'A census of human RNA-binding proteins', *Nature Reviews Genetics*, 15: 829-45.

- Gold, Vicki A. M., Piotr Chroscicki, Piotr Bragoszewski, and Agnieszka Chacinska. 2017. 'Visualization of cytosolic ribosomes on the surface of mitochondria by electron cryotomography', *EMBO reports*, 18: 1786-800-800.
- Graber, Tyson E., Sarah Hébert-Seropian, Arkady Khoutorsky, Alexandre David, Jonathan W. Yewdell, Jean-Claude Lacaille, and Wayne S. Sossin. 2013. 'Reactivation of stalled polyribosomes in synaptic plasticity', *Proceedings of the National Academy of Sciences*, 110: 16205-10.
- Grimm, Jonathan B., Brian P. English, Jiji Chen, Joel P. Slaughter, Zhengjian Zhang, Andrey Revyakin, Ronak Patel, John J. Macklin, Davide Normanno, Robert H. Singer, Timothée Lionnet, and Luke D. Lavis. 2015. 'A general method to improve fluorophores for live-cell and single-molecule microscopy', *Nat. Methods*, 12: 244–50.
- Gropman, A. L., M. Summar, and J. V. Leonard. 2007. 'Neurological implications of urea cycle disorders', *Journal of Inherited Metabolic Disease*, 30: 865-79.
- Guo, Xiufang, Greg T. Macleod, Andrea Wellington, Fangle Hu, Sarvari Panchumarthi, Miriam Schoenfield, Leo Marin, Milton P. Charlton, Harold L. Atwood, and Konrad E. Zinsmaier. 2005. 'The GTPase dMiro Is Required for Axonal Transport of Mitochondria to Drosophila Synapses', *Neuron*, 47: 379-93.
- Häberle, Johannes, Nathalie Boddaert, Alberto Burlina, Anupam Chakrapani, Marjorie Dixon, Martina Huemer, Daniela Karall, Diego Martinelli, Pablo Sanjurjo Crespo, René Santer, Aude Servais, Vassili Valayannopoulos, Martin Lindner, Vicente Rubio, and Carlo Dionisi-Vici. 2012. 'Suggested guidelines for the diagnosis and management of urea cycle disorders', *ORPHANET JOURNAL OF RARE DISEASES*, 7: 32.
- Hakim, Vicky, Laurie D. Cohen, Rina Zuchman, Tamar Ziv, and Noam E. Ziv. 2016. 'The effects of proteasomal inhibition on synaptic proteostasis', *The EMBO Journal*, 35: 2238-62-62.
- Hall, Catherine N., Miriam C. Klein-Flügge, Clare Howarth, and David Attwell. 2012. 'Oxidative Phosphorylation, Not Glycolysis, Powers Presynaptic and Postsynaptic Mechanisms Underlying Brain Information Processing', *J. Neurosci.*, 32: 8940–51.
- Handley, Renee R., Suzanne J. Reid, Rudiger Brauning, Paul Maclean, Emily R. Mears, Imche Fourie, Stefano Patassini, Garth J. S. Cooper, Skye R. Rudiger, Clive J. McLaughlan, Paul J. Verma, James F. Gusella, Marcy E. MacDonald, Henry J. Waldvogel, C. Simon Bawden, Richard L. M. Faull, and Russell G. Snell. 2017. 'Brain urea increase is an early Huntington's disease pathogenic event observed in a prodromal transgenic sheep model and HD cases', *Proceedings of the National Academy of Sciences*, 114: E11293-E302.
- Hansen, Jens Jacob, Alexandra Dürr, Isabelle Cournu-Rebeix, Costa Georgopoulos, Debbie Ang, Marit Nyholm Nielsen, Claire-Sophie Davoine, Alexis Brice, Bertrand Fontaine, Niels Gregersen, and Peter Bross. 2002. 'Hereditary Spastic Paraplegia SPG13 Is Associated with a Mutation in the Gene Encoding the Mitochondrial Chaperonin Hsp60', *The American Journal of Human Genetics*, 70: 1328-32.
- Harbauer, Angelika B. 2017. 'Mitochondrial health maintenance in axons', *Biochem. Soc. Trans.*, 45: 1045–52.
- Harbauer, Angelika B., J. Tabitha Hees, Simone Wanderoy, Inmaculada Segura, Whitney Gibbs, Yiming Cheng, Martha Ordonez, Zerong Cai, Romain Cartoni, Ghazaleh Ashrafi, Chen Wang, Fabiana Perocchi, Zhigang He, and Thomas L. Schwarz. 2022. 'Neuronal mitochondria transport Pink1 mRNA via synaptojanin 2 to support local mitophagy', *Neuron*, 110: 1516-31.e9.
- Harris, Julia J., Renaud Jolivet, and David Attwell. 2012. 'Synaptic Energy Use and Supply', *Neuron*, 75: 762–77.
- Hasan, Saadia, Michael S. Fernandopulle, Stewart W. Humble, Ashley M. Frankenfield, Haorong Li, Ryan Prestil, Kory R. Johnson, Brent J. Ryan, Richard Wade-Martins,

- Michael E. Ward, and Ling Hao. 2023. 'Multi-modal proteomic characterization of lysosomal function and proteostasis in progranulin-deficient neurons', *Molecular Neurodegeneration*, 18: 87.
- Hees, J. Tabitha, Inmaculada Segura, Andrea Schneider, Martina Schifferer, Thomas Misgeld, and Angelika B. Harbauer. 2024. 'ER-associated biogenesis of PINK1 preprotein for neuronal mitophagy', *bioRxiv*: 2024.06.21.600039.
- Hees, J. Tabitha, Simone Wanderoy, Jana Lindner, Marlena Helms, Hariharan Murali Mahadevan, and Angelika B. Harbauer. 2024. 'Insulin signalling regulates Pink1 mRNA localization via modulation of AMPK activity to support PINK1 function in neurons', *Nature Metabolism*, 6: 514-30.
- Hémono, Mickaële, Alexandre Haller, Johana Chicher, Anne-Marie Duchêne, and Richard Patryk Ngondo. 2022. 'The interactome of CLUH reveals its association to SPAG5 and its co-translational proximity to mitochondrial proteins', *BMC Biology*, 20: 13.
- Hémono, Mickaele, Thalia Salinas-Giegé, Jeanne Roignant, Audrey Vingadassalon, Philippe Hammann, Elodie Ubrig, Patryk Ngondo, and Anne-Marie Duchêne. 2022. 'FRIENDLY (FMT) is an RNA binding protein associated with cytosolic ribosomes at the mitochondrial surface', *The Plant Journal*, 112: 309-21.
- Heo, Seok, Graham H. Diering, Chan Hyun Na, Raja Sekhar Nirujogi, Julia L. Bachman, Akhilesh Pandey, and Richard L. Haganir. 2018. 'Identification of long-lived synaptic proteins by proteomic analysis of synaptosome protein turnover', *Proc. Natl. Acad. Sci. U.S.A.*, 115: E3827–E36.
- Hobson, Benjamin D., Se Joon Choi, Eugene V. Mosharov, Rajesh K. Soni, David Sulzer, and Peter A. Sims. 2022. 'Subcellular proteomics of dopamine neurons in the mouse brain', *Elife*, 11: e70921.
- Hüttelmaier, Stefan, Daniel Zenklusen, Marcell Lederer, Jason Dichtenberg, Mike Lorenz, XiuHua Meng, Gary J. Bassell, John Condeelis, and Robert H. Singer. 2005. 'Spatial regulation of β -actin translation by Src-dependent phosphorylation of ZBP1', *Nature*, 438: 512–15.
- Jernberg, Jennifer N., Caitlyn E. Bowman, Michael J. Wolfgang, and Susanna Scafidi. 2017. 'Developmental regulation and localization of carnitine palmitoyltransferases (CPTs) in rat brain', *Journal of Neurochemistry*, 142: 407-19.
- Joazeiro, Claudio A. P. 2019. 'Mechanisms and functions of ribosome-associated protein quality control', *Nature Reviews Molecular Cell Biology*, 20: 368-83.
- Ju, Yeon Ha, Mridula Bhalla, Seung Jae Hyeon, Ju Eun Oh, Seonguk Yoo, Uikyue Chae, Jea Kwon, Wuhyun Koh, Jiwoon Lim, Yongmin Mason Park, Junghee Lee, Il-Joo Cho, Hyunbeom Lee, Hoon Ryu, and C. Justin Lee. 2022. 'Astrocytic urea cycle detoxifies A β -derived ammonia while impairing memory in Alzheimer's disease', *Cell Metabolism*, 34: 1104-20.e8.
- Jung, Jane, Jiyeon Ohk, Hyeyoung Kim, Christine E. Holt, Hyun Jung Park, and Hosung Jung. 2022. 'mRNA transport, translation, and decay in adult mammalian central nervous system axons', *Neuron*.
- Kauppinen, Risto A., Talvinder S. Sihra, and David G. Nicholls. 1987. 'Aminooxyacetic acid inhibits the malate-aspartate shuttle in isolated nerve terminals and prevents the mitochondria from utilizing glycolytic substrates', *Biochimica et Biophysica Acta (BBA) - Molecular Cell Research*, 930: 173-78.
- Kijima, Kazuki, Chikahiko Numakura, Hiroko Izumino, Kazuo Umetsu, Atsuo Nezu, Toshihide Shiiki, Masafumi Ogawa, Yoshito Ishizaki, Takeshi Kitamura, Yasunobu Shozawa, and Kiyoshi Hayasaka. 2005. 'Mitochondrial GTPase mitofusin 2 mutation in Charcot–Marie–Tooth neuropathy type 2A', *Human Genetics*, 116: 23-27.
- Kim, Tae-Young, Ding Wang, Allen K. Kim, Edward Lau, Amanda J. Lin, David A. Liem, Jun Zhang, Nobel C. Zong, Maggie P. Y. Lam, and Peipei Ping. 2012. 'Metabolic Labeling

- Reveals Proteome Dynamics of Mouse Mitochondria', *Mol. Cell. Proteomics*, 11: 1586–94.
- Klinge, Sebastian, Felix Voigts-Hoffmann, Marc Leibundgut, and Nenad Ban. 2012. 'Atomic structures of the eukaryotic ribosome', *Trends in Biochemical Sciences*, 37: 189-98.
- Kolberg, Liis, Uku Raudvere, Ivan Kuzmin, Priit Adler, Jaak Vilo, and Hedi Peterson. 2023. 'g:Profiler—interoperable web service for functional enrichment analysis and gene identifier mapping (2023 update)', *Nucleic Acids Research*, 51: W207-W12.
- Krebs, H. A. 1973. 'The discovery of the ornithine cycle of urea synthesis', *Biochemical Education*, 1: 19-23.
- Kuzniewska, Bozena, Dominik Cysewski, Michal Wasilewski, Paulina Sakowska, Jacek Milek, Tomasz M. Kulinski, Maciej Winiarski, Pawel Kozielowicz, Ewelina Knapska, Michal Dadlez, Agnieszka Chacinska, Andrzej Dziembowski, and Magdalena Dziembowska. 2020. 'Mitochondrial protein biogenesis in the synapse is supported by local translation', *EMBO reports*, 21: e48882.
- Latham, Vaughan M., Edward H. S. Yu, Antonella N. Tullio, Robert S. Adelstein, and Robert H. Singer. 2001. 'A Rho-dependent signaling pathway operating through myosin localizes β -actin mRNA in fibroblasts', *Current Biology*, 11: 1010-16.
- Lécuyer, Eric, Hideki Yoshida, Neela Parthasarathy, Christina Alm, Tomas Babak, Tanja Cerovina, Timothy R. Hughes, Pavel Tomancak, and Henry M. Krause. 2007. 'Global Analysis of mRNA Localization Reveals a Prominent Role in Organizing Cellular Architecture and Function', *Cell*, 131: 174-87.
- Lee, Chien-Der, and Benjamin P Tu. 2015. 'Glucose-Regulated Phosphorylation of the PUF Protein Puf3 Regulates the Translational Fate of Its Bound mRNAs and Association with RNA Granules', *Cell Reports*, 11: 1638-50.
- Li, Weihang, Anna Maekiniemi, Hanae Sato, Christof Osman, and Robert H. Singer. 2022. 'An improved imaging system that corrects MS2-induced RNA destabilization', *Nature Methods*, 19: 1558-62.
- Li, Xing, Hyaeyeong Kim, Jacob L. Litke, Jiahui Wu, and Samie R. Jaffrey. 2020. 'Fluorophore-Promoted RNA Folding and Photostability Enables Imaging of Single Broccoli-Tagged mRNAs in Live Mammalian Cells', *Angewandte Chemie International Edition*, 59: 4511-18.
- Liao, Ya-Cheng, Michael S. Fernandopulle, Guozhen Wang, Heejun Choi, Ling Hao, Catherine M. Drerup, Rajan Patel, Seema Qamar, Jonathon Nixon-Abell, Yi Shen, William Meadows, Michele Vendruscolo, Tuomas P. J. Knowles, Matthew Nelson, Magdalena A. Czekalska, Greta Musteikyte, Mariam A. Gachechiladze, Christina A. Stephens, H. Amalia Pasolli, Lucy R. Forrest, Peter St George-Hyslop, Jennifer Lippincott-Schwartz, and Michael E. Ward. 2019. 'RNA Granules Hitchhike on Lysosomes for Long-Distance Transport, Using Annexin A11 as a Molecular Tether', *Cell*, 179: 147-64.e20.
- Lin, Michael T., and M. Flint Beal. 2006. 'Mitochondrial dysfunction and oxidative stress in neurodegenerative diseases', *Nature*, 443: 787–95.
- Lionnet, Timothée, Kevin Czaplinski, Xavier Darzacq, Yaron Shav-Tal, Amber L. Wells, Jeffrey A. Chao, Hye Yoon Park, Valeria de Turreis, Melissa Lopez-Jones, and Robert H. Singer. 2011. 'A transgenic mouse for in vivo detection of endogenous labeled mRNA', *Nat. Methods*, 8: 165–70.
- Loedige, Inga, Artem Baranovskii, Samantha Mendonsa, Sayaka Dantsuji, Niko Popitsch, Laura Breimann, Nadja Zerna, Vsevolod Cherepanov, Miha Milek, Stefan Ameres, and Marina Chekulaeva. 2023. 'mRNA stability and m6A are major determinants of subcellular mRNA localization in neurons', *Molecular Cell*, 83: 2709-25.e10.
- Lykke-Andersen, Jens, and Eric J. Bennett. 2014. 'Protecting the proteome: Eukaryotic cotranslational quality control pathways', *Journal of Cell Biology*, 204: 467-76.

- Ma, Zhao, Xiaotian Wu, Christopher J. Krueger, and Antony K. Chen. 2017. 'Engineering Novel Molecular Beacon Constructs to Study Intracellular RNA Dynamics and Localization', *Genomics, Proteomics & Bioinformatics*, 15: 279-86.
- Maciel, Renata, Dana M. Bis, Adriana P. Rebelo, Cima Saghira, Stephan Züchner, and Mario A. Saporta. 2018. 'The human motor neuron axonal transcriptome is enriched for transcripts related to mitochondrial function and microtubule-based axonal transport', *Experimental Neurology*, 307: 155-63.
- Mao, Shiqi, Yachen Ying, Ruonan Wu, and Antony K. Chen. 2020. 'Recent Advances in the Molecular Beacon Technology for Live-Cell Single-Molecule Imaging', *iScience*, 23: 101801.
- Mathieson, Toby, Holger Franken, Jan Kosinski, Nils Kurzawa, Nico Zinn, Gavain Sweetman, Daniel Poeckel, Vikram S. Ratnu, Maike Schramm, Isabelle Becher, Michael Steidel, Kyung-Min Noh, Giovanna Bergamini, Martin Beck, Marcus Bantscheff, and Mikhail M. Savitski. 2018. 'Systematic analysis of protein turnover in primary cells', *Nat. Commun.*, 9: 1–10.
- McFarland, Robert, Robert W. Taylor, and Douglass M. Turnbull. 2010. 'A neurological perspective on mitochondrial disease', *The Lancet Neurology*, 9: 829-40.
- Miller-Fleming, Leonor, Wing Hei Au, Laura Raik, Pedro Guiomar, Jasper Schmitz, Ha Yoon Cho, Aron Czako, and Alexander J. Whitworth. 2024. 'Clu1/Clu form mitochondria-associated granules upon metabolic transitions and regulate mitochondrial protein translation via ribosome interactions', *bioRxiv*: 2024.08.17.608283.
- Miller, Melanie A., Joseph Russo, Anthony D. Fischer, Florencia A. Lopez Leban, and Wendy M. Olivas. 2014. 'Carbon source-dependent alteration of Puf3p activity mediates rapid changes in the stabilities of mRNAs involved in mitochondrial function', *Nucleic Acids Research*, 42: 3954-70.
- Mink, J. W., R. J. Blumenshine, and D. B. Adams. 1981. 'Ratio of central nervous system to body metabolism in vertebrates: its constancy and functional basis', *American Journal of Physiology-Regulatory, Integrative and Comparative Physiology*.
- Misgeld, T., and T. L. Schwarz. 2017. 'Mitostasis in Neurons: Maintaining Mitochondria in an Extended Cellular Architecture', *Neuron*, 96: 651-66.
- Mitchell, Sarah F., and Roy Parker. 2014. 'Principles and Properties of Eukaryotic mRNPs', *Molecular Cell*, 54: 547-58.
- Müller-McNicoll, Michaela, and Karla M. Neugebauer. 2013. 'How cells get the message: dynamic assembly and function of mRNA–protein complexes', *Nat. Rev. Genet.*, 14: 275–87.
- Muslimov, Ilham A., Margaret Titmus, Edward Koenig, and Henri Tiedge. 2002. 'Transport of Neuronal BC1 RNA in Mauthner Axons', *J. Neurosci.*, 22: 4293–301.
- Nijssen, Jik, Julio Aguila, Rein Hoogstraaten, Nigel Kee, and Eva Hedlund. 2018. 'Axon-Seq Decodes the Motor Axon Transcriptome and Its Modulation in Response to ALS', *Stem Cell Rep.*, 11: 1565–78.
- Nolte, Hendrik, Thomas D. MacVicar, Frederik Tellkamp, and Marcus Krüger. 2018. 'Instant Clue: A Software Suite for Interactive Data Visualization and Analysis', *Scientific Reports*, 8: 12648.
- Oleynikov, Yuri, and Robert H. Singer. 2003. 'Real-Time Visualization of ZBP1 Association with β -Actin mRNA during Transcription and Localization', *Current Biology*, 13: 199-207.
- Olivas, Wendy, and Roy Parker. 2000. 'The Puf3 protein is a transcript-specific regulator of mRNA degradation in yeast', *The EMBO Journal*, 19: 6602-11-11.
- Otero, Maria G., Matías Alloatti, Lucas E. Cromberg, Angels Almenar-Queralt, Sandra E. Encalada, Victorio M. Pozo Devoto, Luciana Bruno, Lawrence S. B. Goldstein, and

- Tomás L. Falzone. 2014. 'Fast axonal transport of the proteasome complex depends on membrane interaction and molecular motor function', *J. Cell Sci.*, 127: 1537–49.
- Panza, Emanuele, Diego Martinelli, Pamela Magini, Carlo Dionisi Vici, and Marco Seri. 2019. 'Hereditary Spastic Paraplegia Is a Common Phenotypic Finding in ARG1 Deficiency, P5CS Deficiency and HHH Syndrome: Three Inborn Errors of Metabolism Caused by Alteration of an Interconnected Pathway of Glutamate and Urea Cycle Metabolism', *Front. Neurol.*, 10: 428346.
- Park, Hye Yoon, Hyungsik Lim, Young J. Yoon, Antonia Follenzi, Chiso Nwokafor, Melissa Lopez-Jones, Xiuhua Meng, and Robert H. Singer. 2014. 'Visualization of Dynamics of Single Endogenous mRNA Labeled in Live Mouse', *Science*, 343: 422–24.
- Pickrell, Alicia M, and Richard J Youle. 2015. 'The Roles of PINK1, Parkin, and Mitochondrial Fidelity in Parkinson's Disease', *Neuron*, 85: 257-73.
- Picón-Pagès, Pol, Joan Garcia-Buendia, and Francisco J. Muñoz. 2019. 'Functions and dysfunctions of nitric oxide in brain', *Biochimica et Biophysica Acta (BBA) - Molecular Basis of Disease*, 1865: 1949–67.
- Pla-Martín, David, Désirée Schatton, Janica L. Wiederstein, Marie-Charlotte Marx, Salim Khiati, Marcus Krüger, and Elena I. Rugarli. 2020. 'CLUH granules coordinate translation of mitochondrial proteins with mTORC1 signaling and mitophagy', *The EMBO Journal*, 39: e102731.
- Pollard, Thomas. 2007. 'The Function of Mitochondria in Presynaptic Development at the Neuromuscular Junction', *Mol. Biol. Cell*.
- Poulopoulos, Alexandros, Alexander J. Murphy, Abdulkadir Ozkan, Patrick Davis, John Hatch, Rory Kirchner, and Jeffrey D. Macklis. 2019. 'Subcellular transcriptomes and proteomes of developing axon projections in the cerebral cortex', *Nature*, 565: 356–60.
- Price, John C., Shenheng Guan, Alma Burlingame, Stanley B. Prusiner, and Sina Ghaemmaghami. 2010. 'Analysis of proteome dynamics in the mouse brain', *Proc. Natl. Acad. Sci. U.S.A.*, 107: 14508–13.
- Qin, Jane Yuxia, Li Zhang, Kayla L. Clift, Imge Hulus, Andy Peng Xiang, Bing-Zhong Ren, and Bruce T. Lahn. 2010. 'Systematic Comparison of Constitutive Promoters and the Doxycycline-Inducible Promoter', *PLoS One*, 5: e10611.
- Rae, Caroline D., Joseph A. Baur, Karin Borges, Gerald Dienel, Carlos Manlio Díaz-García, Starlette R. Douglass, Kelly Drew, João M N Duarte, Jordi Duran, Oliver Kann, Tibor Kristian, Dasfne Lee-Liu, Britta E. Lindquist, Ewan C. McNay, Michael B. Robinson, Douglas L. Rothman, Benjamin D. Rowlands, Timothy A. Ryan, Joseph Scafidi, Susanna Scafidi, C. William Shuttleworth, Raymond A. Swanson, Gökhan Uruk, Nina Vardjan, Robert Zorec, and Mary C. McKenna. 2024. 'Brain energy metabolism: A roadmap for future research', *Journal of Neurochemistry*, 168: 910-54.
- Rangaraju, Vidhya, Marcel Lauterbach, and Erin M. Schuman. 2019. 'Spatially Stable Mitochondrial Compartments Fuel Local Translation during Plasticity', *Cell*, 176: 73–84.e15.
- Rath, Sneha, Rohit Sharma, Rahul Gupta, Tslil Ast, Connie Chan, Timothy J. Durham, Russell P. Goodman, Zenon Grabarek, Mary E. Haas, Wendy H. W. Hung, Pallavi R. Joshi, Alexis A. Jourdain, Sharon H. Kim, Anna V. Kotrys, Stephanie S. Lam, Jason G. McCoy, Joshua D. Meisel, Maria Miranda, Apekshya Panda, Anupam Patgiri, Robert Rogers, Shayan Sadre, Hardik Shah, Owen S. Skinner, Tsz-Leung To, Melissa A Walker, Hong Wang, Patrick S. Ward, Jordan Wengrod, Chen-Ching Yuan, Sarah E. Calvo, and Vamsi K. Mootha. 2021. 'MitoCarta3.0: an updated mitochondrial proteome now with sub-organelle localization and pathway annotations', *Nucleic Acids Research*, 49: D1541-D47.

- Ruthardt, Nadia, Don C. Lamb, and Christoph Bräuchle. 2011. 'Single-particle Tracking as a Quantitative Microscopy-based Approach to Unravel Cell Entry Mechanisms of Viruses and Pharmaceutical Nanoparticles', *Mol. Ther.*, 19: 1199–211.
- Saal, Lena, Michael Briese, Susanne Kneitz, Michael Glinka, and Michael Sendtner. 2014. 'Subcellular transcriptome alterations in a cell culture model of spinal muscular atrophy point to widespread defects in axonal growth and presynaptic differentiation', *RNA*, 20: 1789–802.
- Saint-Georges, Yann, Mathilde Garcia, Thierry Delaveau, Laurent Jourden, Stephane Le Crom, Sophie Lemoine, Veronique Tanty, Frederic Devaux, and Claude Jacq. 2008. 'Yeast Mitochondrial Biogenesis: A Role for the PUF RNA-Binding Protein Puf3p in mRNA Localization', *PLoS One*, 3: e2293.
- Schatton, Désirée, Giada Di Pietro, Karolina Szczepanowska, Matteo Veronese, Marie-Charlotte Marx, Kristina Braunöhler, Esther Barth, Stefan Müller, Patrick Giavalisco, Thomas Langer, Aleksandra Trifunovic, and Elena I. Rugarli. 2022. 'CLUH controls astrin-1 expression to couple mitochondrial metabolism to cell cycle progression', *Elife*, 11: e74552.
- Schatton, Désirée, David Pla-Martin, Marie-Charlotte Marx, Henriette Hansen, Arnaud Mourier, Ivan Nemazanyy, Alberto Pessia, Peter Zentis, Teresa Corona, Vangelis Kondylis, Esther Barth, Astrid C. Schauss, Vidya Velagapudi, and Elena I. Rugarli. 2017. 'CLUH regulates mitochondrial metabolism by controlling translation and decay of target mRNAs', *J. Cell Biol.*, 216: 675–93.
- Schon, Eric A, and Serge Przedborski. 2011. 'Mitochondria: The Next (Neurode)Generation', *Neuron*, 70: 1033-53.
- Schuhmacher, Jan S., Susanne tom Dieck, Savvas Christoforidis, Cedric Landerer, Jimena Davila Gallesio, Lena Hersemann, Sarah Seifert, Ramona Schäfer, Angelika Giner, Agnes Toth-Petroczy, Yannis Kalaidzidis, Katherine E. Bohnsack, Markus T. Bohnsack, Erin M. Schuman, and Marino Zerial. 2023. 'The Rab5 effector FERRY links early endosomes with mRNA localization', *Molecular Cell*, 83: 1839-55.e13.
- Schwarz, Thomas L. 2013. 'Mitochondrial Trafficking in Neurons', *Cold Spring Harbor Perspect. Biol.*, 5: a011304.
- Sen, Aditya, and Rachel T. Cox. 2016. 'Clueless is a conserved ribonucleoprotein that binds the ribosome at the mitochondrial outer membrane', *Biology Open*, 5: 195-203.
- Sen, Aditya, Vanessa T. Damm, and Rachel T. Cox. 2013. 'Drosophila Clueless Is Highly Expressed in Larval Neuroblasts, Affects Mitochondrial Localization and Suppresses Mitochondrial Oxidative Damage', *PLoS One*, 8: e54283.
- Sheng, Zu-Hang, and Qian Cai. 2012. 'Mitochondrial transport in neurons: impact on synaptic homeostasis and neurodegeneration', *Nat. Rev. Neurosci.*, 13: 77–93.
- Shigeoka, Toshiaki, Hosung Jung, Jane Jung, Benita Turner-Bridger, Jiyeon Ohk, Julie Qiaojin Lin, Paul S Amieux, and Christine E Holt. 2016. 'Dynamic Axonal Translation in Developing and Mature Visual Circuits', *Cell*, 166: 181-92.
- Shin, Jung-Bum, Jocelyn F. Krey, Ahmed Hassan, Zoltan Metlagel, Andrew N. Tauscher, James M. Pagana, Nicholas E. Sherman, Erin D. Jeffery, Kateri J. Spinelli, Hongyu Zhao, Phillip A. Wilmarth, Dongseok Choi, Larry L. David, Manfred Auer, and Peter G. Barr-Gillespie. 2013. 'Molecular architecture of the chick vestibular hair bundle', *Nature Neuroscience*, 16: 365-74.
- Slobodin, Boris, and Jeffrey E. Gerst. 2010. 'A novel mRNA affinity purification technique for the identification of interacting proteins and transcripts in ribonucleoprotein complexes', *RNA*, 16: 2277–90.
- Snider, William D., and Vivekanand Palavali. 1990. 'Early axon and dendritic outgrowth of spinal accessory motor neurons studied with dii in fixed tissues', *J. Comp. Neurol.*, 297: 227–38.

- Song, Wenjiao, Grigory S. Filonov, Hyaeyeong Kim, Markus Hirsch, Xing Li, Jared D. Moon, and Samie R. Jaffrey. 2017. 'Imaging RNA polymerase III transcription using a photostable RNA–fluorophore complex', *Nature Chemical Biology*, 13: 1187-94.
- Spillane, Mirela, Andrea Ketschek, Tanuja T. Merianda, Jeffery L. Twiss, and Gianluca Gallo. 2013. 'Mitochondria Coordinate Sites of Axon Branching through Localized Intraxonal Protein Synthesis', *Cell Rep.*, 5: 1564–75.
- Taanman, Jan-Willem. 1999. 'The mitochondrial genome: structure, transcription, translation and replication', *Biochimica et Biophysica Acta (BBA) - Bioenergetics*, 1410: 103–23.
- Taylor, Anne M., Mathew Blurton-Jones, Seog Woo Rhee, David H. Cribbs, Carl W. Cotman, and Noo Li Jeon. 2005. 'A microfluidic culture platform for CNS axonal injury, regeneration and transport', *Nat. Methods*, 2: 599–605.
- Tom Dieck, Susanne, Lisa Kochen, Cyril Hanus, Maximilian Heumüller, Ina Bartnik, Belquis Nassim-Assir, Katrin Merk, Thorsten Mosler, Sakshi Garg, Stefanie Bunse, David A. Tirrell, and Erin M. Schuman. 2015. 'Direct visualization of newly synthesized target proteins in situ', *Nat. Methods*, 12: 411–14.
- Tsai, Becky Pinjou, Xiaorong Wang, Lan Huang, and Marian L. Waterman. 2011. 'Quantitative Profiling of In Vivo-assembled RNA-Protein Complexes Using a Novel Integrated Proteomic Approach', *Mol. Cell. Proteomics*, 10.
- Turner-Bridger, Benita, Maximilian Jakobs, Leila Muresan, Hovy Ho-Wai Wong, Kristian Franze, William A. Harris, and Christine E. Holt. 2018. 'Single-molecule analysis of endogenous β -actin mRNA trafficking reveals a mechanism for compartmentalized mRNA localization in axons', *Proceedings of the National Academy of Sciences*, 115: E9697-E706.
- Turner, Nicholas L., Thomas Macrina, J. Alexander Bae, Runzhe Yang, Alyssa M. Wilson, Casey Schneider-Mizell, Kisuk Lee, Ran Lu, Jingpeng Wu, Agnes L. Bodor, Adam A. Bleckert, Derrick Brittain, Emmanouil Froudarakis, Sven Dorkenwald, Forrest Collman, Nico Kemnitz, Dodam Ih, William M. Silversmith, Jonathan Zung, Aleksandar Zlateski, Ignacio Tartavull, Szi-chieh Yu, Sergiy Popovych, Shang Mu, William Wong, Chris S. Jordan, Manuel Castro, JoAnn Buchanan, Daniel J. Bumbarger, Marc Takeno, Russel Torres, Gayathri Mahalingam, Leila Elabbady, Yang Li, Erick Cobos, Pengcheng Zhou, Shelby Suckow, Lynne Becker, Liam Paninski, Franck Polleux, Jacob Reimer, Andreas S. Tolia, R. Clay Reid, Nuno Maçarico da Costa, and H. Sebastian Seung. 2022. 'Reconstruction of neocortex: Organelles, compartments, cells, circuits, and activity', *Cell*, 185: 1082-100.e24.
- Tutucci, Evelina, Maria Vera, Jeetayu Biswas, Jennifer Garcia, Roy Parker, and Robert H. Singer. 2018. 'An improved MS2 system for accurate reporting of the mRNA life cycle', *Nat. Methods*, 15: 81–89.
- van Spronsen, Myrrhe, Marina Mikhaylova, Joanna Lipka, Max A Schlager, Dave J van den Heuvel, Marijn Kuijpers, Phebe S Wulf, Nanda Keijzer, Jeroen Demmers, Lukas C Kapitein, Dick Jaarsma, Hans C Gerritsen, Anna Akhmanova, and Casper C Hoogenraad. 2013. 'TRAK/Milton Motor-Adaptor Proteins Steer Mitochondrial Trafficking to Axons and Dendrites', *Neuron*, 77: 485-502.
- Verstreken, Patrik, Cindy V. Ly, Koen J. T. Venken, Tong-Wey Koh, Yi Zhou, and Hugo J. Bellen. 2005. 'Synaptic Mitochondria Are Critical for Mobilization of Reserve Pool Vesicles at Drosophila Neuromuscular Junctions', *Neuron*, 47: 365–78.
- Voigt, Franka, Hui Zhang, Xianying A. Cui, Désirée Triebold, Ai Xin Liu, Jan Eglinger, Eliza S. Lee, Jeffrey A. Chao, and Alexander F. Palazzo. 2017. 'Single-Molecule Quantification of Translation-Dependent Association of mRNAs with the Endoplasmic Reticulum', *Cell Reports*, 21: 3740-53.

- Waterham, Hans R., Janet Koster, Carlo W. T. van Roermund, Petra A. W. Mooyer, Ronald J. A. Wanders, and James V. Leonard. 2007. 'A Lethal Defect of Mitochondrial and Peroxisomal Fission', *New England Journal of Medicine*, 356: 1736-41.
- Wickens, Marvin, David S. Bernstein, Judith Kimble, and Roy Parker. 2002. 'A PUF family portrait: 3'UTR regulation as a way of life', *Trends in Genetics*, 18: 150-57.
- Wu, Bin, Jiahao Chen, and Robert H. Singer. 2014. 'Background free imaging of single mRNAs in live cells using split fluorescent proteins', *Sci. Rep.*, 4: 1–3.
- Wu, Bin, Carolina Eliscovich, Young J. Yoon, and Robert H. Singer. 2016. 'Translation dynamics of single mRNAs in live cells and neurons', *Science*, 352: 1430–35.
- Wu, Bin, Veronika Miskolci, Hanae Sato, Evelina Tutucci, Charles A. Kenworthy, Sara K. Donnelly, Young J. Yoon, Dianne Cox, Robert H. Singer, and Louis Hodgson. 2015. 'Synonymous modification results in high-fidelity gene expression of repetitive protein and nucleotide sequences', *Genes Dev.*, 29: 876–86.
- Wu, Colin Chih-Chien, Amy Peterson, Boris Zinshteyn, Sergi Regot, and Rachel Green. 2020. 'Ribosome Collisions Trigger General Stress Responses to Regulate Cell Fate', *Cell*, 182: 404-16.e14.
- Xu, Jingshu, Paul Begley, Stephanie J. Church, Stefano Patassini, Katherine A. Hollywood, Mia Jüllig, Maurice A. Curtis, Henry J. Waldvogel, Richard L. M. Faull, Richard D. Unwin, and Garth J. S. Cooper. 2016. 'Graded perturbations of metabolism in multiple regions of human brain in Alzheimer's disease: Snapshot of a pervasive metabolic disorder', *Biochimica et Biophysica Acta (BBA) - Molecular Basis of Disease*, 1862: 1084-92.
- Yang, Geng, Ting Song, Meng Wang, Mengyue Li, QingQing Su, Zhengxin Xie, Xiaoxue Xie, Hanxi Zhang, Yi Feng, Chunhui Wu, Yiyao Liu, and Hong Yang. 2022. 'Recent Advancements in Nanosystem-Based Molecular Beacons for RNA Detection and Imaging', *ACS Applied Nano Materials*, 5: 3065-86.
- Yoon, Young J., Bin Wu, Adina R. Buxbaum, Sulagna Das, Albert Tsai, Brian P. English, Jonathan B. Grimm, Luke D. Lavis, and Robert H. Singer. 2016. 'Glutamate-induced RNA localization and translation in neurons', *Proc. Natl. Acad. Sci. U.S.A.*, 113: E6877–E86.
- Zaninello, Marta, Tim Schlegel, Hendrik Nolte, Mujeeb Pirzada, Elisa Savino, Esther Barth, Ines Klein, Hauke Wüstenberg, Tesmin Uddin, Lisa Wolff, Brunhilde Wirth, Helmar C. Lehmann, Jean-Michel Cioni, Thomas Langer, and Elena I. Rugarli. 2024. 'CLUH maintains functional mitochondria and translation in motoneuronal axons and prevents peripheral neuropathy', *Science Advances*, 10: eadn2050.
- Zappulo, Alessandra, David van den Bruck, Camilla Ciolli Mattioli, Vedran Franke, Koshi Imami, Erik McShane, Mireia Moreno-Estelles, Lorenzo Calviello, Andrei Filipchuk, Esteban Peguero-Sanchez, Thomas Müller, Andrew Woehler, Carmen Birchmeier, Enrique Merino, Nikolaus Rajewsky, Uwe Ohler, Esteban O. Mazzoni, Matthias Selbach, Altuna Akalin, and Marina Chekulaeva. 2017. 'RNA localization is a key determinant of neurite-enriched proteome', *Nature Communications*, 8: 583.
- Zecha, Jana, Chen Meng, Daniel Paul Zolg, Patroklos Samaras, Mathias Wilhelm, and Bernhard Kuster. 2018. 'Peptide Level Turnover Measurements Enable the Study of Proteoform Dynamics*', *Molecular & Cellular Proteomics*, 17: 974-92.
- Zhao, Junjun, Albert Hiu Ka Fok, Ruolin Fan, Pui-Yi Kwan, Hei-Lok Chan, Louisa Hoi-Ying Lo, Ying-Shing Chan, Wing-Ho Yung, Jiandong Huang, Cora Sau Wan Lai, and Kwok-On Lai. 2020. 'Specific depletion of the motor protein KIF5B leads to deficits in dendritic transport, synaptic plasticity and memory', *Elife*, 9: e53456.
- Zhao, Ru-Zhou, Shuai Jiang, Lin Zhang, and Zhi-Bin Yu. 2019. 'Mitochondrial electron transport chain, ROS generation and uncoupling (Review)', *Int. J. Mol. Med.*, 44: 3–15.

- Zhu, Qianlong, Durvis Hulen, Tongyao Liu, and Margaret Clarke. 1997. 'The cluA- mutant of Dictyostelium identifies a novel class of proteins required for dispersion of mitochondria', *Proceedings of the National Academy of Sciences*, 94: 7308-13.
- Züchner, Stephan, Irina V. Mersiyanova, Maria Muglia, Nisrine Bissar-Tadmouri, Julie Rochelle, Elena L. Dadali, Mario Zappia, Eva Nelis, Alessandra Patitucci, Jan Senderek, Yesim Parman, Oleg Evgrafov, Peter De Jonghe, Yuji Takahashi, Shoji Tsuji, Margaret A. Pericak-Vance, Aldo Quattrone, Esra Battaloglu, Alexander V. Polyakov, Vincent Timmerman, J. Michael Schröder, and Jeffery M. Vance. 2004. 'Mutations in the mitochondrial GTPase mitofusin 2 cause Charcot-Marie-Tooth neuropathy type 2A', *Nat. Genet.*, 36: 449-51.
- Züchner, Stephan, and Jeffery M. Vance. 2005. 'Emerging pathways for hereditary axonopathies', *J. Mol. Med.*, 83: 935-43.

Erklärung zur Dissertation

gemäß der Promotionsordnung vom 12. März 2020

□Hiermit versichere ich an Eides statt, dass ich die vorliegende Dissertation selbstständig und ohne die Benutzung anderer als der angegebenen Hilfsmittel und Literatur angefertigt habe. Alle Stellen, die wörtlich oder sinngemäß aus veröffentlichten und nicht veröffentlichten Werken dem Wortlaut oder dem Sinn nach entnommen wurden, sind als solche kenntlich gemacht. Ich versichere an Eides statt, dass diese Dissertation noch keiner anderen Fakultät oder Universität zur Prüfung vorgelegen hat; dass sie - abgesehen von unten angegebenen Teilpublikationen und eingebundenen Artikeln und Manuskripten - noch nicht veröffentlicht worden ist sowie, dass ich eine Veröffentlichung der Dissertation vor Abschluss der Promotion nicht ohne Genehmigung des Promotionsausschusses vornehmen werde. Die Bestimmungen dieser Ordnung sind mir bekannt. Darüber hinaus erkläre ich hiermit, dass ich die Ordnung zur Sicherung guter wissenschaftlicher Praxis und zum Umgang mit wissenschaftlichem Fehlverhalten der Universität zu Köln gelesen und sie bei der Durchführung der Dissertation zugrundeliegenden Arbeiten und der schriftlich verfassten Dissertation beachtet habe und verpflichte mich hiermit, die dort genannten Vorgaben bei allen wissenschaftlichen Tätigkeiten zu beachten und umzusetzen. Ich versichere, dass die eingereichte elektronische Fassung der eingereichten Druckfassung vollständig entspricht."

Teilpublikationen:

Marta Zaninello, Tim Schlegel *et al.*, CLUH maintains functional mitochondria and translation in motoneuronal axons and prevents peripheral neuropathy. *Sci. Adv.* **10**, eadn2050(2024). DOI:10.1126/sciadv.adn2050

29.11.2024, Tim Schlegel